Effectiveness of Damaged Fireproofing in Structural Steel Members Subjected to Fire

By

Ataollah Taghipour Anvari
B.S., Azarbaijan Shahid Madani University, 2015

THESIS

Submitted as partial fulfillment of the requirements
for the degree of Master of Science in Civil Engineering
in the Graduate College of the
University of Illinois at Chicago, 2017

Chicago, Illinois

Defense Committee:

Dr. Mustafa Mahamid, Advisor, Civil and Materials Engineering
Dr. Michael J. McNallen, Chair and Co-Advisor, Civil and Materials Engineering
Dr. Eduard Karpov, Civil and Materials Engineering

ACKNOWLEDGMENTS

I would like to express my gratitude to my advisors Prof. Mustafa Mahamid and Prof. Michael McNallen for their support, guidance and encouragement to accomplish all the steps of the research. It has been an honor to complete my master program under their supervision. Also, It is my pleasure to thank all my committee members for their patience and constructive comments.

Sincere thanks to my labmates, Kamel Bilal and Ines Torra, for their helpful discussions and comments. Also, I would like to thank all my friends helped me during course of my studies.

I wish to gratefully acknowledge the funding for this research was provided by COE Seed Funding. I would like to thank them for their resources and support

Last but not the least, warm thanks to my family for their true love, encouragement and support in all my pursuits.

Ataollah Taghipour Anvari
July 2017

TABLE OF CONTENTS

CHAPTER PAGE

1. INTRODUCTION 1

1.1 General 1

1.2 Literature review 4

1.3 Problem Statement and Research scope 8

2. MODELLING 10

2.1 Thermal Analysis 11

2.1.1 Thermal loading 11

2.1.2 Fire scenarios 13

2.2 Structural analysis 16

2.2.1 Boundary conditions 16

2.2.2 Loading 17

2.2.3 Failure criteria 18

2.3 Element Selection 21

2.3.1 Thermal Analysis 21

2.3.2 Structural Analysis 24

2.4 Thermal Material Properties 27

2.4.1 Structural Steel 27

2.4.2 Concrete 31

2.5 Mechanical Material Properties 34

2.5.1 Structural Steel Mechanical Properties 34

2.5.2 Concrete Mechanical Properties 38

3. MODEL VALIDATION 42

3.1 General 42

TABLE OF CONTENTS (Continued)

CHAPTER PAGE

3.2 Thermal Analysis Validation 44

3.3 Structural Analysis Validation 45

4. DAMAGED FIREPROOFING 49

4.1 General 49

4.2 Steel Beam's geometries 50

4.3 Types of the Fire Protection Damage 51

4.4 Loading 52

4.5 Failure Criteria 53

4.6 Parametric studies results 53

4.6.1 The Effect of Damage Penetration 54

4.6.2 Effect of fire protection's damage length 70

5. CONCLUSIONS AND FUTURE WORK 96

5.1 Summary 96

5.2 Conclusions 97

5.3 Future Work 98

REFERENCES 100

Vita 102

LIST OF TABLES

TABLE PAGE

Table 2-1. ASTM E119 fire time-temperature 14

Table 2-2. Thermal conductivity of structural steel at various temperatures (Eurocode3) 27

Table 2-3. Specific heat of structural steel at various temperatures (Eurocode3) 28

Table 2-4. Thermal expansion of structural steel at various temperatures (Eurocode3) 29

Table 2-5. Thermal conductivity of concrete at various temperatures (Eurocode2) 31

Table 2-6. Thermal expansion of concrete at various temperatures (Eurocode2) 32

Table 2-7. Specific heat of concrete at various temperatures (Eurocode2) 33

Table 2-8. Reduction factor of yield strength and modulus of elasticity of steel material relative to 20 °C (Eurocode3) 35

Table 2-9. Stress- strain relationships for steel material at elevated temperatures (Eurocode3) .. 36

Table 2-10. The variation of concrete unit mass at high temperatures (Eurocode2) 38

Table 2-11. Reduction factors of material properties of concrete at elevated temperatures (Eurocode2) 40

Table 3-1. Steel bridge girder dimensions and loading condition 44

Table 4-1. The properties of the selected steel cross sections 51

Table 4-2. Fire resistance of the members with fully damaged fire protection 65

Table 4-3. Fire resistance of the members 50%damaged penetration fire protection 65

Table 4-4. Fire resistance of the beams (Minute) 91

Table 4-5. Fire resistance of damaged members as function of fire resistance of fully protected members 92

LIST OF FIGURES

FIGURE PAGE

Figure 1-1. Concrete encased beam with partial loss of concrete fire protection 8

Figure 2-1. Fire temperature application regions 12

Figure 2-2. Standard fire time-temperature curves 15

Figure 2-3. Applied loads and beam sections 18

Figure 2-4. 3D discretization of a typical steel beam with concrete fireproofing 19

Figure 2-5. Cross section and mesh of concrete finite element 20

Figure 2-6. Cross section and mesh of steel beam 20

Figure 2-7. SOLID70 Geometry. Adopted from (ANSYS Element reference, 2016) 21

Figure 2-8. SHELL131 geometry. Adopted from (ANSYS Element reference, 2016) 22

Figure 2-9. SURF152 geometry with optional extra nodes to define convection and radiation properties. Adopted from (ANSYS Element reference, 2016) 23

Figure 2-10. TARGE170 and CONTA174 element geometry. Adopted from (ANSYS Element reference, 2016) 23

Figure 2-11. SOLID185 Element geometry 24

Figure 2-12. SHELL181 Element geometry. 25

Figure 2-13. LINK180 Element geometry. 25

Figure 2-14. Thermal conductivity of structural steel at various temperatures (Eurocode3) 28

Figure 2-15. Specific heat of structural steel at various temperatures (Eurocode3) 29

Figure 2-16. Thermal expansion of structural steel at various temperatures (Eurocode3) 30

Figure 2-17. Thermal conductivity of concrete at various temperatures (Eurocode2) 31

Figure 2-18. Thermal expansion of concrete at various temperatures (Eurocode2) 32

LIST OF FIGURES (Continued)

FIGURE PAGE

Figure 2-19. Specific heat of concrete at various temperatures (Eurocode2) 33

Figure 2-20. Reduction factor of yield strength and modulus of elasticity of steel material relative to 20 °C (Eurocode3) 35

Figure 2-21. Stress- strain curves for steel material at elevated temperatures (Eurocode3) 37

Figure 2-22. The variation of concrete unit mass at high temperatures (Eurocode2) 39

Figure 2-23. Reduction of concrete material properties at elevated temperatures (Eurocode2) ... 40

Figure 2-24. Drucker-Prager concrete model. 41

Figure 3-1. Schematic elevation of Steel bridge girder. Adopted form (Aziz et al., 2015) 42

Figure 3-2. 3D discretization of steel bridge girder 43

Figure 3-3. Comparison of measured temperature and thermal analysis results 45

Figure 3-4. Steel bridge girder at failure time a. Structural analysis b. Experimental test. Adopted from (Aziz et al., 2015) 46

Figure 3-5. Comparison of mid-span deflection in structural analysis and experiment 47

Figure 3-6. Steel girder placement in the furnace. Adopted from (Aziz et al., 2015) 47

Figure 3-7. LVDT set-up to measure mid-span deflection and out-of-plane displacement. Adopted from (Aziz et al., 2015) 48

Figure 4-1. a) Fully fireproofed beam (without any fire protection damage 52

Figure 4-2 Temperature of various parts of W12×22 with full and half damage penetration and fully fireproofed during the fire exposure 55

Figure 4-3. Temperature of various parts of W12×22 with full and half damage penetration and fully fireproofed during the fire exposure 55

LIST OF FIGURES (Continued)

FIGURE PAGE

Figure 4-4. Temperature of various parts of W14×30 with full and half damage penetration and fully fireproofed during the fire exposure..... 56

Figure 4-5. Temperature of various parts of W14×74 with full and half damage penetration and fully fireproofed during the fire exposure..... 56

Figure 4-6. Temperature of various parts of W18×40 with full and half damage penetration and fully fireproofed during the fire exposure..... 57

Figure 4-7. Temperature of various parts of W18×86 with full and half damage penetration and fully fireproofed during the fire exposure..... 57

Figure 4-8. Temperature of various parts of W21×44 with full and half damage penetration and fully fireproofed during the fire exposure..... 58

Figure 4-9. Temperature of various parts of W21×93 with full and half damage penetration and fully fireproofed during the fire exposure..... 58

Figure 4-10. Comparison of the temperature of different parts of W12×22 and W12×50 with full damage penetration during the fire exposure..... 61

Figure 4-11. Comparison of the temperature of different parts of W14×30 and W14×74 with full damage penetration during the fire exposure..... 61

Figure 4-12. Comparison of the temperature of different parts of W18×40 and W18×86 with full damage penetration during the fire exposure..... 62

Figure 4-13. Comparison of the temperature of different parts of W21×44 and W21×93 with full damage penetration during the fire exposure..... 62

Figure 4-14. Mid-span deflection of W12×22 with no damage and with 12.7cm damage length66

LIST OF FIGURES (Continued)

FIGURE PAGE

Figure 4-15. Mid-span deflection of W12×50 with no damage and with 12.7cm damage length 66

Figure 4-16. Mid-span deflection of W14×30 with no damage and with 12.7cm damage length 67

Figure 4-17. Mid-span deflection of W14×86 with no damage and with 12.7cm damage length 67

Figure 4-18. Mid-span deflection of W18×40 with no damage and with 12.7cm damage length 68

Figure 4-19. Mid-span deflection of W18×86 with no damage and with 12.7cm damage length 68

Figure 4-20. Mid-span deflection of W21×44 with no damage and with 12.7cm damage length 69

Figure 4-21. Mid-span deflection of W21×93 with no damage and with 12.7cm damage length 69

Figure 4-22. Temperature of various parts of W12×22 with 30% of span damage and fully fireproofed during the fire exposure 71

Figure 4-23. Temperature of various parts of W12×50 with 30% of span damage and fully fireproofed during the fire exposure 71

Figure 4-24. Temperature of various parts of W14×30 with 30% of span damage and fully fireproofed during the fire exposure 72

Figure 4-25. Temperature of various parts of W14×74 with 30% of span damage and fully fireproofed during the fire exposure 72

Figure 4-26. Temperature of various parts of W18×40 with 30% of span damage and fully fireproofed during the fire exposure 73

Figure 4-27. Temperature of various parts of W18×86 with 30% of span damage and fully fireproofed during the fire exposure 73

Figure 4-28. Temperature of various parts of W21x44 with 30% of span damage and fully fireproofed during the fire exposure 74

LIST OF FIGURES (Continued)

FIGURE PAGE

Figure 4-29. Temperature of various parts of W21×93 with 30% of span damage and fully fireproofed during the fire exposure 74

Figure 4-30. Mid-span deflection of W12×22 with 50% loading and various damage length..... 75

Figure 4-31. Mid-span deflection of W12×22 with 70% loading and various damage length..... 75

Figure 4-32. Mid-span deflection of W12×22 with 90% loading and various damage length..... 76

Figure 4-33. Mid-span deflection of W12×50 with 50% loading and various damage length..... 77

Figure 4-34. Mid-span deflection of W12×50 with 70% loading and various damage length..... 77

Figure 4-35. Mid-span deflection of W12×50 with 90% loading and various damage length..... 78

Figure 4-36. Mid-span deflection of W14×30 with 50% loading and various damage length..... 79

Figure 4-37. Mid-span deflection of W14×30 with 70% loading and various damage length..... 79

Figure 4-38. Mid-span deflection of W14×30 with 90% loading and various damage length..... 80

Figure 4-39. Mid-span deflection of W14×74 with 50% loading and various damage length..... 81

Figure 4-40. Mid-span deflection of W14×74 with 70% loading and various damage length..... 81

Figure 4-41. Mid-span deflection of W14×74 with 90% loading and various damage length..... 82

Figure 4-42. Mid-span deflection of W18×40 with 50% loading and various damage length..... 83

Figure 4-43. Mid-span deflection of W18×40 with 70% loading and various damage length..... 83

Figure 4-44. Mid-span deflection of W18×40 with 90% loading and various damage length..... 84

Figure 4-45. Mid-span deflection of W18×86 with 50% loading and various damage length..... 85

Figure 4-46. Mid-span deflection of W18×86 with 70% loading and various damage length..... 85

Figure 4-47. Mid-span deflection of W18×86 with 90% loading and various damage length..... 86

Figure 4-48. Mid-span deflection of W21×44 with 50% loading and various damage length..... 87

LIST OF FIGURES (Continued)

FIGURE PAGE

Figure 4-49. Mid-span deflection of W21×44 with 70% loading and various damage length..... 87

Figure 4-50. Mid-span deflection of W21×44 with 90% loading and various damage length..... 88

Figure 4-51. Mid-span deflection of W21×93 with 50% loading and various damage length..... 89

Figure 4-52. Mid-span deflection of W21×93 with 70% loading and various damage length..... 89

Figure 4-53. Mid-span deflection of W21×93 with 90% loading and various damage length..... 90

Figure 4-54. The mid-span deflecting of W12x22 with 30% of span damage length during fire exposure 95

Figure 4-55. The mid-span deflecting of W21x44 with 30% of span damage length during fire exposure 95

LIST OF ABBREVIATIONS

AFP	Active Fire Protection
ASTM	American Society for Testing and Materials
CFD	Computational Dynamic Fluids
FEM	Finite Element Method
PFP	Passive Fire Protection
EC	Eurocode
AISC	American Institute of Steel Construction

SUMMARY

Structural steel systems' advantages over other structural systems have made structural steel a dominant material as a construction material in the United States. One of the disadvantages of steel structures is the strength reduction at elevated temperatures. Therefore, preserving the stability of steel structures during fire events is an challenge facing engineers, architects and contractors. For this reason, various passive fire protection methods are proposed to prevent or delay temperature increase within the cross-section. However, during the service life of a structure, there is a probability of damage development in the fire protections due to physical accidents, long-term weathering, improper material application and other circumstances. These methods have been tested in an excellent condition and, the proposed design methods of the fire protections have considered the full protection of the structural members. Concrete encasement is known as a passive fire protection method from past decades which was used widely in various industries. The goal of this study is to evaluate the fire resistance of the steel beams with partial loss of concrete as a fireproofing material. Fire protection's partial loss raises the question regarding the effectiveness of such damages on the fire resistance of the beams which is very essential for structures at refinery and oil plants where a high amount of flammable material are processed.

Finite element analyses were utilized to study the thermal and structural response of the beams. Developed finite element models for both thermal and structural analysis were validated by comparing the finite element analyses' results with experimental results by other researchers. ASTM E119 fire temperature for 4 hours was applied to the beams. The fire resistance of beams with damages with varying penetrations and lengths at the bottom flange of the beams were investigated. Thermal analysis results showed that the temperature at the damage region increases

at a high rate due to direct exposure to fire. It was found that small area of damage can cause significant reduction in fire resistance of the beams which leads to earlier failure than steel beams with full fire protection. The penetration of the damage had a minor reduction in the fire resistance of the beams. Furthermore, the longer damaged region's length leads to a faster degradation of the load carrying capacity and increment of deflection of the beams. As the damage parts' length increases, the fire resistance reduces. However; beyond a certain limit the increase in the damage region's length does have any further effect.

CHAPTER 1. INTRODUCTION

1.1 General

High strength, ductility and other advantages made structural steel attractive material and option to engineers. However, structural steel has lower fire resistance than concrete. Fire is a potential hazard to structures, occupants and users. Structures in petrochemicals, oil and gas refinery plants are the main concern of fire safety issues. The function of these structures is to support pipes those include high amount of flammable material. Due to the high conductivity of steel, the temperature within steel structures' members increases during exposure to fire, and the high temperature is transferred to other members rapidly. The strength and stiffness properties of steel degrade at elevated temperature; hence, steel structures are susceptible to strength loss and instability during fire events.

Various methods are employed to keep steel structures safe against a fire incident to reduce the adverse effects of fire. Fire protection systems are intended to extinguish, control or reduce the spread of the fire and smoke. The design of fire protection systems generally depends on the

type of the flammable material, the amount of the existing flammable material, the size of the intended place and the type of the structure's usage.

The designed fire protection systems should satisfy the required performance as specified in related design codes and standards. Fire protection systems are categorized into two main categories, active and passive fire protection systems. Active Fire Protection (AFP) system usually contain a detection system that automatically activates the system to extinguish the fire during a fire incident. Sprinklers systems are examples of active fire protection systems that are used widely in most types of buildings. Passive Fire Protection (PFP) system is intended to slow the spread of the fire or smoke in a structure during a fire incident. Firewalls and spray applied fireproofing are examples of passive fire protection systems. In the case of protecting the structural members, spray applied fireproofing, gypsum boards, concrete encasement are some of the common methods of passive fireproofing. In these methods, the structural members are covered by fire protection material to reduce the heat flow rate into the structural components. By reducing the heat transfer rate to the structural members, the structure's performance is preserved upon evacuation of occupants and extinguishing the fire. The main characteristic of fire protection material is the weak heat conductivity properties. The fire resistance of the members depends mainly on the thickness of the fire protection material covered the member.

Concrete encasement is one of the traditional fire protection methods had been utilized in gas and oil refineries and drilling plants. In this method, the steel members are covered by concrete. Due to low thermal conductivity of concrete, it plays an important role as a thermal insulator. The fire resistance of members is mainly dependent on the thickness of the concrete. The durability of concrete against weather exposure, impact and corrosion are the advantages of concrete

encasement method for exposed structures, oil and gas drilling plants (NIST, 2004). Nevertheless, the fragility, spalling of the concrete, impacts and other incidents can lead to the reduction of fire endurance of the structural elements. The objective of this study is to investigate the structural response of steel structural beams with partial loss of concrete fireproofing. By investigating the real behavior of such members under fire exposure, the potential hazards can be predicted and prohibited during a fire incident. The procedure and details are presented in the problem statement and research objective sections.

1.2 Literature review

Milke et al. (2003) investigated the effect of the loss of spray-applied fire protection in the reduction of fire resistance of steel columns. An estimated Spray applied fire protection thickness was considered for each section regarding the fire exposure time. 3D finite element thermal analysis was carried out to study the impact of temperature increment in regions with fire protection loss exposed to ASTM E119 standard fire. Authors studied two steel sections with different protection loss areas for one and two hours of fire exposure. Columns were studied without any load application. Therefore, to determine the fire resistance of the members, ASTM E119 temperature endpoint criteria were the governing limit state. Results showed that with small loss area of fire protection the fire resistance of the member would reduce. The extension of the damaged area is a primary factor in reducing the fire resistance of the member. Also, massive columns with similar protection loss and fire exposure condition showed more fire resistance due to higher thermal capacity where compared with lighter columns.

Kang et al. (2008) performed a numerical analysis study to find out the effect of partial loss of the spray-applied fire protection on steel beams under ISO 834 standard fire exposure. To figure out the influence of partial loss of fire protection, the reduction in actual load bearing capacity was calculated, and the deflection of the steel beams was measured. Four standard hot-rolled I- shape sections with two spray-applied fire protection thickness were studied. The material properties of the steel sections at elevated temperatures were input to ABAQUS according to Eurocode2. However, constant thermal material properties for spray-applied fire protection material was utilized. Coupled thermal and structural finite element analysis were carried out for each model was created in ABAQUS. Beams were assumed to be simply supported with

continuous lateral supports. It was shown that the load bearing capacity is influenced by the damage location, damage penetration and the dimensions of the cross section. They concluded that the area of the fire protection loss has a significant effect on the reduction of the member's moment capacity. Cases with larger damaged areas experienced more reduction in their moment capacity. However, by increasing the damaged area, the reduction rate in moment capacity is reducing. It was indicated that the decrease in moment capacity is higher in cases with damaged fire protection in the flange than the web of the cross section. Also, a closer damaged regions in the web of the cross section to the flanges causes more reduction in moment capacity of the beams. Also, the damage areas with higher width to thickness ratio cause more decrease in the moment capacity of the cross section at early stages of fire exposure. Furthermore, with same cross section's depth, the lighter cross sections suffer more reduction in their moment capacity.

Tomecek and Milke (1993) performed heat transfer finite element analysis to determine the thermal response of the columns with missing fire protection to figure out the relationship between the fire resistance reduction, the location and missing amount of fire protection. The thickness of fire protection material was specified from recommended Underwriters Laboratories (Underwriters' Laboratories, 1992) equations. Three columns sizes with three variable fire protection thicknesses and two protection loss locations were selected. Models were simulated in two-dimensional models using FIRES-T3 heat transfer computer models. The columns were exposed to ASTM E119 standard fire, and the temperature endpoint criteria specified in ASTM E119 was considered to determine the fire resistance of the columns. They concluded that with the same area of fire protection loss, the lighter columns experience more reduction in their fire resistance. The fire resistance of the columns with larger protection loss area reduced,

significantly. Also, it was shown that the location of fire protection loss, the size of the column and amount of the protection loss affects the fire resistance of the columns. Because of the shadow effect of the flange on the web, the effect of fire protection loss of the flanges was more than the columns with protection loss in the web. Also, the columns with higher fire rating experienced more fire resistance reduction with the same amount of protection loss. As an example, the same amount of protection loss reduced the fire resistance of W10x49 by 2% for one- hour fire rating and 28% for three-hour fire rating.

Dwaikat and Kodur (2012) developed a simple approach to predict the temperature profile of the steel cross-sections with damaged fire protection. The results of the proposed approach were validated through comparing the temperature profile of the cross section resulted by the thermal finite element analysis using ANSYS. Results from this study showed that the partial loss of fire protection causes a rapid increment of the temperature of the cross-section. Therefore, a severe degradation in the strength of the material of the cross-section was observed. Also, if the member is restrained, extra axial forces would be produced. The analysis showed that partial loss of the fire insulation could reduce the fire protection of a column from 3 hours to 90 minutes.

Wang and Li (2009) performed an experimental study to evaluate the influence of partial loss of fire protection on the behavior of the steel columns. The experimental study included two H-shape steel columns with damage length of 7% and 14% of the column length at both ends of the columns. The thickness of the fire protection was 20 mm for both columns. A constant axial load equivalent to 55% of the capacity of the specimens was applied during the test. The temperature of the furnace followed ISO 834 standard fire temperature. The temperature

distribution along the column was simulated by finite element analysis and compared with the experimental results. The material properties of the steel at elevated temperatures were adopted from the equations provided by Chinese Technical Code for Fire Safety of Steel Buildings. Additionally, authors presented a continuum model to determine the ultimate capacity of the columns with partial fire protection loss. The experimental results showed that the length of the damage has a major contribution to the reduction of column's fire resistance. Experimental and analytical results indicated that the failure occurs at the part of the column with damaged fire protection. Furthermore, the damaged part length and load eccentricity have a significant effect on the fire resistance of columns. The mode of failure was yielding in the column with shorter damaged fire protection part. However, for the column with a larger length of fire protection buckling failure mode controlled. The shorter length of the damaged part results in higher critical temperature. Also, the rotational stiffness has minor effect when the damage length at the end of the column is shorter.

Faber et al. (2004) carried out a parametric study to investigate the reduction of fire resistance of cross sections with damaged fire protection. They performed transient finite element analysis using ABAQUS under ISO834 fire exposure. Two cross sections with four fire protection thicknesses and three different thermal material properties were studied. The fire resistance of members with various damaged areas and fire protection loss at the middle of the members' span were compared with fire resistance of members without any damage. It was concluded that small damage areas reduce the fire endurance of the members significantly. Furthermore, members with thicker fire protection experienced more fire resistance reduction. The comparison between the cases with different damage locations showed that the effect of partial loss of fire protection in

flanges is more significant than the partial loss of fire protection in the web. The authors recommended periodic monitoring and maintenance to prohibit any damage in fire protection of the structural elements.

1.3 Problem Statement and Research scope

The proposed methods in codes to design fire protections for structural members are based on the assumption that the structural members will be completely fireproofed and will not have any missing part. Nevertheless, during the service life of a structure, physical impacts, inappropriate application of fire protection material and fire protection removal at connection regions lead to missing portions of fire protection along or across the depth of the structural members. In Figure 1-1 a concrete encased beam with partial loss of concrete fireproofing is illustrated. The partial loss of fire protection results in a sharp rise in the temperature of the steel member and reduction in the strength and stiffness properties of the steel sections.

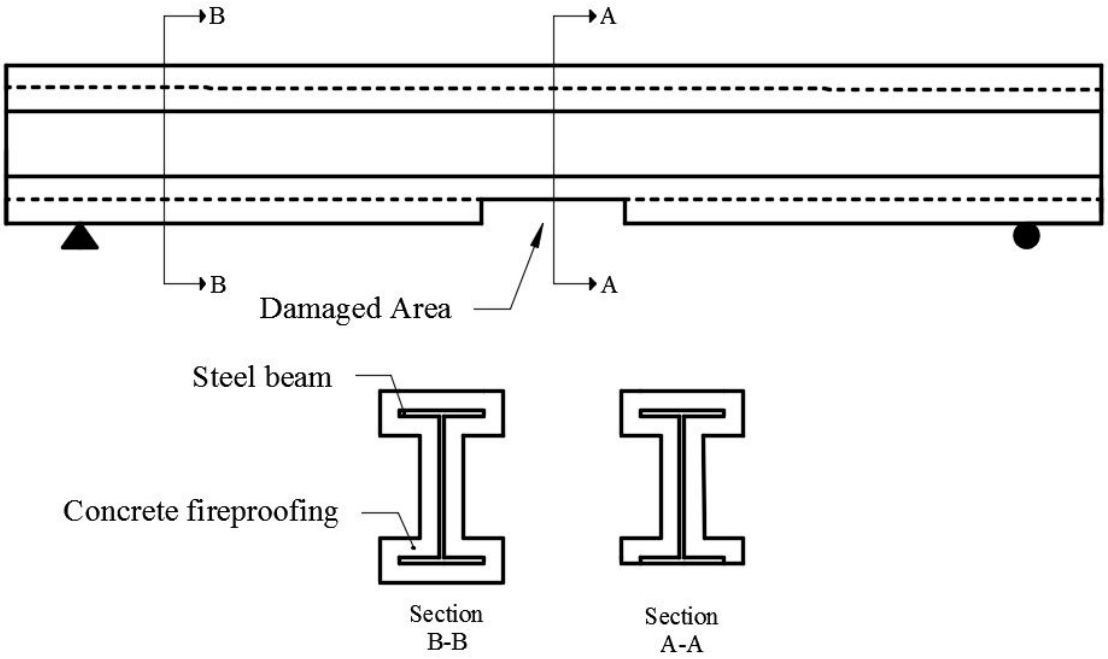

Figure 1-1. Concrete encased beam with partial loss of concrete fire protection

Therefore, to understand the effect of such damages due to the partial loss of the fire protection, more studies are needed to evaluate the reliability of the members with damaged fire protection within a structure. Previous studies on the behavior of members with partial loss of fire protection have shown that the partial loss of fire protection can have a considerable negative influence on the deformation and load-carrying capacity of the structural components that can lead to the collapse of a structure. Most of the previous experimental and analytical studies were focused on the effect of the partial loss of fire protection on columns. Also, studies have been done on evaluating the effectiveness of damages on the fire resistance of the members with spray-applied fire protection. However, in most of petrochemical and oil refineries plants most of the structures are protected by application of concrete encasement method. In addition to that structures at oil and refinery plants are more likely to exposed to fire and severe conditions.

The aim of this study is to evaluate the performance of the steel beams with partial loss of concrete encasement fireproofing and determine the potential risk of such damages. Finite element method (FEM) was employed in this study. Nonlinear thermal and structural finite element models were developed by ANSYS (ANSYS Inc., 2016). The material properties of concrete and steel at elevated temperatures were calculated according to the proposed equations by Eurocodes (EC2, 2004; EC3, 2005). To understand the influence of the cross-sections' properties, different cross-sections were selected for analysis. Damaged fireproofing with various areas and damage penetration were simulated to evaluate the behavior of structural members due to partial loss in fire protection.

CHAPTER 2. MODELLING

Numerical analysis was used in this study to investigate the behavior of the damaged fireproofed steel beams under fire loading. Many types of instruments are required to explore the behavior of the beams with damaged fireproofing by actual experiments. Experiments are dependent on many parameters which should be controlled during the test, such as the type of the material, the temperature of the furnace, and these tests are expensive. In this study, 3D finite element models were developed. ANSYS 17.1 (ANSYS Inc., 2016) was utilized to develop finite element models. Finite element models for thermal and structural parts were validated with test results that had been provided by other researchers (Aziz et al., 2015; Aziz, 2015). Details on validations purposes are provided in chapter 3.

Direct method and load transfer methods are two type of methods to carry out fire resistance finite element analysis (ANSYS Coupled-field Analysis Guide, 2016). Coupled- field elements are used in direct coupling method analysis which involves just one kind of analysis. However, in load transfer method analysis, the fire resistance analysis is performed by two types of analysis in different fields. In this study, to determine fire resistance of the beams with damaged fireproofing, finite element models were created based on the load transfer method. Thermal and

structural finite element models, to perform analysis in two different fields, were established. Results from the thermal analysis were input to structural analysis as nodal temperature load during the fire exposure time. Both thermal and structural models were meshed similar to each other to avoid any error in mapping the temperature distribution from thermal analysis to structural analysis.

2.1 Thermal Analysis

Thermal models were created to determine the distribution of the temperature within the structural member due to a fire exposure. Thermal analysis is independent of structural analysis, and it is assumed that any deflection does not influence the temperature distribution along the member and during the fire exposure. Thermal analysis is only dependent on the high-temperature material properties. All parts of the model meshed with thermal elements. SHELL131, SOLID70, SURF152, TARGE170 and CONTA174 (ANSYS Element reference, 2016) are thermal elements used in the thermal analysis.

2.1.1 Thermal loading

It is assumed that the studied members are exposed to fire with uniform temperature distribution. The temperature of the fire was applied through various time steps during the finite element analysis. It was assumed that the member is exposed to the fire from three sides to account for the effect of the slabs on the beams. The temperature at the top side of the beams was assumed as room temperature during the fire exposure. To avoid any stress concentration due to thermal expansion at the supports, the fire loading was applied 30 cm away from both ends of the beam's length. Figure 2-1 shows the regions of fire exposure of the members.

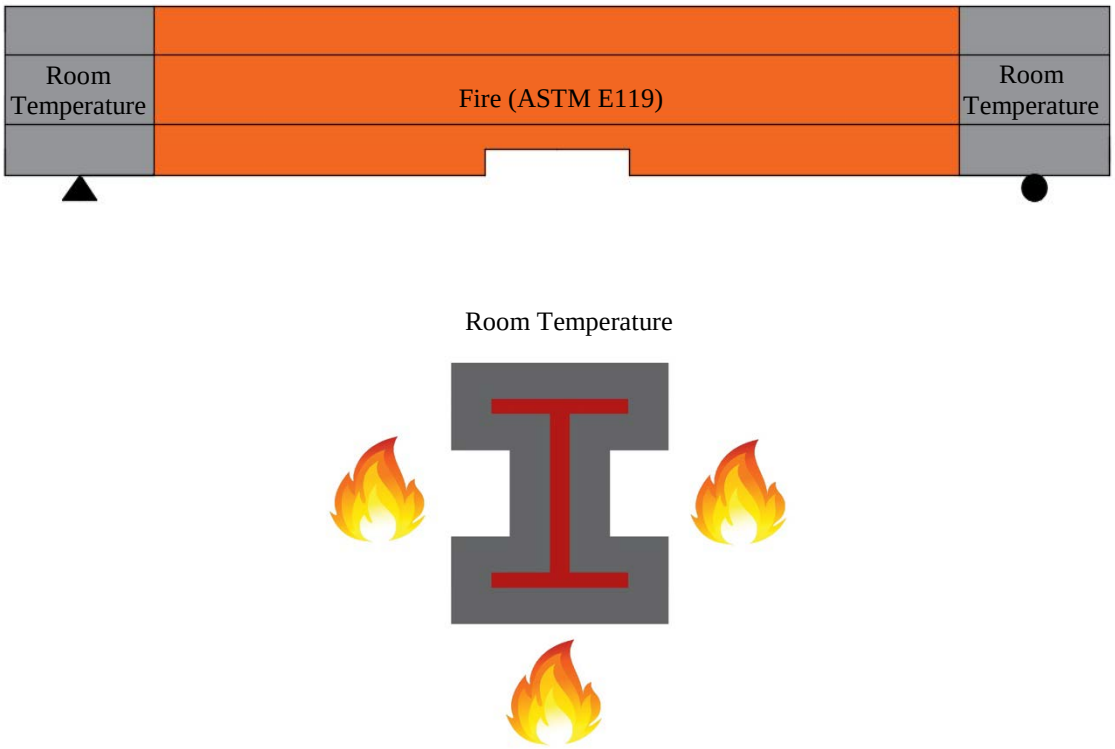

Figure 2-1. Fire temperature application regions

The thermal convection was applied using the SURF152 element. SURF152 elements were implemented on exposed parts of the models. The bulk temperature was applied according to the standard time-temperature fire curve (ASTM E119, 2016). The bulk temperature of room temperature $(20℃)$ was applied to the SURF152 elements on the top surface of the beams.

Heat convention coefficient of $25\ \mathrm{W/m^2K}$ and Stefan-Boltzman constant of $5.67 \times 10^{-8}\ \mathrm{W/m^2.°K^4}$ was used for thermal analysis as it is recommended in Eurocode1 (EC1, 2002). It was assumed that all three sides of the members receive 70% of the fire radiation. According to the recommendation of Eurocode2 and 3, the radiation factor of 0.7 was used.

2.1.2 Fire scenarios

The intensity of fire temperature has a significant effect on the design of the structural elements. The distribution of temperature around and within the cross section of fire-proofed beams is governed by several parameters such as enclosure type, existing flammable material, and ventilation. To take into account these parameters for a specific case, it requires to build and solve computational dynamic fluids (CFD) models. The objective of this study was to determine the effect of the damages of fireproofing material on the response of the steel beams without considering any specific cases. Therefore, the thermal analysis was done considering the provided time-temperature relationships in the specific standards and codes.

In standard fire scenarios it is assumed that the temperature of the fire increases without any decay duration of the fire exposure. However, realistic fire scenarios define the severity of fires in a real exposure depending on the fuel load, ventilation condition, design philosophy and the existing fire extinguisher systems. In realistic fire scenarios, the time-temperatures curves include a decay in fire temperature as cooling phase after the maximum temperature is achieved. The growth and the decay of fire in realistic fire scenarios are influenced by the activity of any active fireproofing, ventilation and the amount of fuel.

Most of the fire resistant tests used the standard fire time-temperature curves specified by specific standards and codes. Hydrocarbon fire and external fire time-temperature curves are alternative design fires from Eurocode1 (EC1, 2002) for elements engulfed in fire flames and structural members exposed to low temperature, respectively (NIST Technical Note 1681, 2010).

In Figure 2-2 the time- temperature curves of ASTM E119, Standard fire, hydrocarbon fire and external fire are shown. In this study ASTM E119 time-temperature fire curve was applied to all members. ASTM E119 fire time-temperature is defined by several distinct points as it is shown in Table 2-1.

Standard time-temperature curve (EC1, 2002):

$\theta = 20 + 345\ \log_{10}(8t + 1)$ (Eq. 2-1)

External fire time-temperature curve (EC1, 2002):

$\theta = 660\ (1 - 0.687e^{-32t} - 0.313e^{-3.8t}) + 20$ (Eq. 2-2)

Hydrocarbon fire time-temperature curve(EC1, 2002):

$\theta = 1080\ (1 - 0.325e^{-0.167t} - 0.675e^{-2.5t}) + 20$ (Eq. 2-3)

Table 2-1. ASTM E119 fire time-temperature

Time (Min)	Temperature (℃)
0	20
5	538
10	704
30	843
60	927
120	1010
240	1093
480	1260

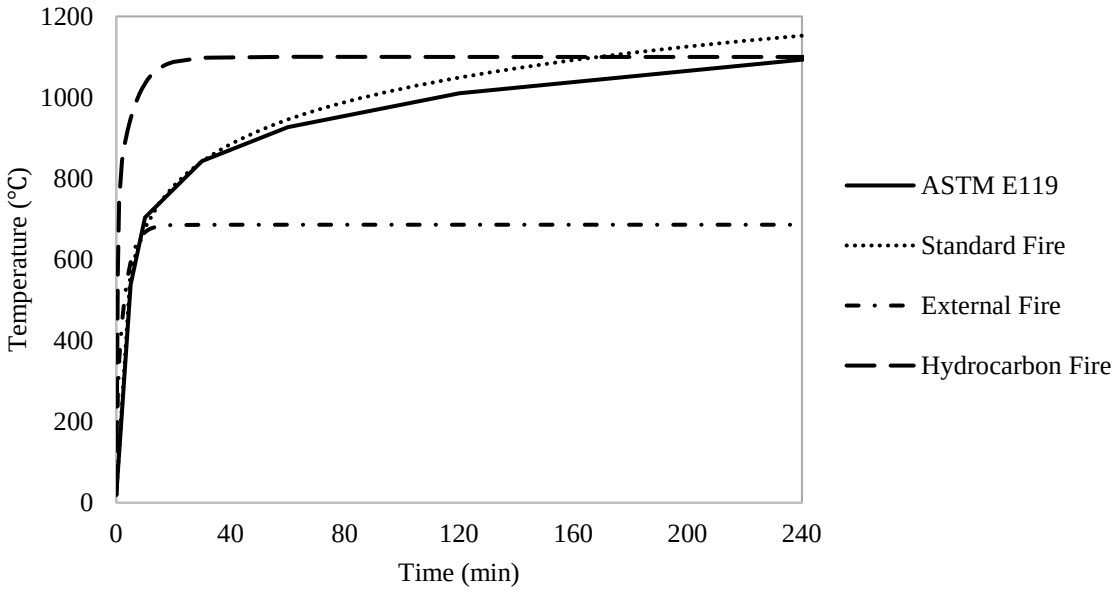

Figure 2-2. Standard fire time-temperature curves

2.2 Structural analysis

The structural finite element models were created to determine the fire resistance of the members under severe fire loading. Structural analysis was carried out in several time steps. The temperature of each node at different parts of the member during the fire exposure was mapped to the structural finite element models.

2.2.1 Boundary conditions

Application of accurate boundary conditions is important to get accurate results. Axial restrains on the beams causes axial stress due to thermal expansion. For members within a structure, the axial stiffness can be produced due to the existence of the adjacent columns and frames. For most cases, the adjacent frames and members are not identical; therefore, the axial stiffness can be different for each beam. End rotational and axial restraint can increase the fire response of the member (Gewain and Troup, 2001). Because the goal of this study is to determine the effect of damaged fireproofing on the structural behavior of the beams without considering any specific frame, all beams were assumed to be simply supported. In Figure 2-3 a layout of structural model and beam sections is illustrated.

In the structural analysis, three types of restrains were applied. Pin support was applied as zero displacements in Y and Z axis direction at the nodes in a row at 15 cm from the one end of the beams. Roller support was applied as zero displacements in Y axis on a row of nodes at 15 cm distance from the other end of the beams. The lateral bracings had been implemented on the edge of one side of the top flange of the beams with appropriate distances according to the strength properties of the cross-section, to avoid lateral torsional buckling failure mode of the beams during

fire analysis. This allows obtaining the actual capacity at the beam in yielding limit state that mostly controls in actual structures.

2.2.2 Loading

To consider the existing stress and deformation within the member before fire exposure, at the first time step of the structural analysis, structural loads were applied without any thermal load. At other time steps, the resulted temperature distribution within the members' cross section from thermal analysis was applied to the structural analysis as nodal loads (ANSYS Thermal Analysis Guide, 2016). Structural loads include a uniform distributed load along the beam and two point loads at a distance of one-third span from both ends. The uniform structural load was calculated according to the weight of the steel cross-section and the weight of the fireproofing concrete. The point loads were calculated to produce a bending moment in the middle third of the member equal to 50%, 70% and 90% of the member bending capacity including the bending moment generated by the uniform load. It was assumed that the strength is the only limit state of failure. Therefore, the moment capacity is the plastic moment limit state according to AISC 360-10 (AISC, 2010).

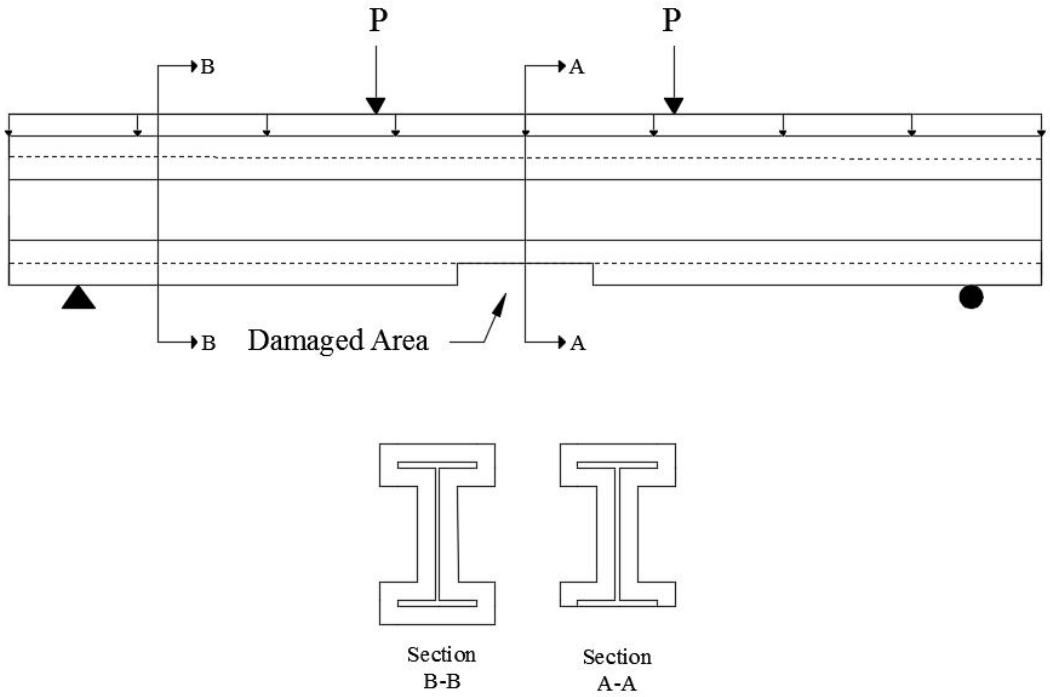

Figure 2-3. Applied loads and beam sections

2.2.3 Failure criteria

To determine the fire resistance of each of the studied case, the structural analysis was checked according to deflection and strength limit states. The models were continuously laterally braced, and no lateral torsional buckling occured. The deflection limit state of ASTM E119 was used in this study. When the both deflection and the rate of the deflection at mid-span of the beam exceeded the maximum amount, as shown below in Eq. 2-4 and Eq.2-5, that point was defined as the failure time of the beam.

Maximum deflection (ASTM E119, 2016) = $\frac{L_c^2}{400d}$ in or mm (Eq. 2-4)

Maximum deflection rate (ASTM E119, 2016) = $\frac{L_c^2}{9000d}$ in or mm/min (Eq. 2-5)

Where:

L_c = Clear span of the beam

d = The distance between the extreme fiber of the beam in the compression zone and the extreme fiber of the beam in the tensile zone.

In some models, the ultimate strain based on the defined stress-strain relationship was exceeded. When the strain exceeds the ultimate strain, the material loses its strength, and the finite element model does not converge. In such models, the strength limit state governs, and it happens before the mid-span deflection achieves its maximum value. Three-dimensional model of a concrete encased fire proofed beam is shown in Figure 2-4, cross-section in Figure 2-5, and bare steel beam in Figure 2-6.

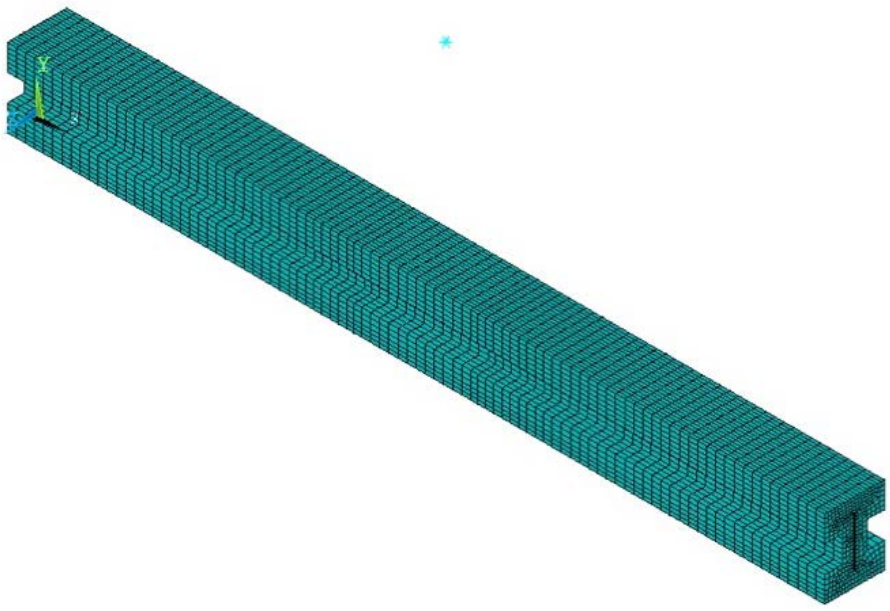

Figure 2-4. 3D discretization of a typical steel beam with concrete fireproofing

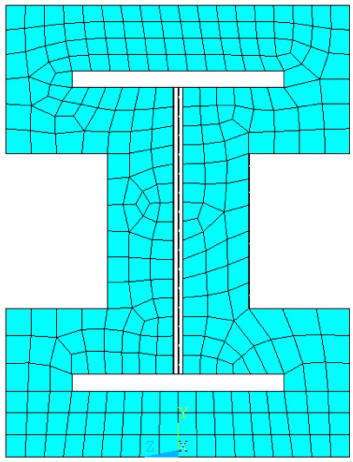

Figure 2-5. Cross section and mesh of concrete finite element

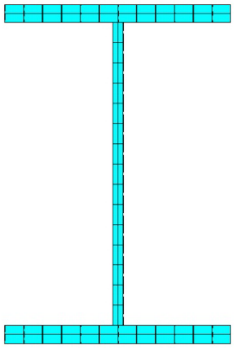

Figure 2-6. Cross section and mesh of steel beam

2.3 Element Selection

2.3.1 Thermal Analysis

- **SOLID70:**

This type of element has eight nodes. At each node, the temperature is the only degree of freedom. SOLID70 is used for simulating solid structures. It has through thickness conduction capability, and it is applicable for steady-state and transient thermal analysis. This element was used to simulate concrete fireproofing and concrete slab on the steel beam for validation purposes models. SOLID70 was replaced with SOLID185, an equivalent solid three-dimensional element, for structural analysis. The geometry and location of the nodes at SOLID70 is illustrated in Figure 2-7.

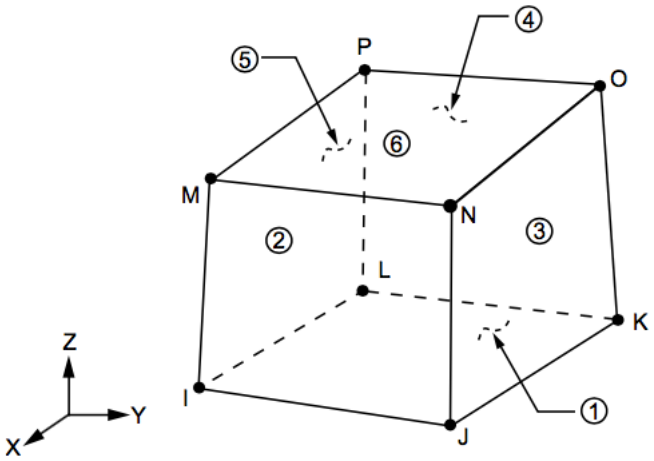

Figure 2-7. SOLID70 Geometry. Adopted from (ANSYS Element reference, 2016)

- **SHELL131:**

SHELL131 is a three-dimensional layered element. This element has in-plane and through thickness thermal conduction capability. SHELL131 is applicable for three-dimensional transient analysis. This element has four nodes. Each node has up to 32 degrees of freedom depending on

the number of layers. For structural analyses, SHELL181 has been used as an equivalent three-dimensional element. SHELL131 is used to simulate steel beams. Two layered SHELL131 elements were applied in all analysis done by this study. The geometry and location of the nodes at SHELL131 is shown in Figure 2-8. SHELL181 element was used as an equivalent element for structural analyses.

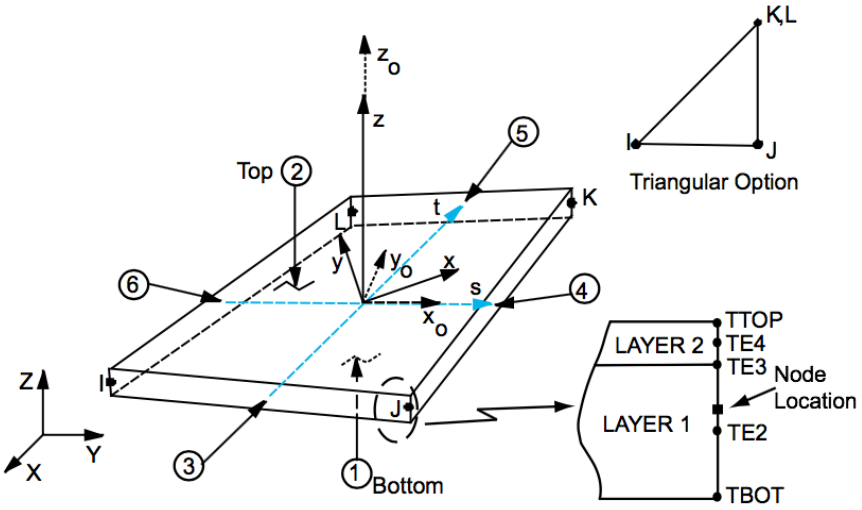

Figure 2-8. SHELL131 geometry. Adopted from (ANSYS Element reference, 2016)

- **SURF152:**

SURF152 is a three-dimensional thermal element. This element was overlaid on three-dimensional elements for surface loads and effects applications in thermal analysis. SURF152 was used with four nodes in this study. SURF152 shares node with underlying solid or shell elements to simulate heat conduction, radiation and convection. An extra node away from base elements was used to apply environment temperature for convection and radiation effects. The temperature of the fire during thermal analysis was applied to the extra node. SURF152 was applied on the surface of the concrete fireproofing and exposed parts of the steel beams. The geometry and location of the nodes at SURF152 is presented in Figure 2-9.

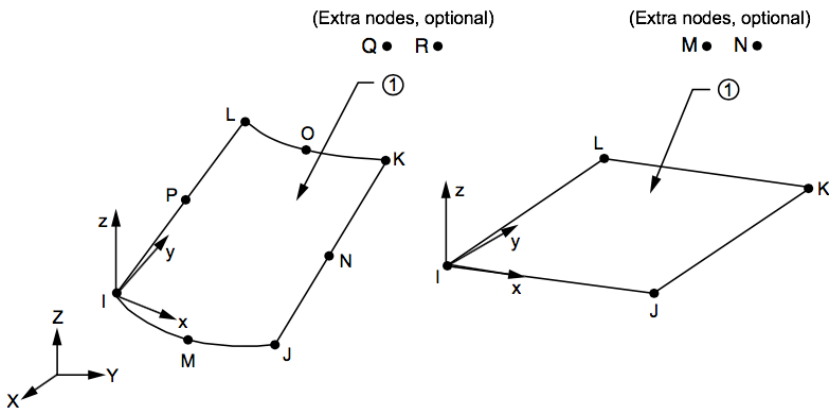

Figure 2-9. SURF152 geometry with optional extra nodes to define convection and radiation properties. Adopted from (ANSYS Element reference, 2016)

- **TARGE170 and CONTA174:**

TARGE170 is used to represent target surfaces accompanied contact element. This element overlays on solid and shell elements to account for the boundary of the body. Target elements are associated with contact elements. For thermal analysis, TARGE170 and CONTA174 elements are used to enable thermal transfer between various elements and materials. In thermal analysis, CONTA174 elements with four nodes with a temperature degree of freedom at each node was used. The geometry of TARGE170 and CONTA174 are demonstrated in Figure 2-10. Theses elements were applied between the concrete fireproofing or slab and the steel girder to simulate the heat transfer between two parts.

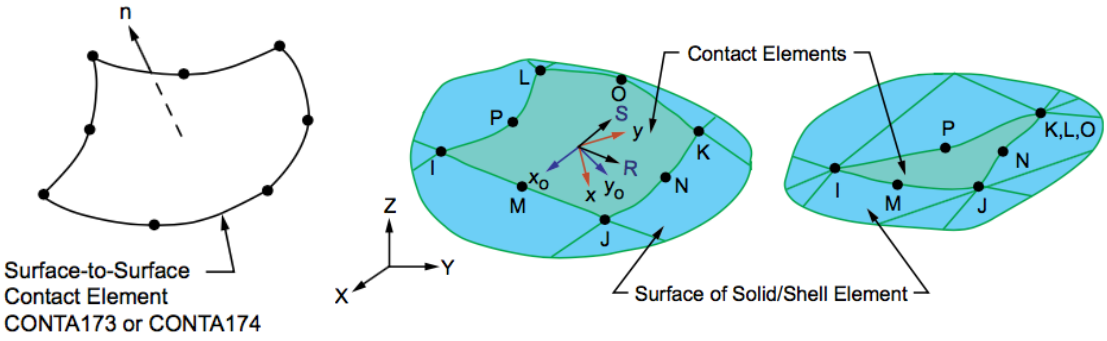

Figure 2-10. TARGE170 and CONTA174 element geometry. Adopted from (ANSYS Element reference, 2016)

2.3.2 Structural Analysis

- **SOLID185:**

This element is a common element to model 3D solid structures. This element has eight nodes with three degrees of freedom at each node (Transition in X, Y, and Z-axis). It is well suited type of elements for analysis which include, plasticity, large deflection and strain. Resulted temperature from thermal analysis can be applied as body load to each node. SOLID185 was used to simulate concrete slabs on top of the beams. Figure 2-11 shows the geometry and the nodes of SOLID185.

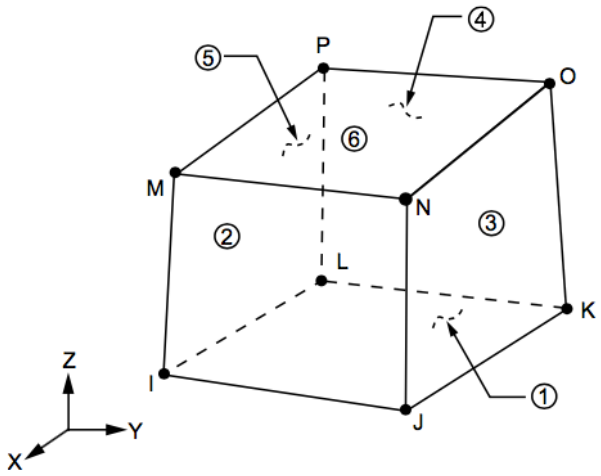

Figure 2-11. SOLID185 Element geometry.
Adopted from (ANSYS ADPL Element reference, 2016)

- **SHELL181:**

This element is suitable to use in simulating structures with a thin thickness. This element has four nodes with six-degree freedom including translation in X, Y, Z directions and rotation about X, Y , Z-axes. SHELL181 has large rotation and strain capabilities in nonlinear analysis. This element is suitable for analysis that may include buckling analysis. The geometry of

SHELL181 is displayed in Figure2-12. For all structural analysis, the two-layered SHELL181 element was used to mesh steel beams.

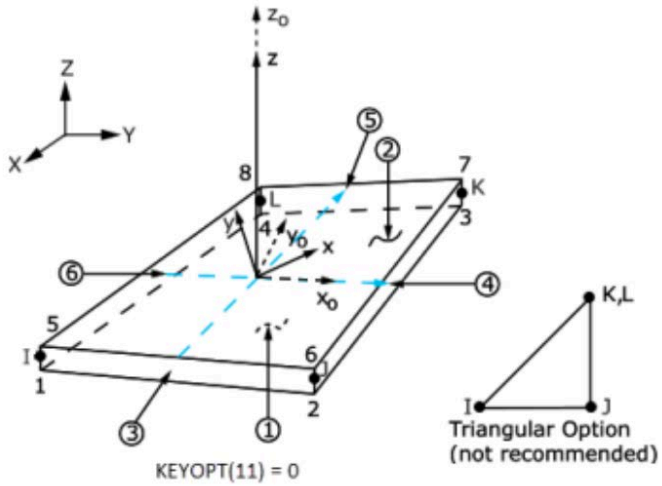

Figure 2-12. SHELL181 Element geometry.
Adopted from (ANSYS Element reference, 2016)

- **LINK180:**

LINK180 is a three-dimensional spar element. This type of element was used for modeling steel reinforcing bars in the concrete slabs. LINK180 has two nodes with three translational degrees of freedom in X, Y and Z directions at each node. Figure 2-13 shows the geometry of LINK180. This element has large deflection, plasticity and large strain capabilities.

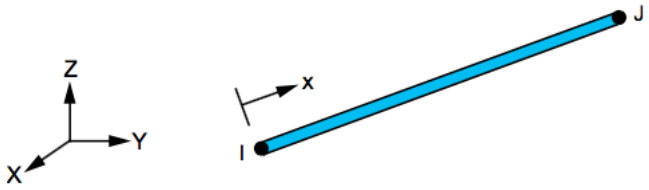

Figure 2-13. LINK180 Element geometry.
Adopted from (ANSYS ADPL Element reference, 2016)

- **TARGE170 and CONTA174:**

To simulate the interaction between the steel girders and concrete slabs, TAGRE170 and CONTA174 as surface to surface contact elements were used. The contact pair model was applied as fully bonded to represent the behavoir of fully composite section. Also, unbonded contact behavior can be used to represent the partial composite behavior.

2.4 Thermal Material Properties

In order to simulate the correct behavior of the material under at various temperatures, high temperature material properties were used for structural steel, concrete and steel reinforcement bars. In following sections, the input material properties for materials is provided.

2.4.1 Structural Steel

The specified structural steel high-temperature material properties in Eurocode3 (EC3, 2005) was applied to develop the finite element models. As it is provided below, thermals conductivity, specific heat and thermal expansion of structural steel are highly dependent on the temperature.

- **Thermal Conductivity**

The thermal conductivity of the structural steel (λ_a) based on the material temperature (θ) was applied as shown in Table 2-2 and Figure 2-14:

Table 2-2. Thermal conductivity of structural steel at various temperatures (Eurocode3)

Temperature Range	Thermal Conductivity (W/mk)	
20˚C < θ < 800˚C	$\lambda_a = 54 - 3.33 \times 10^2\ \theta\ W/mK$	(Eq. 2-6a)
800˚C < θ < 1200˚C	$\lambda_a = 27.3$	(Eq. 2-6b)

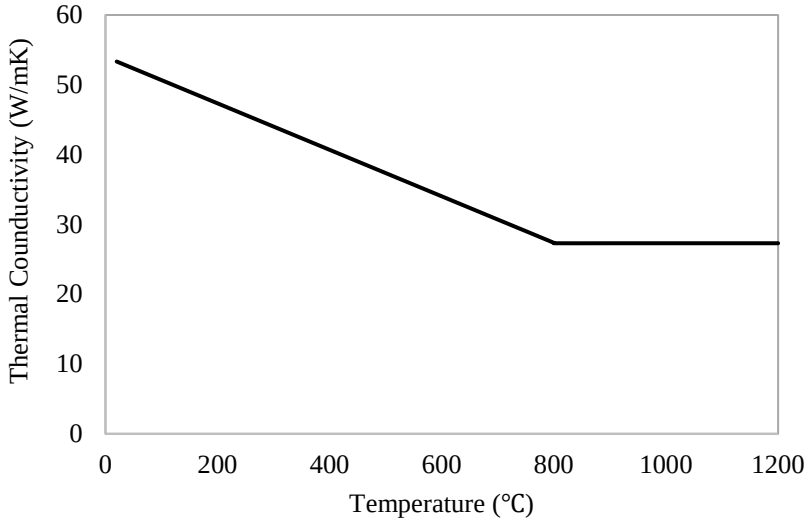

Figure 2-14. Thermal conductivity of structural steel at various temperatures (Eurocode3)

- **Specific Heat**

The specific heat of the structural steel (C_a) based on the material temperature (θ) was applied as shown in Table 2-3 and Figure 2-15:

Table 2-3. Specific heat of structural steel at various temperatures (Eurocode3)

Temperature Range	Specific Heat (J/kgK)	
20˚C < θ < 600˚C	$C_a = 425 + 7.73 \times 10^{-1}\,\theta - 1.96 \times 10^{-3}\,\theta^2 + 2.22 \times 10^{-6}\,\theta^3$	(Eq. 2-7a)
600˚C < θ < 735˚C	$C_a = 666 + 13002\,/(738 - \theta)$ (Eq.8)	(Eq. 2-7b)
735˚C < θ < 900˚C	$C_a = 545 + 17820\,/(\theta - 731)$ (Eq.9)	(Eq. 2-7c)
900˚C < θ < 1200˚C	$C_a = 650$	(Eq. 2-7d)

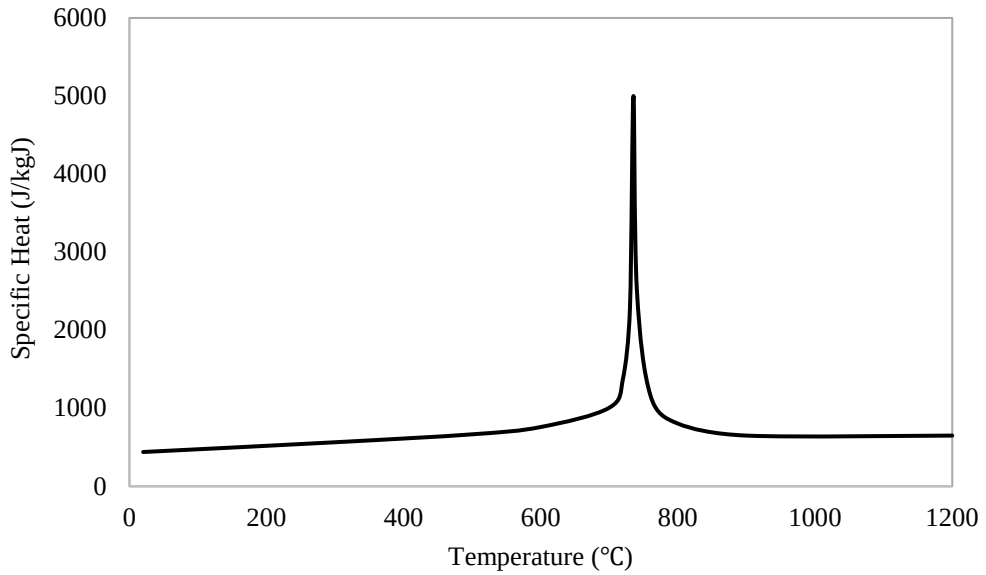

Figure 2-15. Specific heat of structural steel at various temperatures (Eurocode3)

- **Thermal Expansion**

The thermal expansion of the structural steel ($\Delta l/l$) is determined from equations are provided in Table 2-4 and Figure 2-16. θ is the structural steel temperature, l is the length at 20˚C, and Δl is the amount of the thermal expansion.

Table 2-4. Thermal expansion of structural steel at various temperatures (Eurocode3)

Temperature Range	Thermal expansion	
20˚C < θ < 750˚C	$\Delta l/l = 1.2 \times 10^{-5}\,\theta + 0.4 \times 10^{-8}\,\theta^2 - 2.416 \times 10^{-4}$	(Eq. 2-8a)
750˚C < θ < 860˚C	$\Delta l/l = 1.1 \times 10^{-2}$	(Eq. 2-8b)
860˚C < θ < 1200˚C	$\Delta l/l = 2 \times 10^{-5}\theta - 6.2 \times 10^{-3}$	(Eq. 2-8c)

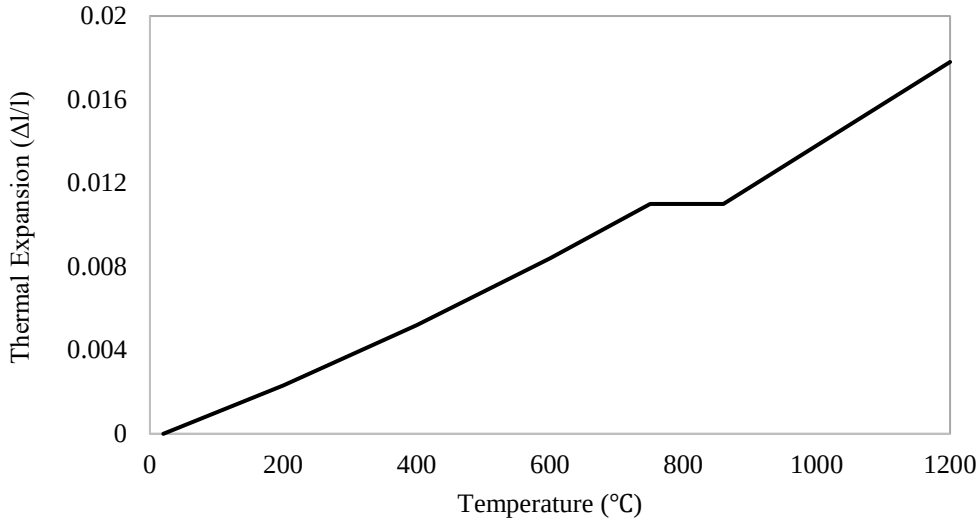

Figure 2-16. Thermal expansion of structural steel at various temperatures (Eurocode3)

2.4.2 Concrete

In the following, sections the input high-temperature thermal material properties of the concrete adopted from Eurocode2 (EC2, 2004) are presented.

- **Thermal conductivity**

The thermal conductivity of concrete (λ_c) based on the material temperature (θ) was applied as shown in Table 2-5 and Figure 2-17. For this study the average between the upper limit and lower limit was utilized.

Table 2-5. Thermal conductivity of concrete at various temperatures (Eurocode2)

Temperature Range	Thermal Conductivity
Upper limit 20˚C < θ < 1200˚C	$\lambda_c = 2 - 0.2451(\theta/100) + 0.0107\,(\theta/100)^2\ W/mK$ (Eq. 2-9a)
Lower limit 20˚C < θ < 1200˚C	$\lambda_c = 1.36 - 0.136(\theta/100) + 0.0057\,(\theta/100)^2\ W/mK$ (Eq. 2-9b)

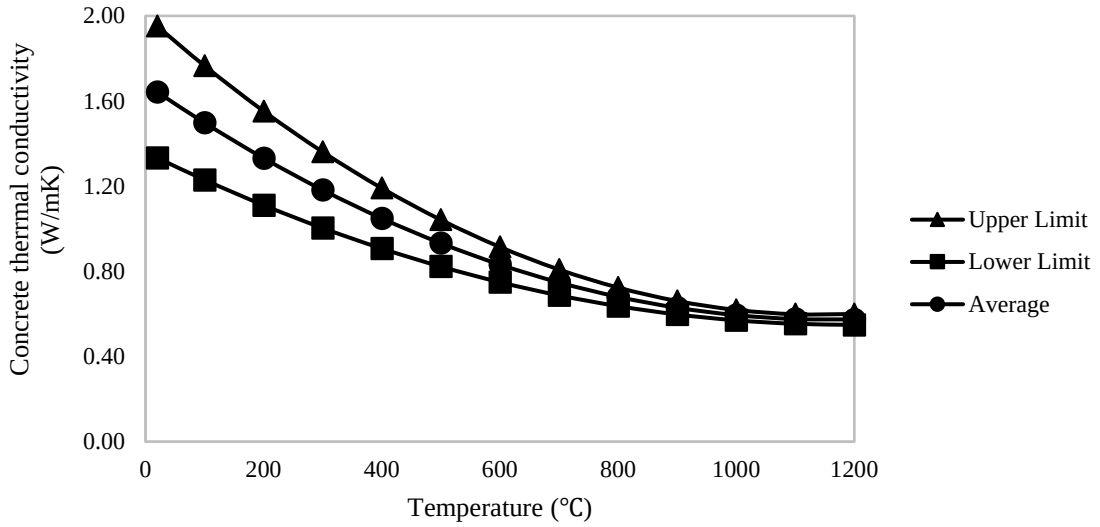

Figure 2-17. Thermal conductivity of concrete at various temperatures (Eurocode2)

- **Thermal Expansion**

The thermal expansion of concrete ($\Delta l/l$) as a function of material temperature (θ) is shown in Table 2-6 and Figure 2-18.

Table 2-6. Thermal expansion of concrete at various temperatures (Eurocode2)

	Temperature Range	Thermal Expansion	
Siliceous aggregate	$20^{\circ}C < \theta < 700^{\circ}C$	$\Delta l/l = -1.8 \times 10^{-4} + 9 \times 10^{-6}\theta + 2.3 \times 10^{-11}\theta^3$	(Eq. 2-10a)
	$700^{\circ}C < \theta < 1200^{\circ}C$	$\Delta l/l = 14 \times 10^{-3}$	(Eq. 2-10b)
Calcareous aggregate	$20^{\circ}C < \theta < 805^{\circ}C$	$\Delta l/l = -1.2 \times 10^{-4} + 6 \times 10^{-6}\theta + 1.4 \times 10^{-11}\theta^3$	(Eq. 2-10c)
	$805^{\circ}C < \theta < 1200^{\circ}C$	$\Delta l/l = 12 \times 10^{-3}$	(Eq. 2-10d)

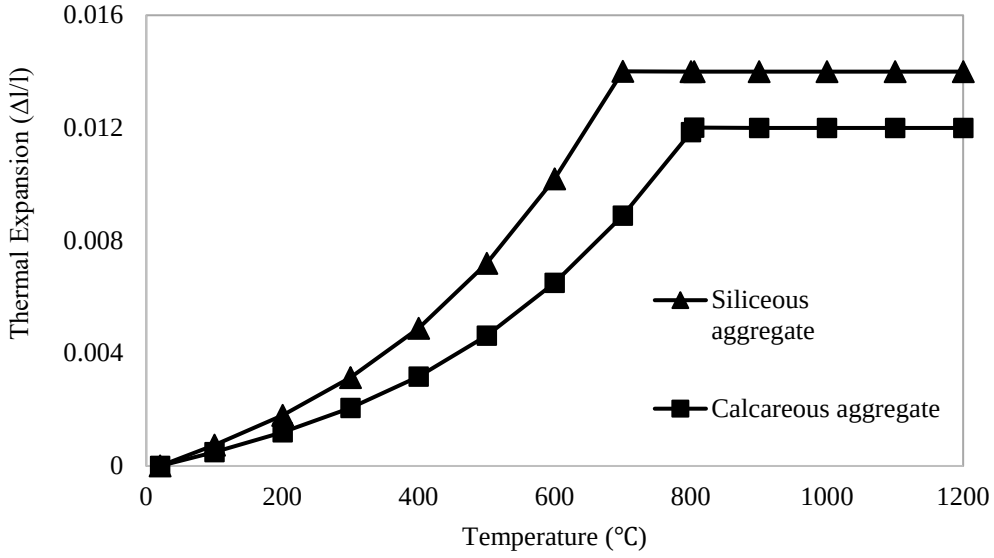

Figure 2-18. Thermal expansion of concrete at various temperatures (Eurocode2)

- **Specific Heat**

The specific heat of the concrete (C_p) based on the material temperature (θ) is shown in Table 2-7 and Figure 2-19. In this study it is assumed that concrete has the moisture of 1.5% of concrete weight.

Table 2-7. Specific heat of concrete at various temperatures (Eurocode2)

Temperature Range	Specific Heat	
20˚C < θ < 100˚C	$C_p = 900$ J/kgK	(Eq. 2-11a)
100˚C < θ < 200˚C	$C_p = 900 + (\theta - 100)$ J/kgK	(Eq. 2-11b)
200˚C < θ < 400˚C	$C_p = 1000 + (\theta - 200)/2$ J/kgK	(Eq. 2-11c)
400˚C < θ < 1200˚C	$C_a = 400$ J/kgK	(Eq. 2-11d)

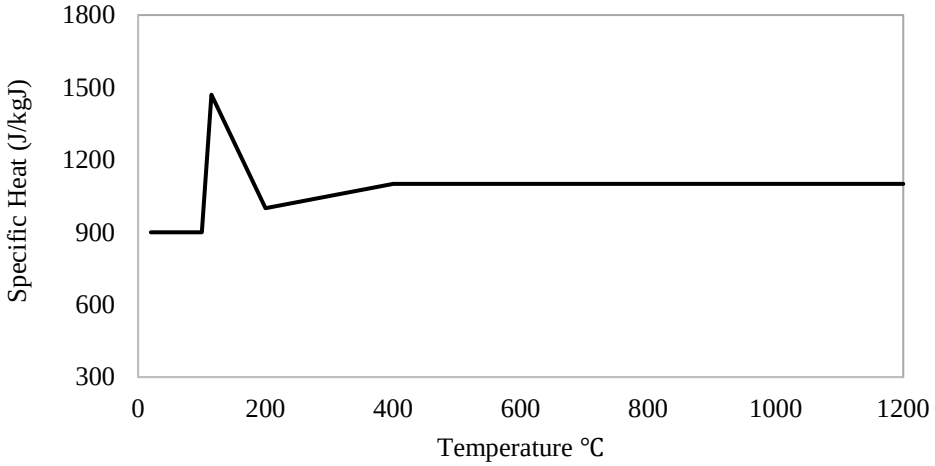

Figure 2-19. Specific heat of concrete at various temperatures (Eurocode2)

2.5 Mechanical Material Properties

In this study, the steel section is the only part that functions as a structural element and supports the load. The concrete is assumed not to have any contribution to the load-carrying capacity. However, for validation purposes to simulate the concrete slab, concrete had a contribution in carrying the load and the overall composite cross-section's capacity. In this section the high-temperature mechanical material properties including, modulus of elasticity, stress-strain curves at elevated temperatures for the structural steel is provided in following sections and adapted from Eurocode3.

2.5.1 Structural Steel Mechanical Properties

- **Unit mass**

To simulate steel material, it was considered that the unit mass of steel is independent of the steel temperature. The unit mass of steel for all analyses is taken as 7850 Kg/m^3.

- **Modulus of elasticity and yield strength**

The modulus of elasticity of the steel at elevated temperatures was calculated according to the reduction factors relative to the material properties at room temperature (20 °C) adopted from the Eurocode3. Modulus of elasticity and yield strength at high temperatures relative to room temperature (20 °C) are shown in Table 2-8 and Figure 2-20.

Table 2-8. Reduction factor of yield strength and modulus of elasticity of steel material relative to 20 °C (Eurocode3)

Steel temperature	Modulus of elasticity	Yield strength
20	1	1
100	1	1
200	0.9	1
300	0.8	1
400	0.7	1
500	0.6	0.78
600	0.31	0.47
700	0.13	0.23
800	0.09	0.11
900	0.0675	0.06
1000	0.045	0.04
1100	0.0225	0.02
1200	0	0

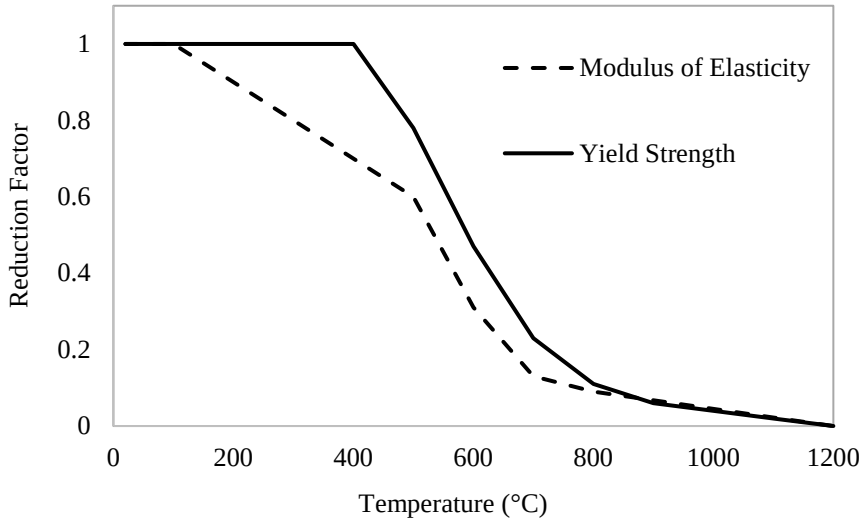

Figure 2-20. Reduction factor of yield strength and modulus of elasticity of steel material relative to 20 °C (Eurocode3)

- **Stress-strain relations at elevated temperatures**

For all steel sections, the stress-strain curves at various temperatures were generated according to the equations provided in Eurocode3, per Table 2-9 and as shown in Figure 2-21.

Table 2-9. Stress- strain relationships for steel material at elevated temperatures (Eurocode3)

Strain Range	Stress	Tangent Modulus
$\varepsilon \le \varepsilon_{p,T}$	$\varepsilon\, E_{a,T}$	$E_{a,T}$
$\varepsilon_{p,T} < \varepsilon < \varepsilon_{y,T}$	$f_{p,T} - c + (\frac{b}{a})\left[a^2 - (\varepsilon_{y,T} - \varepsilon)^2\right]^{0.5}$	$\frac{b(\varepsilon_{y,T} - \varepsilon)}{a\left[a^2 - (\varepsilon_{y,T} - \varepsilon)^2\right]^{0.5}}$
$\varepsilon_{y,T} \le \varepsilon \le \varepsilon_{t,T}$	$f_{y,T}$	0
$\varepsilon_{t,T} < \varepsilon < \varepsilon_{u,T}$	$f_{y,T}\left[1 - \frac{\varepsilon - \varepsilon_{t,T}}{\varepsilon_{u,T} - \varepsilon_{t,T}}\right]$	0
$\varepsilon = \varepsilon_{u,T}$	0	0

Where:

$$\varepsilon_{p,T} = \frac{f_{p,T}}{E_{a,T}} \qquad \varepsilon_{y,T} = 0.02 \qquad \varepsilon_{t,T} = 0.15 \qquad \varepsilon_{u,T} = 0.2$$

$$a^2 = (\varepsilon_{y,T} - \varepsilon_{p,T})(\varepsilon_{y,T} - \varepsilon_{p,T} + \frac{c}{E_{a,T}})$$

$$b^2 = c(\varepsilon_{y,T} - \varepsilon_{p,T})E_{a,T} + c^2$$

$$c = \frac{(f_{y,T} - f_{p,T})^2}{(\varepsilon_{y,T} - \varepsilon_{p,T})E_{a,T} - 2(f_{y,T} - f_{p,T})}$$

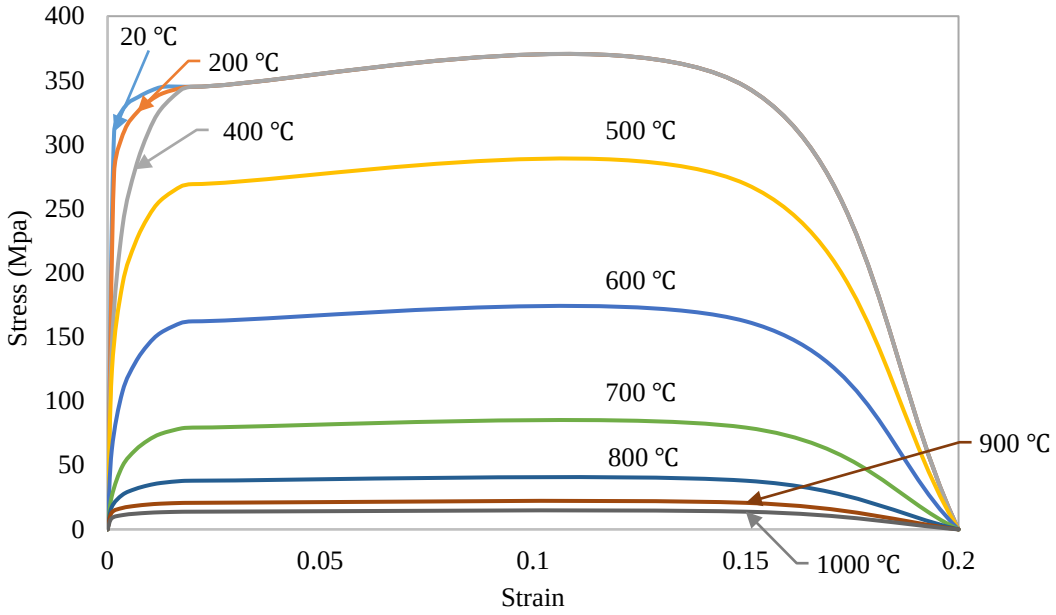

Figure 2-21. Stress- strain curves for steel material at elevated temperatures (Eurocode3)

2.5.2 Concrete Mechanical Properties

- **Unit mass**

It was assumed that the unit mass (density) of the concrete was 2300 kg/m^3. However, due to the water loss at high temperatures, concrete loses its moisture and affects the density of the concrete at high temperatures. The variation of the unit mass of the concrete is determined from Table 2-10. Figure 2-22 shows the variation of concrete unit mass at higher temperatures.

Table 2-10. The variation of concrete unit mass at high temperatures (Eurocode2)

Temperature Range	Unit Mass	
20˚C < θ < 150˚C	$\rho_\theta = \rho_{20}$	(Eq. 2-12a)
115˚C < θ < 200˚C	$\rho_\theta = \rho_{20}(1 - \frac{0.02(\theta - 115)}{85})$	(Eq. 2-12b)
200˚C < θ < 400˚C	$\rho_\theta = \rho_{20}(0.98 - \frac{0.03(\theta - 200)}{200})$	(Eq. 2-12c)
400˚C < θ < 1200˚C	$\rho_\theta = \rho_{20}(0.95 - \frac{0.07(\theta - 400)}{800})$	(Eq. 2-12d)

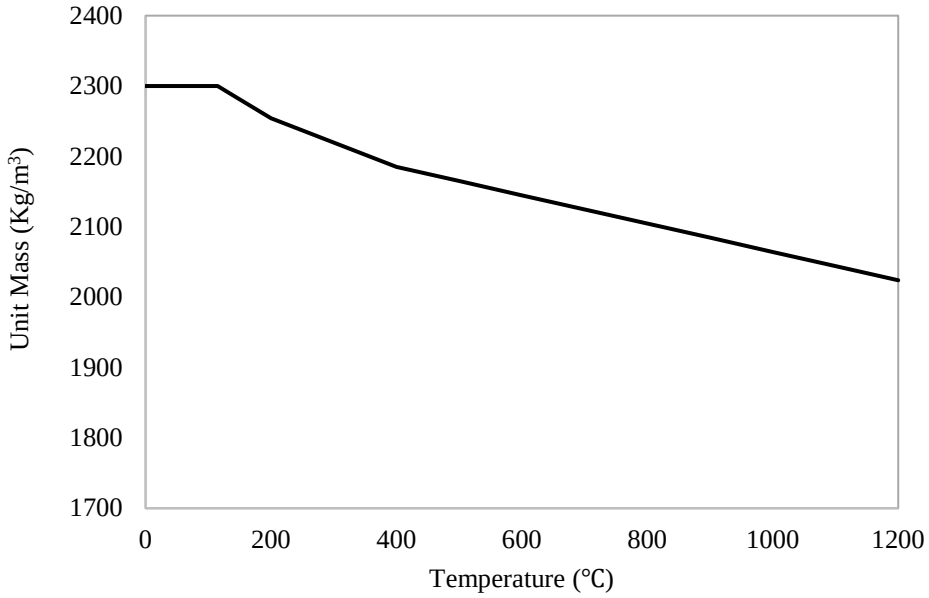

Figure 2-22. The variation of concrete unit mass at high temperatures (Eurocode2)

- **Yield strength and modulus of elasticity**

The average (arithmetic mean) of the reduction factors of two different types of concrete material provided in Eurocode2 were used to determine the yield strength of the concrete at elevated temperatures. Table 2-11 shows the reduction factor of compressive strength of concrete at elevated temperatures. Figure 2-23 shows the reduction of concrete compression strength at elevated temperatures and the average reduction factor is applied in analysis. The modulus of elasticity of concrete at elevated temperatures was defined using the following equation:

$$E = 4700\sqrt{f'_c} \qquad \text{(Eq. 2-13)}$$

Table 2-11. Reduction factors of material properties of concrete at elevated temperatures (Eurocode2)

Concrete temperature	Siliceous aggregate			Calcareous aggregate		
	$f'_{c,\theta}/f'_c$	$\varepsilon_{c,t}$	$\varepsilon_{cu,t}$	$f'_{c,\theta}/f'_c$	$\varepsilon_{c,t}$	$\varepsilon_{cu,t}$
20	1	0.0025	0.02	1	0.0025	0.02
100	1	0.004	0.0225	1	0.004	0.0225
200	0.95	0.0055	0.025	0.97	0.0055	0.025
300	0.85	0.007	0.0275	0.91	0.007	0.0275
400	0.75	0.01	0.03	0.85	0.01	0.03
500	0.6	0.015	0.0325	0.74	0.015	0.0325
600	0.45	0.025	0.035	0.6	0.025	0.035
700	0.3	0.025	0.0375	0.43	0.025	0.0375
800	0.15	0.025	0.04	0.27	0.025	0.04
900	0.08	0.025	0.0425	0.15	0.025	0.0425
1000	0.04	0.025	0.045	0.06	0.025	0.045
1100	0.01	0.025	0.0475	0.02	0.025	0.0475
1200	0	-	-	0	-	-

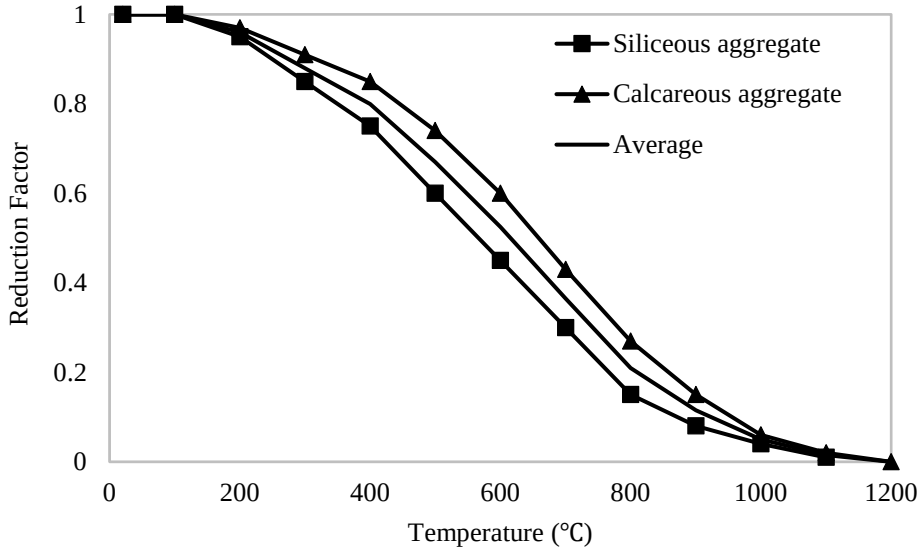

Figure 2-23. Reduction of concrete compressive strength at elevated temperatures (Eurocode2)

- **Stress- strain relations at elevated temperatures**

Drucker-Prager Concrete Model in ANSYS 17.1 was utilized to simulate the concrete. Concrete material properties at elevated temperatures as they are illustrated in Table 2-11 were used to input the Drucker-Prager Concrete Model constants. Figure 2-24 shows applied the Drucker- Prager concrete model. The parameters were determined from Eurocode2 and literature (Cheng et al., 2006).

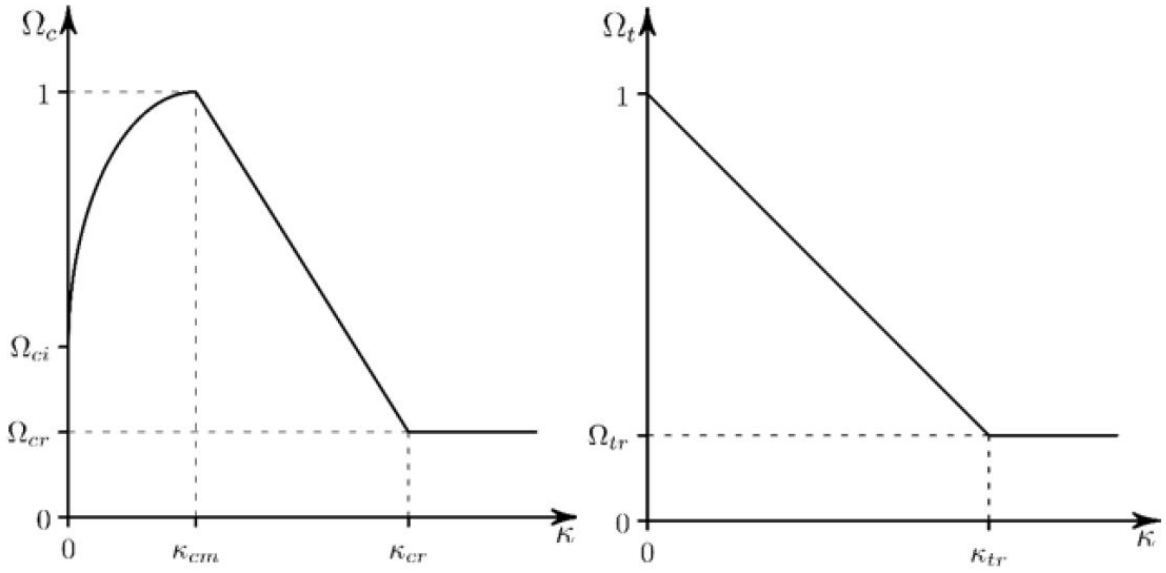

a. Compression **b. Tension**

Figure 2-24. Drucker-Prager concrete model.
Adopted from (ANSYS Material reference, 2016)

CHAPTER 3.MODEL VALIDATION

3.1 General

The finite element models were validated according to the results obtained from experiments performed by (Aziz et al. 2015). The validation process was done for both thermal and structural analysis of a steel bridge girder with a span of 3658 mm. As it is shown in Figure 3-1, the bridge steel girder included a W24x62 steel beam and a concrete slab with a 140 mm thickness on top of it. The temperature of the furnace was controlled to follow the ASTM E119 time-temperature curve. In Figure 3-2 cross section and the finite element model of the bridge steel girder are shown.

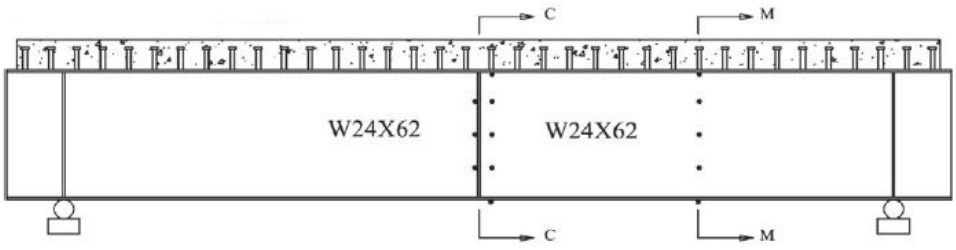

Figure 3-1. Schematic elevation of Steel bridge girder. Adopted form (Aziz et al., 2015)

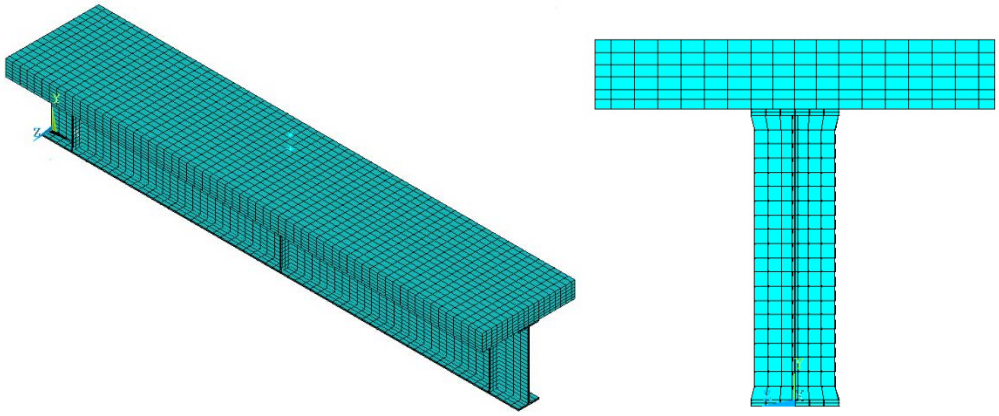

Figure 3-2. 3D discretization of steel bridge girder

Thermal analysis validation includes comparing the temperature of the various parts of the cross section. Mid-span and out of plane deflection of the finite element model was validated according to the experimental results. The concrete of the slab had a compressive strength of about 66 MPa and tensile strength of 3.5 MPa. The modulus of elasticity and yield strength of the steel material were determined according to the three coupon test results (Aziz et al. 2015). The modulus elasticity of the steel used is 240,000 MPa and yield strength of 480 MPa was used at room temperature. The room temperature material properties were used to create the stress-strain relationships for steel and concrete at elevated temperatures. The stress-strain relationships, modulus of elasticity, thermal expansion, thermal conduction and specific heat of the steel and concrete material at elevated temperatures, were calculated according to Eurocode2 and Eurocode3 respectively. More detailed information about the geometry and the loading condition

of the bridge steel girder are shown in Table 3-1. The load was applied at the mid-span of the girder as a point load.

Table 3-1. Steel bridge girder dimensions and loading condition

Geometry	Span	3658 mm	Stiffeners	Mid- span (w× t_{stf})	76.2 × 12.7 mm
	Total Length	4167 mm		Supports (w× t_{stf})	76.2 × 9.5 mm
	Flange Plate ($b_f \times t_f$)	177.8 × 12.7 mm	Capacity	Flexure	1569 KN.m
	Web Plate ($D \times t_w$)	577.9 × 11.1 mm		Shear capacity	1278 KN
	Concrete Slab ($b_{eff} \times t_s$)	813 × 140 mm	Loading	Applied load	691 KN
	End Panel width (S)	254 mm		Applied load/ flexural capacity	40%
Fire	Fire Exposure	ASTM E119		Applied load/ shear capacity	27%

3.2 Thermal Analysis Validation

To validate the finite element thermal analysis, the temperatures at bottom flange, web, top flange and middle of the concrete slab were traced during fire exposure and compared with experimental results. Figure 3-3 shows the comparison of the results for the thermal finite element analysis and measured temperature during the tests. The temperature of the bottom flange and mid-height of the web increased rapidly due to the direct exposure to fire. Due to the heat sink effect of the concrete slab, the rate of temperature increment in the top flange is less than the bottom flange and the web. The temperature measured at the mid-thickness of the slab was low. The lower heat conduction capacity of the concrete compared to the steel is the main reason that the temperature at the mid-thickness of the slab was below 150℃ throughout the test and thermal finite

element analysis. The small errors and mismatches of the measured and finite element thermal responses are due to the differences in the radiation and convection coefficients in compare with the real values. Overall, the comparison between the thermal experimental results and thermal responses of finite element analysis shows good correlation.

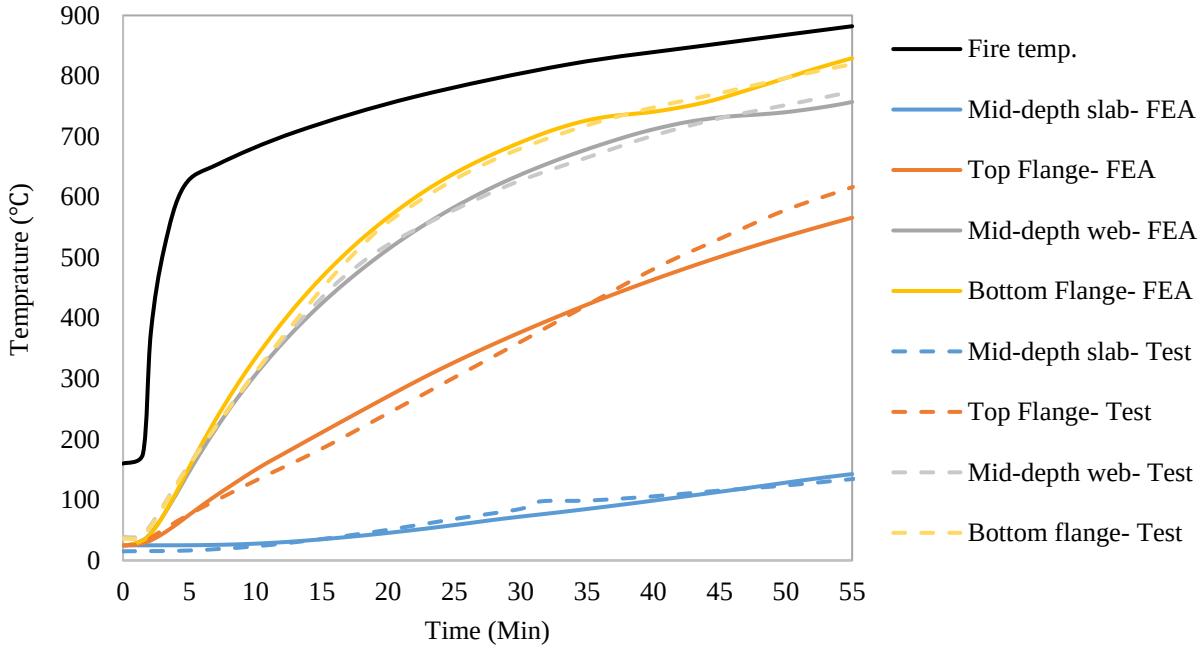

Figure 3-3. Comparison of measured temperature and thermal analysis results

3.3 Structural Analysis Validation

To validate the structural finite element models, the mid-span and the out of plane displacement of the structural model were compared to the measured displacements. The reduction in the modulus of elasticity of the steel material at higher temperature is the main reason for the increase in the mid-span deflection. The mid-span deflection of the girder starts after about 3 minutes as the temperature of the bottom flange and the web reaches 100℃. According to Eurocode3, the degradation of the modulus of elasticity of steel starts after 100℃. Also, when the

temperature of most parts of the section exceeded 400℃, the rate of the mid-span deflection increment slightly increased. The temperature of the bottom flange exceeded 600℃ at about 23 minutes. At this point, mid-span deflection increased with a higher rate. Eventually, at about 39 minutes, the girder failed due to loss of strength at high temperatures. In Figure 3-4 the steel bridge girder in the test and structural analysis at failure time are illustrated.

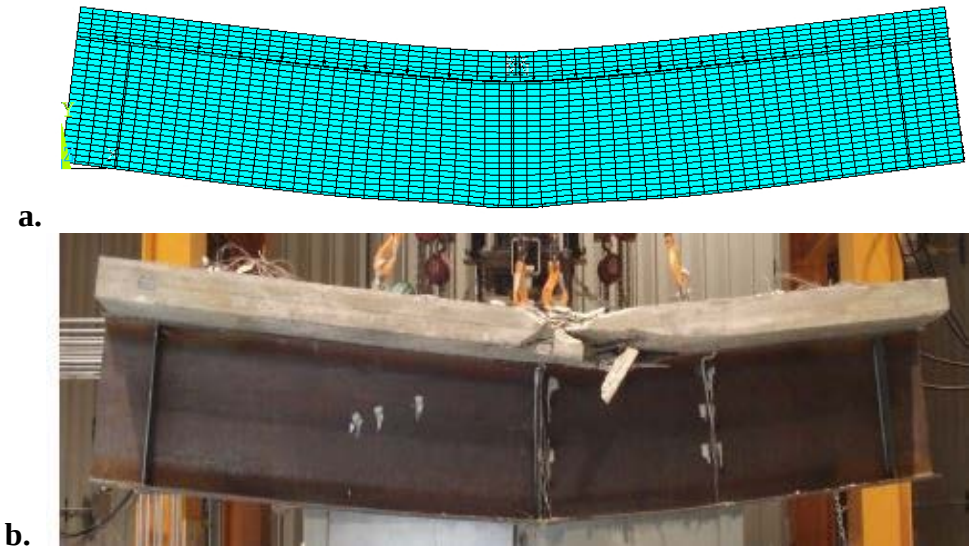

Figure 3-4. Steel bridge girder at failure time a. Structural analysis b. Experimental test. Adopted from (Aziz et al., 2015)

The girder did not experience any buckling or out of plane displacement in the web or lateral torsional buckling during the test and the finite element analysis. Plotted curves in figure 3-5 show a good agreement between the measured mid-span deflection resulted from the test and the results of the developed structural finite element model.

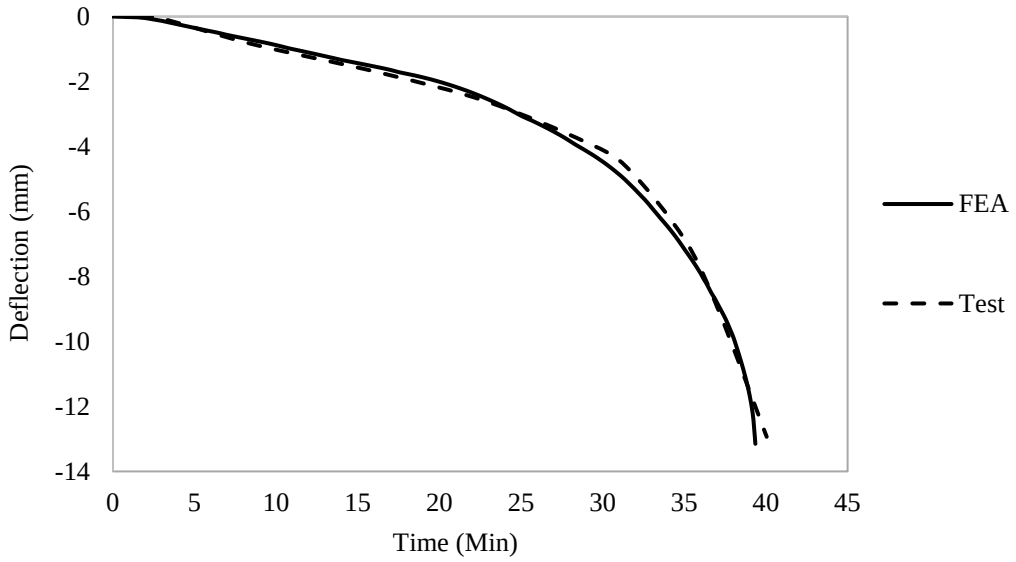

Figure 3-5. Comparison of mid-span deflection in structural analysis and experiment

In Figure 3-6 the placement of the steel girder at the furnace is shown. Also in Figure 3-7 a schematic LVDT set-up to measure the displacements is shown.

Figure 3-6. Steel girder placement in the furnace. Adopted from (Aziz et al., 2015)

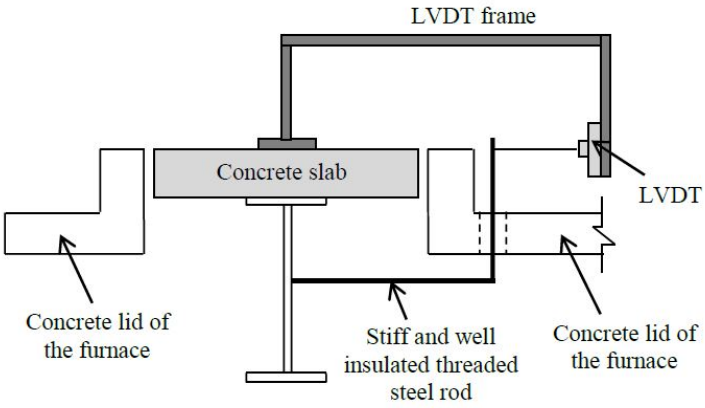

Figure 3-7. LVDT set-up to measure mid-span deflection and out-of-plane displacement. Adopted from (Aziz et al., 2015)

CHAPTER 4. DAMAGED FIREPROOFING

4.1 General

In this chapter, the fire resistance of the beams with damaged fire protection will be estimated by using finite element analysis method. The results of fire tests to investigate the effect of partial loss of the fire protection are more realistic; however, performing fire tests in laboratories needs appropriate facilities, expensive and time-consuming. Therefore, to investigate the effect of partial loss of concrete as a fire protection material, a parametric study was carried out. Finite element models were created by ANSYS as it is described in Chapter two. The validation process of the finite element models is described in Chapter three of this thesis. To achieve the goal of this study more than 278 finite element models were created in ANSYS. For each case, thermal and structural finite element analysis were conducted. A group of beams with varying damage parameters such as fire protection loss areas and penetration were studied to determine the influence of partial loss of the fire protection and, compared to fully protected beams with same size and fireproofing. All studied cases were exposed to ASTM E119 standard fire temperature

from three sides. To account for the effect of the slabs or floors, room temperature was assumed for the top side of the beams. The temperature dependent material properties of the steel and concrete were applied as recommended by Eurocode2 and Eurocode3. The material properties of steel and concrete at elevated temperatures are presented in Chapter two. Strength and deflection failure limit states were investigated to determine the fire resistance of each studied case. The temperature of parts of the steel cross sections and the mid-span deflection of the studied cases are illustrated in the results section.

4.2 Steel Beam's geometries

Eight steel beam sections commonly used in practice were selected in this study to understand the behavior of the various beam sections with fire protection loss. The span for each steel beam varies. In Table 4-1 the properties of selected beam sections and the assigned span length are presented.

Table 4-1. The properties of the selected steel cross sections

Section Size	Span	Area	Depth	Web Thickness	Flanges		Plastic Modulus	
					Width	Thickness		
		A	d	t_w	b_f	t_f	Z_x	Z_y
in×lbs/ft	m	cm^2	cm	cm	cm	cm	cm^3	cm^3
W 12 × 22	4.27	41.81	31.27	0.66	10.24	1.08	480.14	59.98
W 12 × 50	4.27	94.84	30.96	0.94	20.52	1.63	1178.23	349.04
W 14 × 30	4.88	57.10	35.15	0.69	17.09	0.98	775.11	147.32
W 14 × 74	4.88	140.64	35.99	1.14	25.58	1.99	2064.77	663.68
W 18 × 40	8.23	76.13	45.47	0.80	15.28	1.33	1284.75	163.87
W 18 × 86	8.23	163.23	46.71	1.22	28.17	1.96	3047.99	793.13
W 21 × 44	9.75	83.87	52.58	0.89	16.51	1.14	1563.33	167.15
W 21 × 93	9.75	176.13	54.91	1.47	21.39	2.36	3621.54	568.63

4.3 Types of the Fire Protection Damage

In this study, two types of fire protection damages were examined to scrutinize the fire protection damage effect on the fire resistance of the beams. For both damage types, the fire protection loss's location is in the middle of the span. The damage area was equal to 5 inches by the width of the beam. However, the penetration of the fire protection damage varies. In the second type of the fire protection damage, the length of damaged area was equal to a range of a certain amount of the percentage of the beam's span by the total width of the beams. Figure 4-1 shows sketches of the beams with full fire protection damaged fireproofed sections.

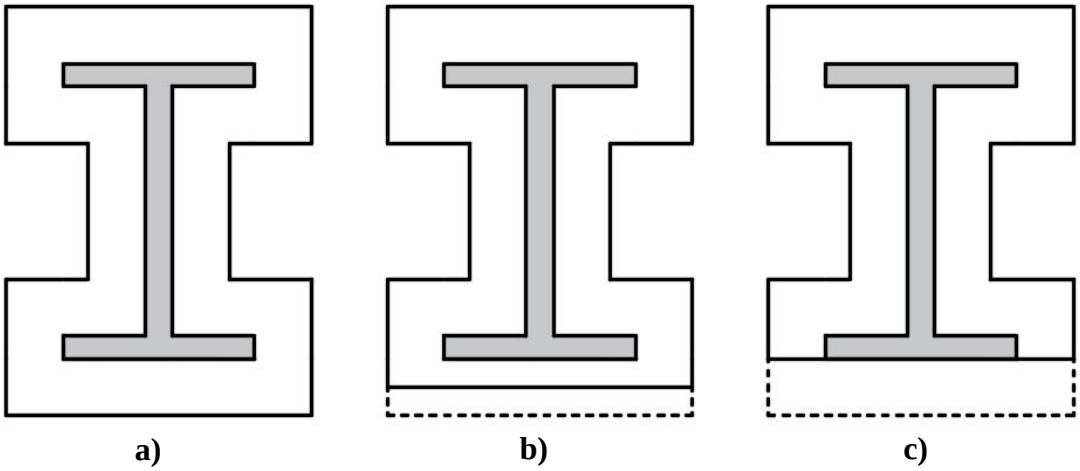

Figure 4-1. a) Fully fireproofed beam (without any fire protection damage
b) Damaged fire protection with half of thickness of fire protection
c) Fully damaged fire protection

4.4 Loading

To investigate the effect of the load level on the fire resistance of each studied case, different load levels were applied in this parametric study. The load level of the studied cases in this study is related to the bending capacity of the beams. The load was applied to produce the existing stress within the cross section prior the fire exposure. A uniform load equal to the self-weight of the steel beam's cross-section and the concrete fireproofing that covered the steel beam was applied to the beams. Two concentrated loads at one-third of the span from both ends of the beams were applied. The total induced bending moment at the middle of the beam length was equal to 50%, 70% and 90% of the maximum bending moment of the cross sections. The loads were applied at first time step, and they were kept constant during the fire exposure. All studied cases were assumed to have continuous lateral bracing. The moment bending capacity of the steel cross-section was calculated according to the provided plastic modulus in AISC 360-10 (AISC 2010), as they are presented in Table 4-1.

$$\text{Load level} = \frac{M_{applied}}{M_{capacity}} \times 100\% \qquad \text{(Eq. 4-1)}$$

4.5 Failure Criteria

In order to evaluate the fire resistance of the each studied case, flexural, shear and deflection limit states have been investigated. The fire resistance is determined as the time when at least one of the limits mentioned above states is exceeded. The strength of the material degrades at elevated temperature. The ultimate stress of the defined steel material properties starts to decay after the strain exceeds 0.15 until it reaches zero at 0.2 strain. When the strain exceeds 0.15 the ultimate stress at the critical section, the member cannot support the load, and the finite element equations do not converge.

The other structural failure limit is associated with the maximum deflection at the mid-span of the beams. ASTM E119 has defined the maximum total and deflection at mid-span of the beams to determine beams fire resistance rating. The failure limit considered when the deflection limit states exceed the limits presented in Eq. 2-4 and Eq. 2-5, where L is the clear span of the beam and d is the distance between the extreme fibers of the beam in compression and the tensile.

4.6 Parametric studies results

A total of 278 thermal and structural finite element analyses were performed to investigate the influence of different factors on the fire resistance of the members. Thermal analysis results are illustrated as the temperature of the various parts of the steel beams' temperature during the fire exposure time. Structural analysis results are presented as the mid-span deflection of the beams as a function of time.

4.6.1 The Effect of Damage Penetration

The material properties of steel are temperature-dependent. Hence, the thermal analysis is an important part of evaluating the response of structural members. Figures 4-2 to 4-9 show the temperature of the different parts of the steel beams as a function of time.

The legend of the figures is defined in three parts. The first part represents the size of the beam. The second part of the name of each curve defines the part of the beam where the temperature is measured. “TF”, “W”, and “BF” represent the temperature of the top flange, mid-depth of the web and bottom flange at the beam mid-span. The third part the name of curves in the legend of the figures shows the penetration of the damage in the fire protection at the mid-span. “ND”, “t”, “0.5t” correspond to the beams with No Damage, full thickness damage and half-thickness damage of the fire protection material, respectively. As an example W12×22- BF- ND shows the temperature of the bottom flange of fully fireproofed W12×22 at mid-span.

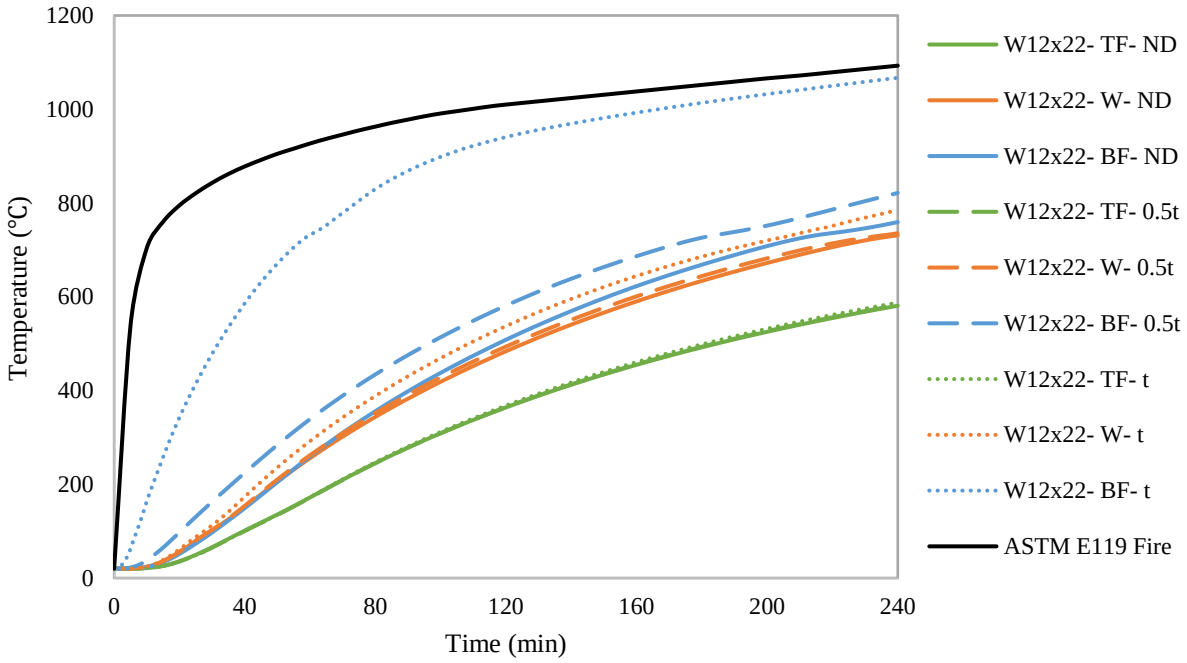

Figure 4-2 Temperature of various parts of W12×22 with full and half damage penetration and fully fireproofed during the fire exposure

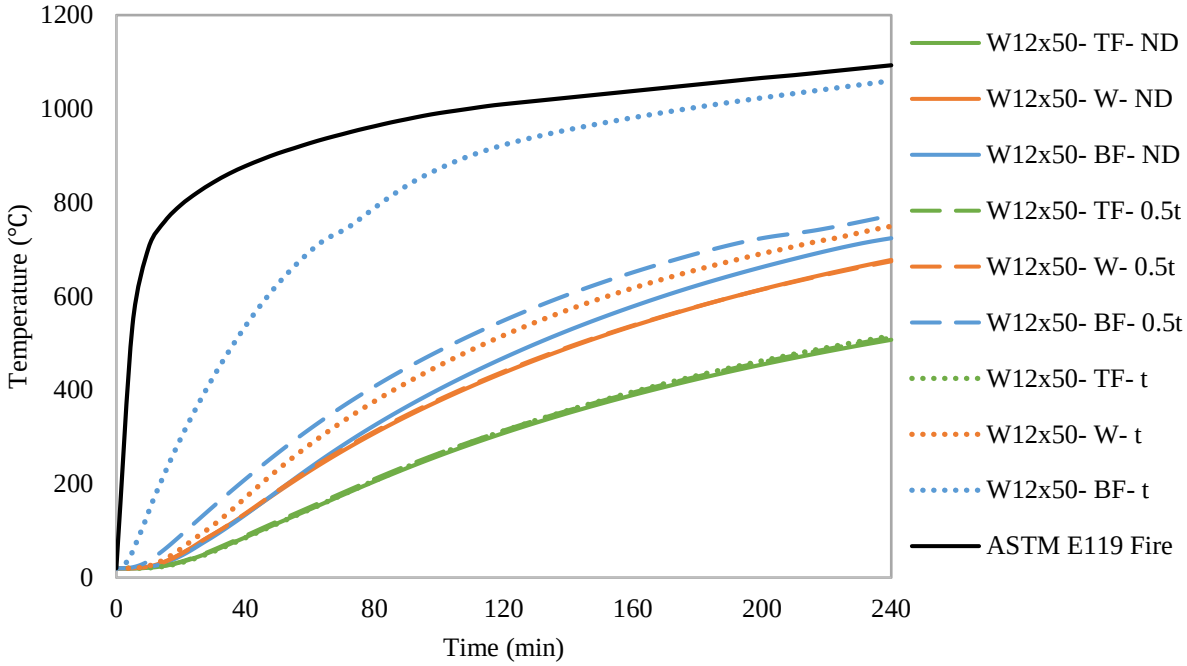

Figure 4-3. Temperature of various parts of W12×22 with full and half damage penetration and fully fireproofed during the fire exposure

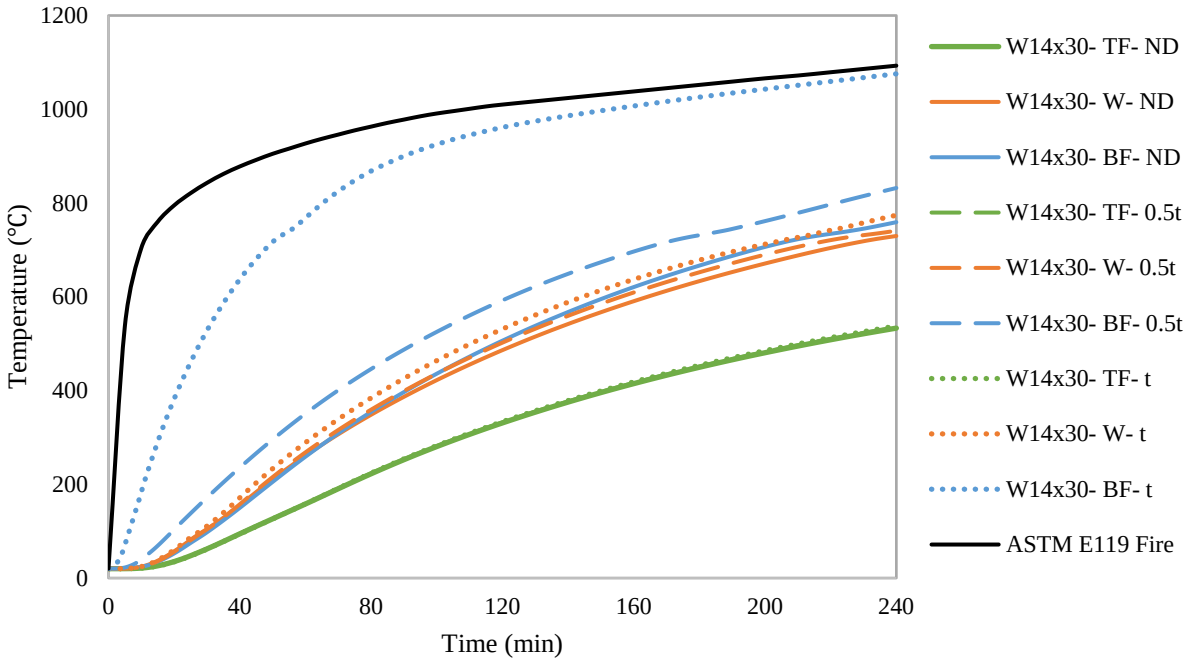

Figure 4-4. Temperature of various parts of W14×30 with full and half damage penetration and fully fireproofed during the fire exposure

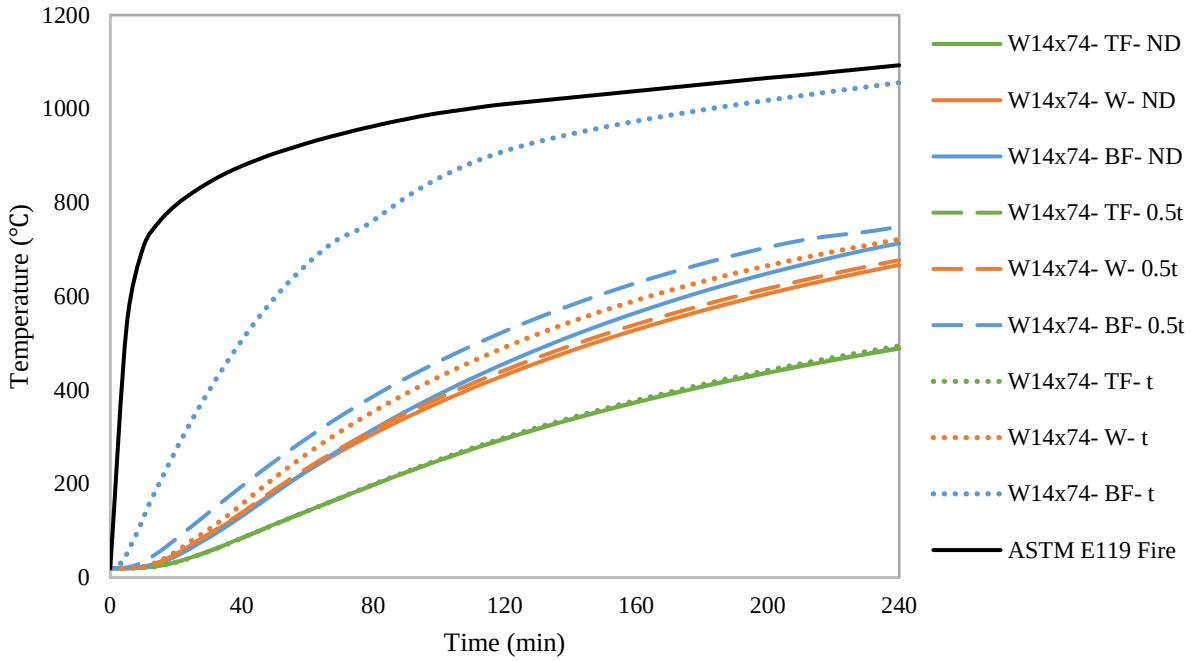

Figure 4-5. Temperature of various parts of W14×74 with full and half damage penetration and fully fireproofed during the fire exposure

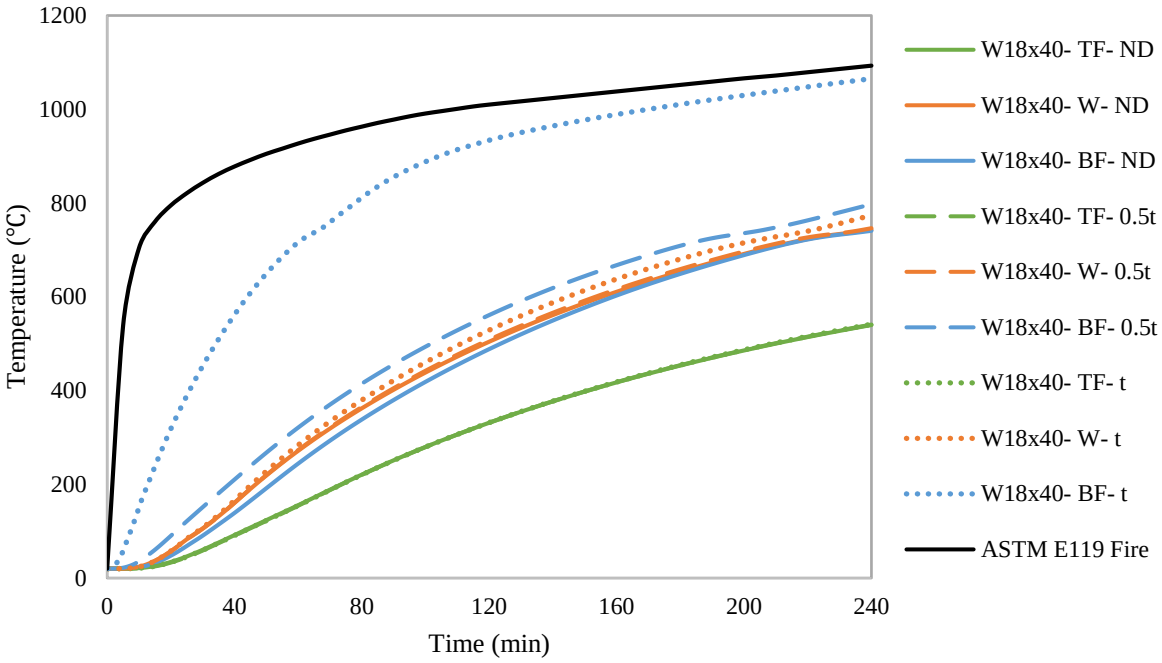

Figure 4-6. Temperature of various parts of W18×40 with full and half damage penetration and fully fireproofed during the fire exposure

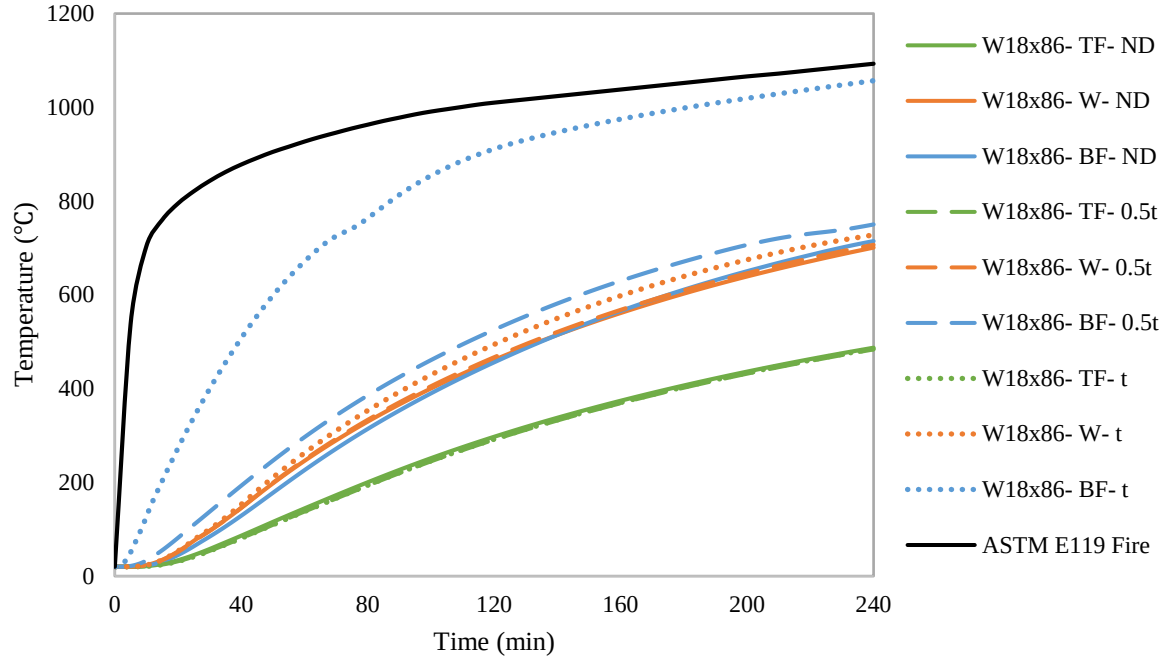

Figure 4-7. Temperature of various parts of W18×86 with full and half damage penetration and fully fireproofed during the fire exposure

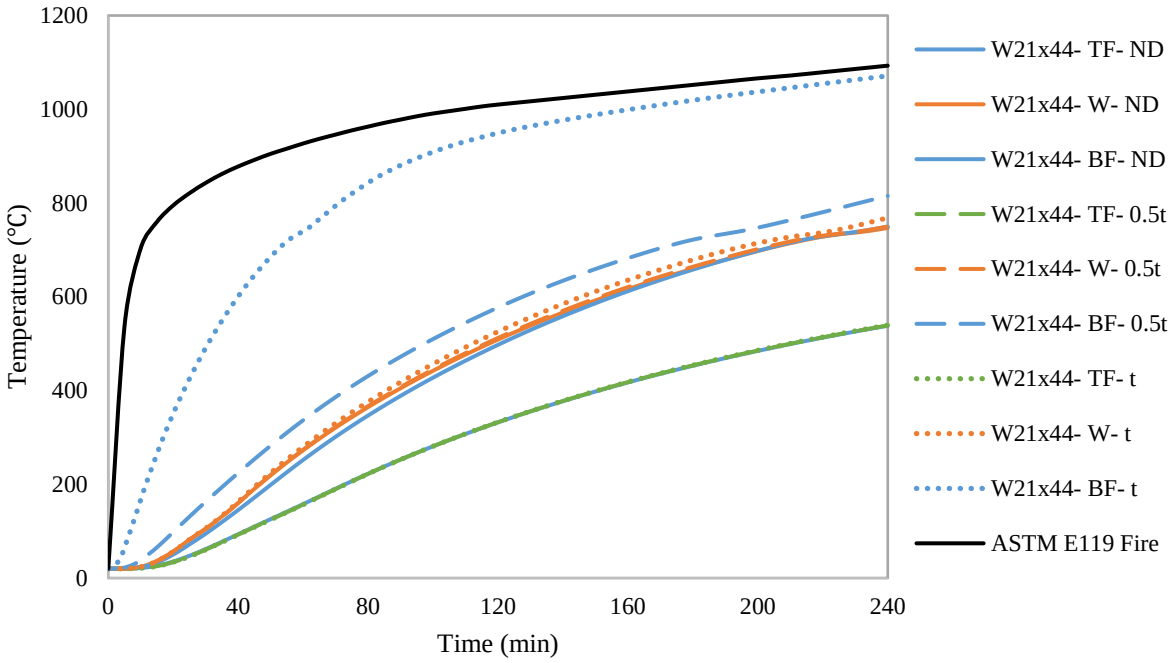

Figure 4-8. Temperature of various parts of W21×44 with full and half damage penetration and fully fireproofed during the fire exposure

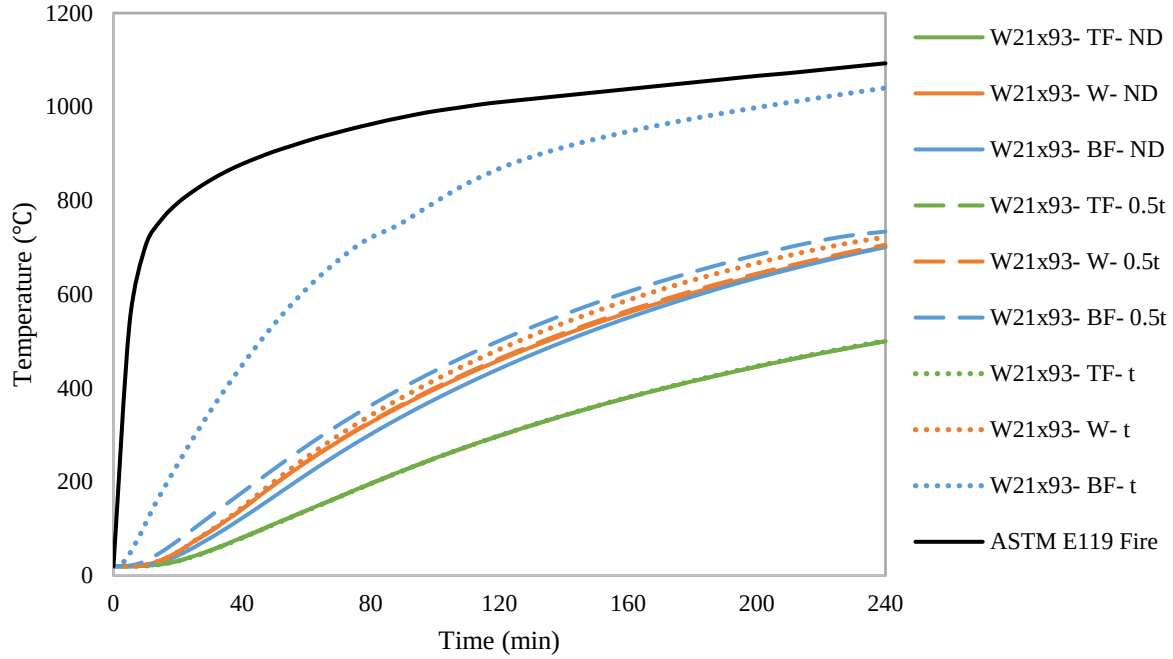

Figure 4-9. Temperature of various parts of W21×93 with full and half damage penetration and fully fireproofed during the fire exposure

The bottom flange and web's temperature rise rate decreases at about 700°C. The sudden rise in the specific heat of the steel material leads to the reduction in the pace of the temperature increase at about 700°C up to 760°C. At this range of temperature due to the phase change of steel material; it absorbs a high amount of heat.

The damage penetration has a minor effect on the temperature of the bottom flanges of the beams' section. But for models with full thickness damage, the bottom flange's temperature increases significantly. As expected, the increase of the bottom flange's temperature of the cases with fully damaged (t) fire protection is more than the cases with half-thickness damage penetration (0.5t). However, the difference between the bottom flanges' temperature of the fully fireproofed members and fully damaged members is more than the difference between the members with 0.5t damage and fully fireproofed members'. As an example, at the end of fire analysis, the bottom flange's temperature of W12x50 with full thickness damaged is about 336 °C more than the bottom flange of the fully fireproofed beam. However, the bottom flange's temperature of W12x50 with full thickness damaged is about 48°C more than the bottom flange of the fully fireproofed beam.

The remaining fire protection material in models with half of the specified fire protection's thickness, prohibits the direct exposure of the steel section to fire. In this case, the remaining thin layer of concrete prevents the heat transfer from fire to steel section through radiation. This results in a lower rate of temperature rise at damaged regions compare to the cases with fully damaged fire protection and eventually leads to lower section's temperature compare to the temperature of fully damaged beams.

The temperature at the top flanges of studied cases with different damage penetration and fully protected members are similar during the fire exposure; therefore, the damaged fire protection part at the bottom flange does not affect the temperature rise at the top flange. The similar temperature rise during the fire exposure is associated with the existing concrete at the top of the top flanges with room temperature at the other side which causes the dissipation of heat.

Furthermore, the deeper the steel beam section the lower the temperature in the web of fully protected members due to longer heat transfer path. However, the web temperature of the fully protected members and members with 0.5t damage are almost same during the fire exposure. The web temperature of members with 0.5t damage is slightly higher than the web temperature of the fully fireproofed members. Also, the web temperature of the members with deeper sections is slightly lower than the web temperature of shallower members. Furthermore, the web temperature of the heavier sections with fully damaged fire protection is more than that of lighter sections. This is attributed to the wider flange of the heavier sections that would result in higher exposure area to the fire.

Figures 4-10 to 4-13 illustrate the temperature of the various parts of the sections with similar section's depth. Higher heat capacity observed for the heavier sections and, this is due to the thicker web and flanges which results in lower temperature increase rate at the different parts of the section during the fire exposure. Moreover, the temperature of the bottom flanges of lighter and heavier sections become closer to each other at later stages of fire exposure. However, the temperature of the lighter sections' web and top flanges increases at a higher rate during fire exposure. The direct exposure of the bottom flanges to fire due to the partial loss of fire protection is the main reason for the higher temperature at the bottom flange than other parts of the section.

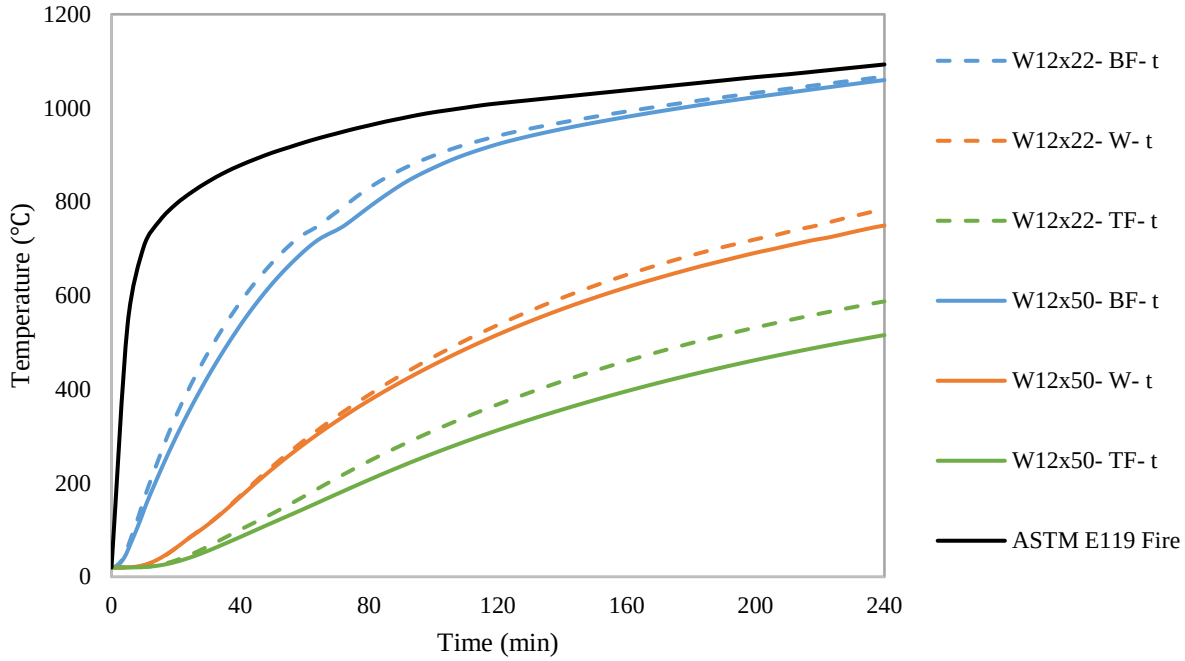

Figure 4-10. Comparison of the temperature of different parts of W12×22 and W12×50 with full damage penetration during the fire exposure

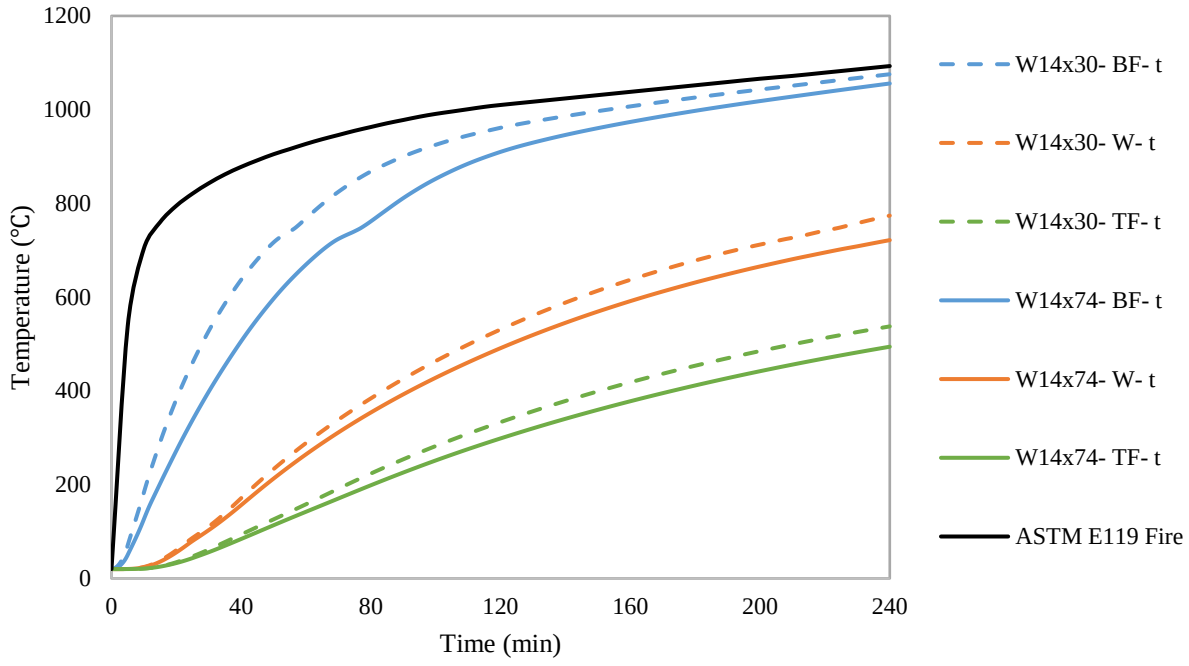

Figure 4-11. Comparison of the temperature of different parts of W14×30 and W14×74 with full damage penetration during the fire exposure

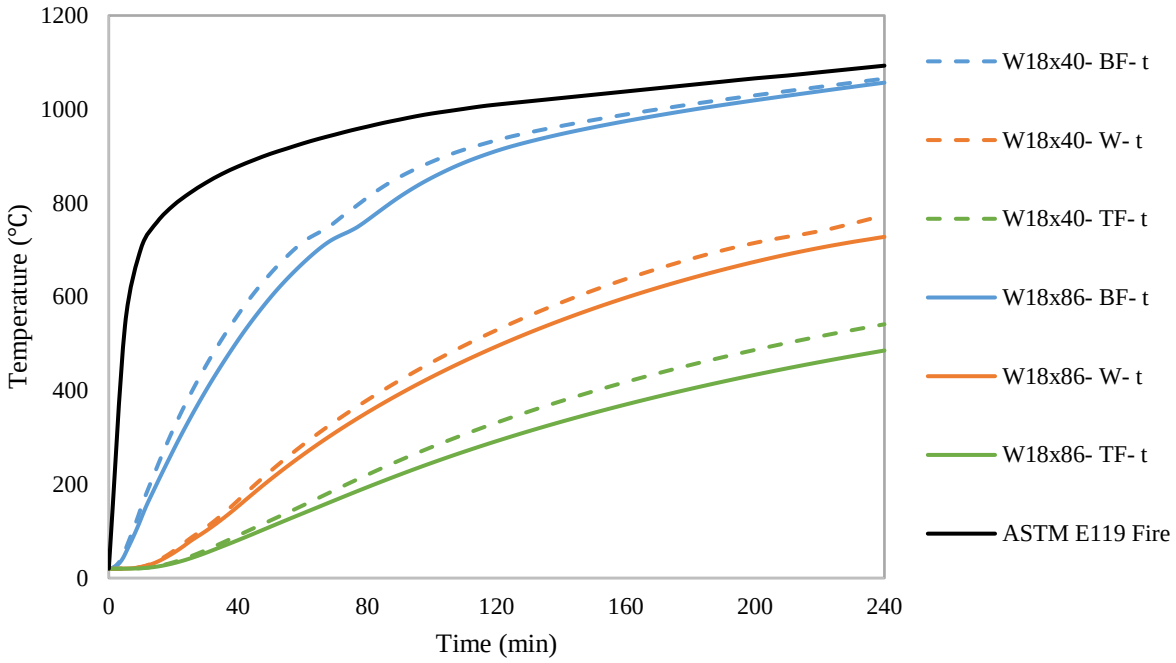

Figure 4-12. Comparison of the temperature of different parts of W18×40 and W18×86 with full damage penetration during the fire exposure

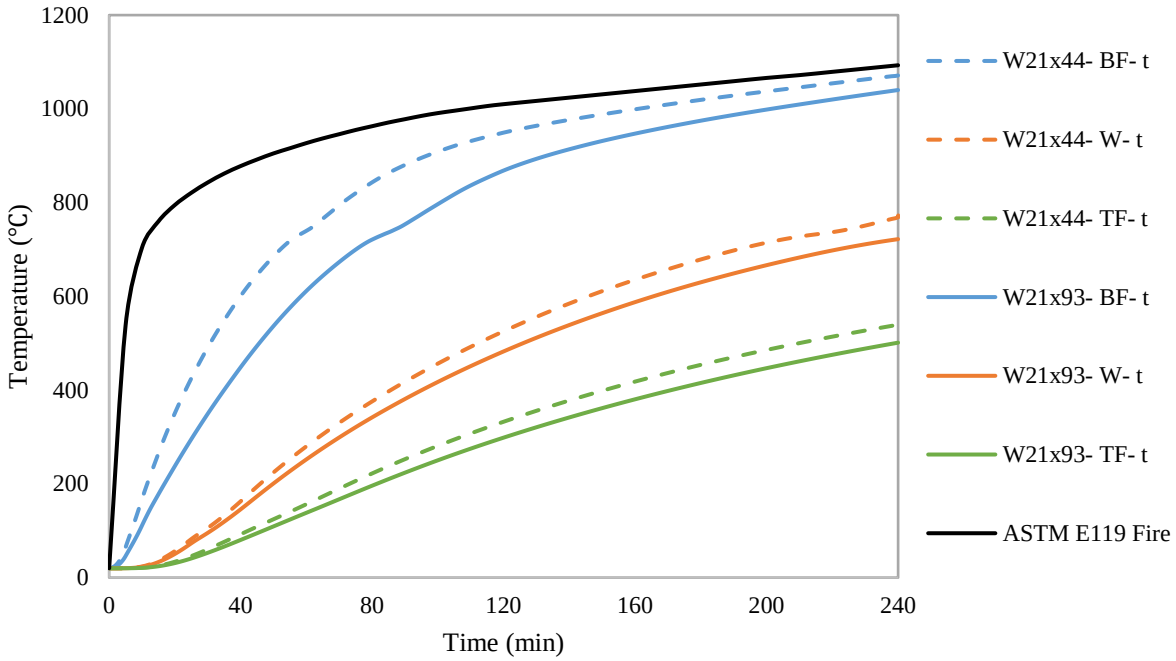

Figure 4-13. Comparison of the temperature of different parts of W21×44 and W21×93 with full damage penetration during the fire exposure

The structural response of the fully fireproofed members and members with t, 0.5t damage are shown in Figures 4-14 to 4-21. The failure time (fire resistance) is presented at the end of each curve. Yielding is the governing limit state for the beams with fully damaged fire protection(t). The loss of fire protection at the middle of the span leads to a higher temperature rise within the cross section and causes high stresses within the cross-section due to the degradation of the steel strength at the with damage locations. Therefore, the spread of plasticity within the critical section forms a plastic hinge at the middle of the span. Finally, the plastic hinge causes high strains and deformations at the damage location part and would lead to beam collapse.

The load level is a significant parameter to determine the fire resistance of the members during a fire incident. By increasing the load level, higher stresses are induced within the beam's cross-sections. The rise of the temperature at the regions with damaged fire protection leads to reaching the capacity of the beam, rapidly. As it is shown in the result of the structural analysis, increasing the load level leads to the reduction of the fire resistance of the beams. Additionally, the fire resistance of the lighter sections reduces at a higher rate than the fire resistance of the heavier sections at higher load levels.

The larger width of the heavier sections results in a larger exposure area; hence, the fire resistance of the heavier sections with fully damaged fire protection and with similar section heights reduces faster than the lighter sections' fire resistance. As it is shown in Table 4-2 by increasing the load level, the fire resistance of the memebers reduces at different rates. However, at higher load levels (90% loading) the fire resistance reduction all beams become closer to a limit about 62%.

The fire resistance of the members with half thickness damage penetration (0.5t) of the fire protection experiences a minor reduction of fire resistance. The deflection of the mid-span of the beams as a function of time for beams with 0.5t damage is close to the fully fireproofed beams. Hence, the damage penetration has a minor effect on the fire resistance of the beams. A summary of fire resistance of the different cases is shown in Tables 4-2 and 4-3. Table 4-2 shows the fire resistance of the both members with full thickness damage and fully fireproofed members. Also, in Table 4-3 fire resistance of the members with 50% damage penetration are compared to the fire resistance of the fully fireproofed members. In both tables, the fire resistance of the each damaged member as a percentage of the fire resistance of same member with full fire protection is presented.

Table 4-2. Fire resistance of the members with fully damaged fire protection

100% Damage Penetration	Fully protected fire resistance (min)				Damaged members fire resistance (min)			Fire resistance after damage compare to fully protected case (%)		
	Sections	Loading			Loading			Loading		
		50%	70%	90%	50%	70%	90%	50%	70%	90%
	W12x22	182	151	126	98	69	46	54	46	37
	W12x50	192	160	136	76	53	48	40	33	35
	W14x30	180	151	127	91	58	40	51	38	31
	W14x76	198	165	138	77	59	48	39	36	35
	W18x40	197	164	139	119	81	54	60	49	39
	W18x86	206	172	145	92	65	52	45	38	36
	W21x44	204	168	142	141	98	65	69	58	46
	W21x93	219	181	152	119	86	63	54	48	41

Table 4-3. Fire resistance of the members 50%damaged penetration fire protection

50% Damage Penetration	Fully protected fire resistance (min)				Damaged members fire resistance (min)			Fire resistance after damage compare to fully protected case (%)		
	Sections	Loading			Loading			Loading		
		50%	70%	90%	50%	70%	90%	50%	70%	90%
	W12x22	182	151	126	170	142	118	93	94	94
	W12x50	192	160	136	176	145	121	92	91	89
	W14x30	180	151	127	166	138	114	92	91	90
	W14x86	198	165	138	182	150	126	92	91	91
	W18x40	197	164	139	188	154	129	95	94	93
	W18x86	206	172	145	191	158	133	93	92	92
	W21x44	204	168	142	196	158	132	96	94	93
	W21x86	219	181	152	209	173	146	95	96	96

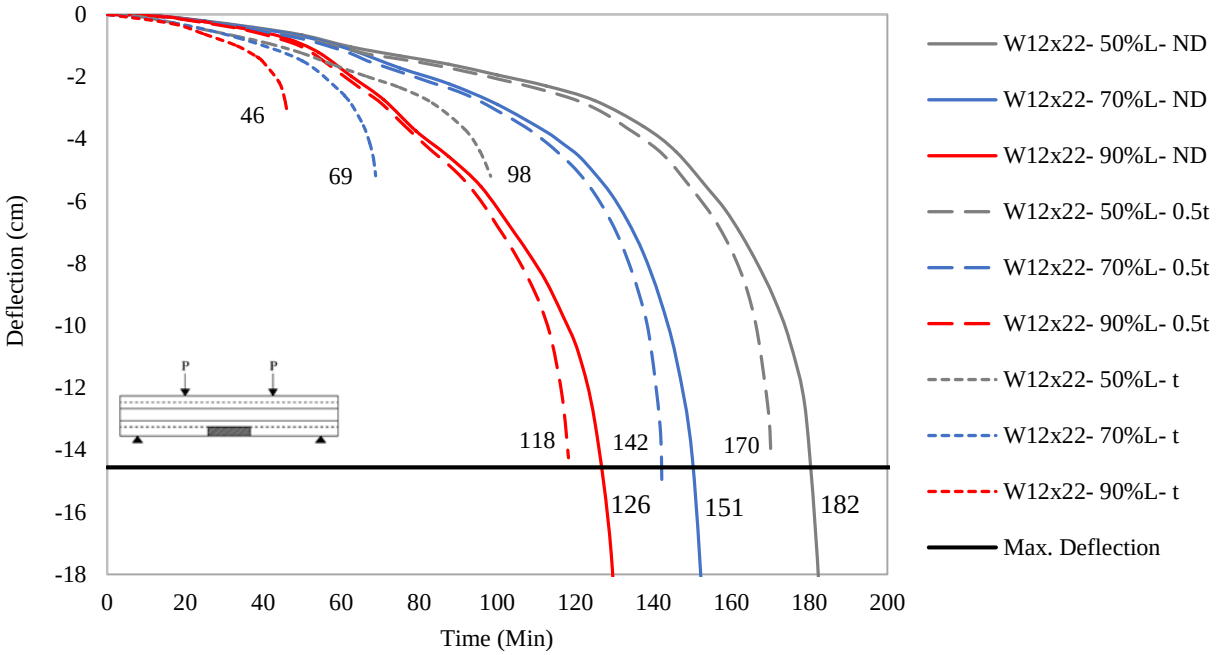

Figure 4-14. Mid-span deflection of W12×22 with no damage and with 12.7cm damage length

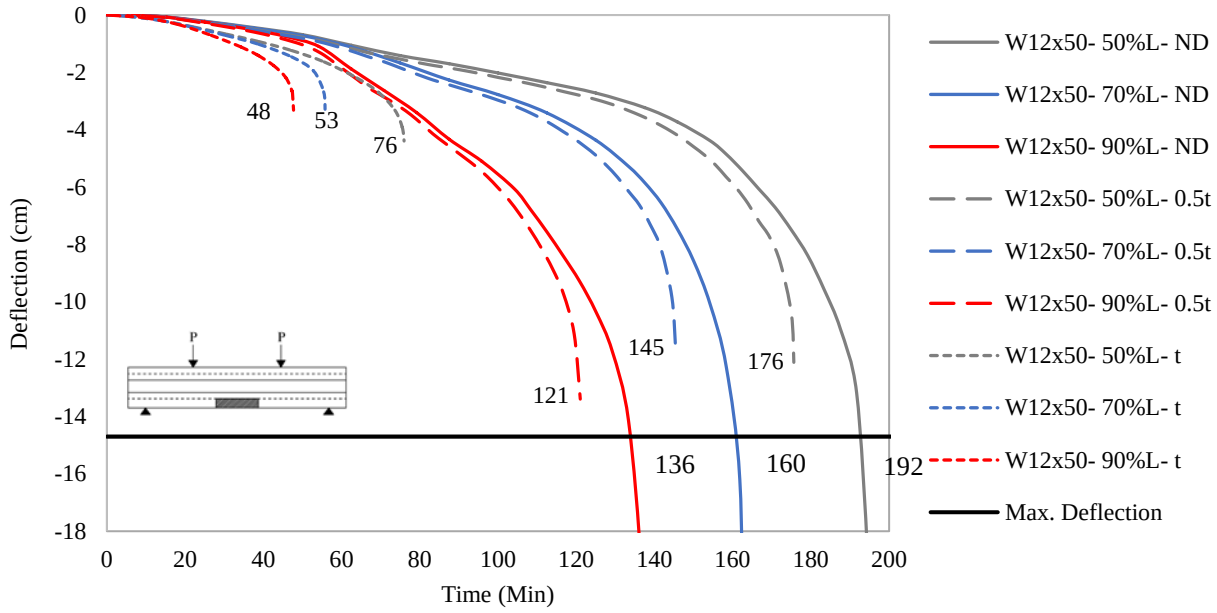

Figure 4-15. Mid-span deflection of W12×50 with no damage and with 12.7cm damage length

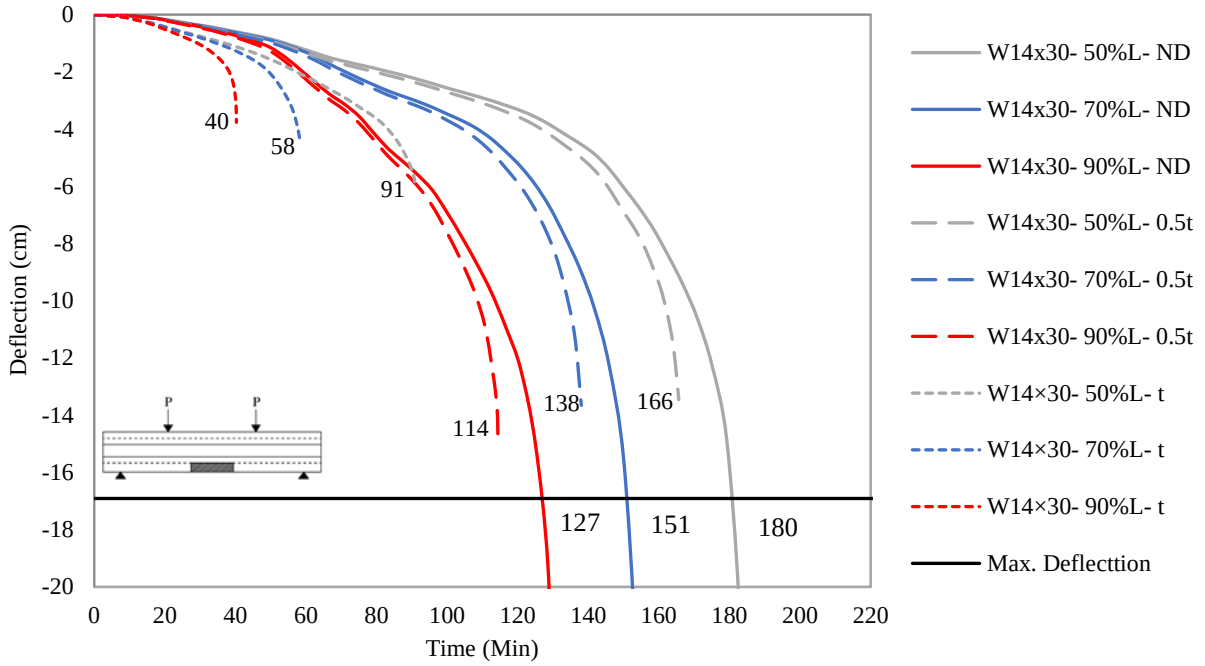

Figure 4-16. Mid-span deflection of W14×30 with no damage and with 12.7cm damage length

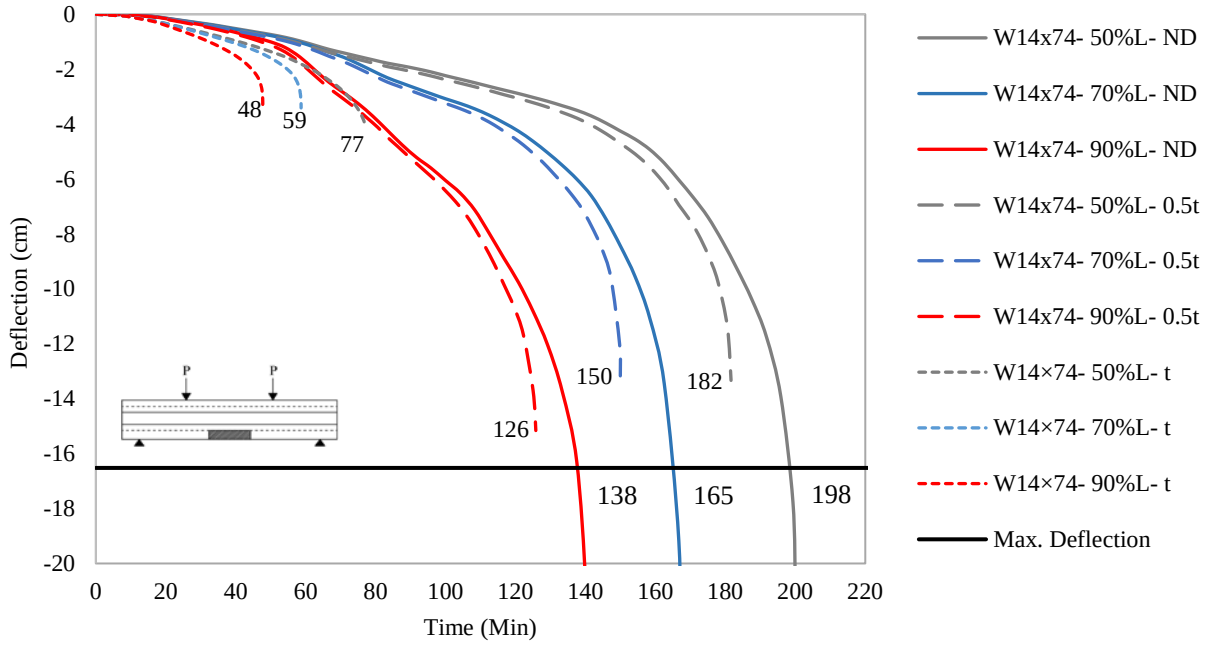

Figure 4-17. Mid-span deflection of W14×86 with no damage and with 12.7cm damage length

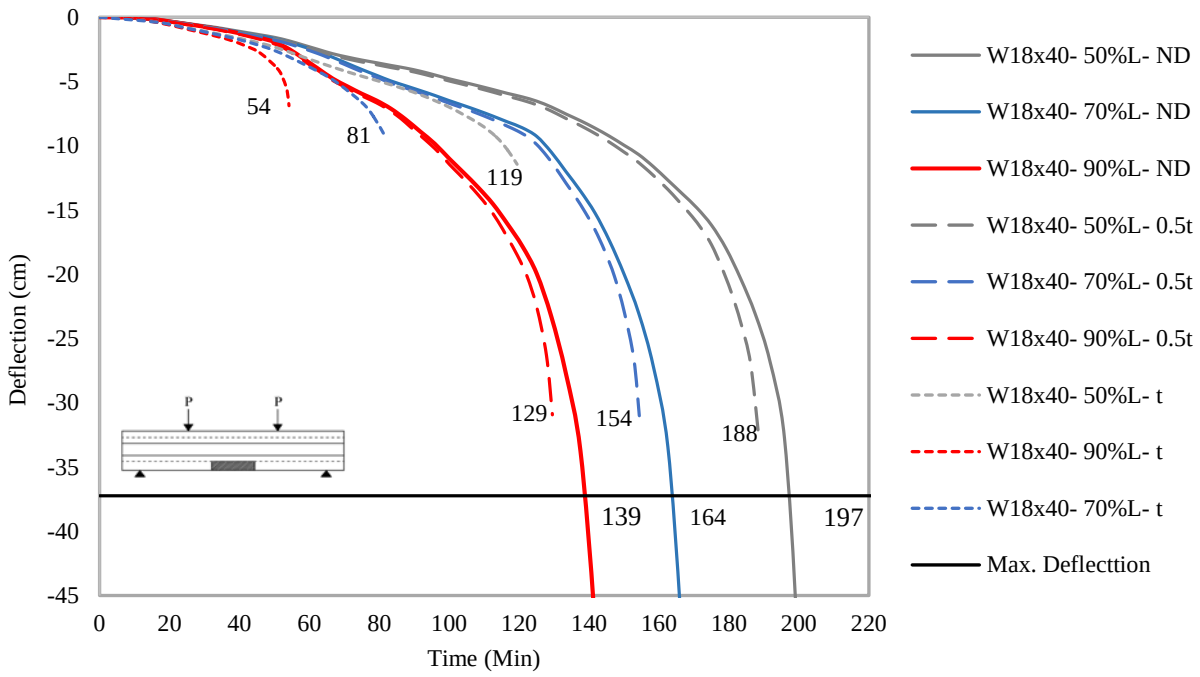

Figure 4-18. Mid-span deflection of W18×40 with no damage and with 12.7cm damage length

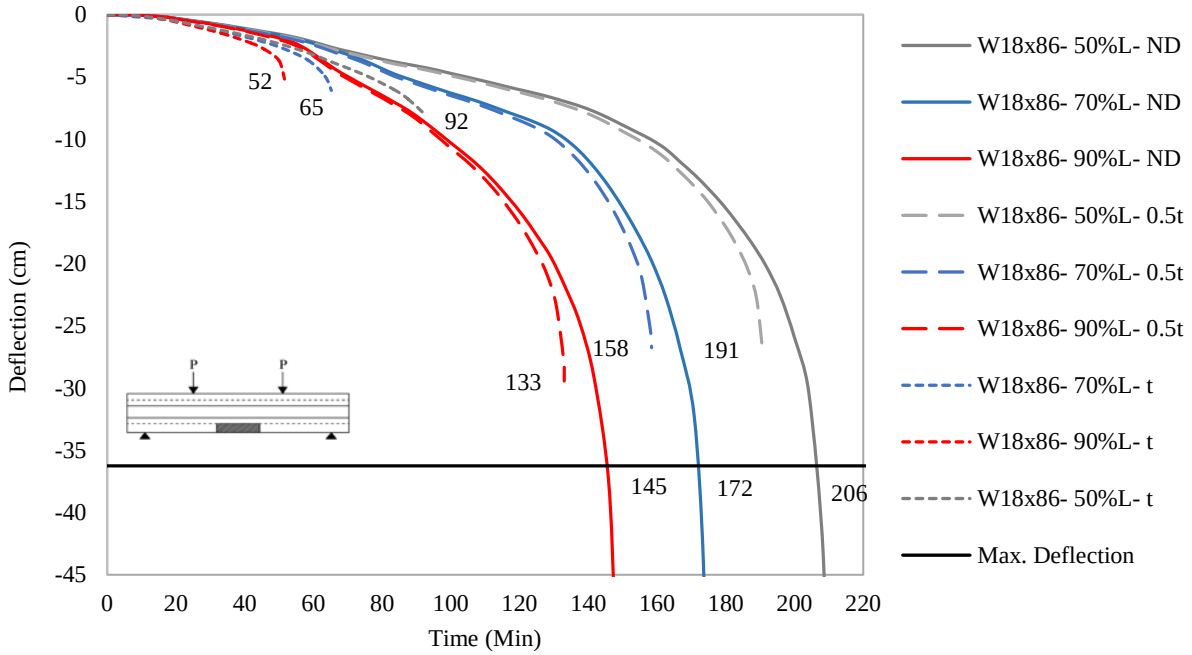

Figure 4-19. Mid-span deflection of W18×86 with no damage and with 12.7cm damage length

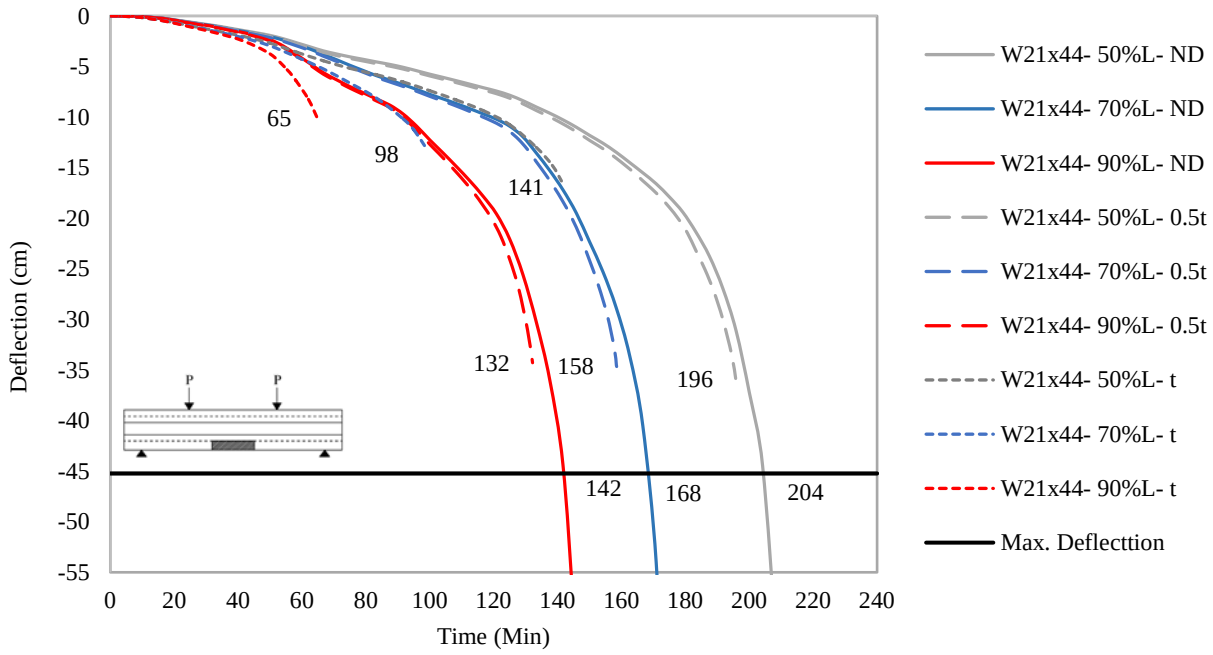

Figure 4-20. Mid-span deflection of W21×44 with no damage and with 12.7cm damage length

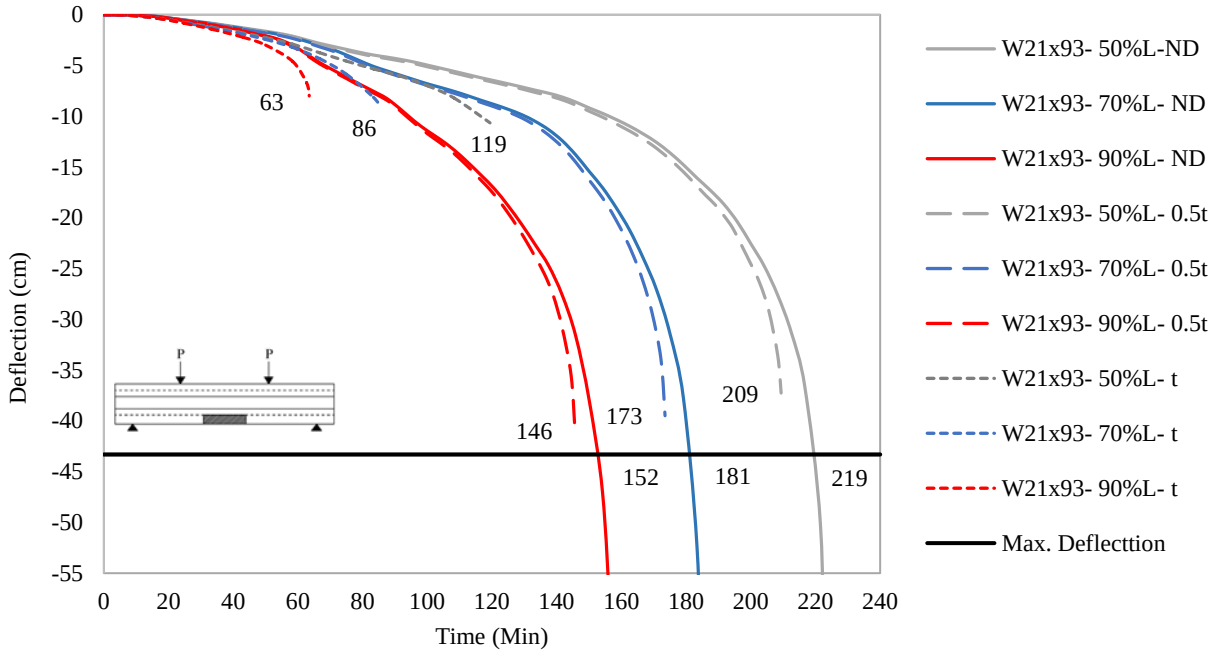

Figure 4-21. Mid-span deflection of W21×93 with no damage and with 12.7cm damage length

4.6.2 Effect of fire protection's damage length

In this series of models, ASTM E119 standard fire is applied from three sides, and room temperature is assumed for the top side of the beams. The temperature of the beams' cross section for different damage scenarios at the mid-span was almost same during the fire exposure. Therefore, only the temperature rise of the various parts of the beams cross-section at the mid-span of the beams for 30% of span damage length is illustrated in Figures 4-22 to 4-29, and they are compared with the temperature of fully fireproofed members' sections.

The temperature of the cross-sections during the fire exposure are similar to the studied cases with t damage in previous group of beams. Top flanges' temperature (TF) during the fire exposure for both damaged and fully fireproofed members are too close to each other. The temperature of top flanges of W18s and W21s are almost same.

In Figures 4-30 to 4-53, the mid-span deflection of the steel beams with a series of fire protection loss lengths are shown as a function of time. The damage part length ranges from 10% to 50% of the span, and it is shown as a percentage of member's span in the legend of the figures. The load levels of 50%, 70% and 90% of the moment capacity of the steel beams were applied. The fire resistance of each studied case is presented on the associated curve. Also, the deflection of fully fireproofed members is included for comparison. Table 4-4 presents the fire resistance of the members with various load levels and damage lengths.

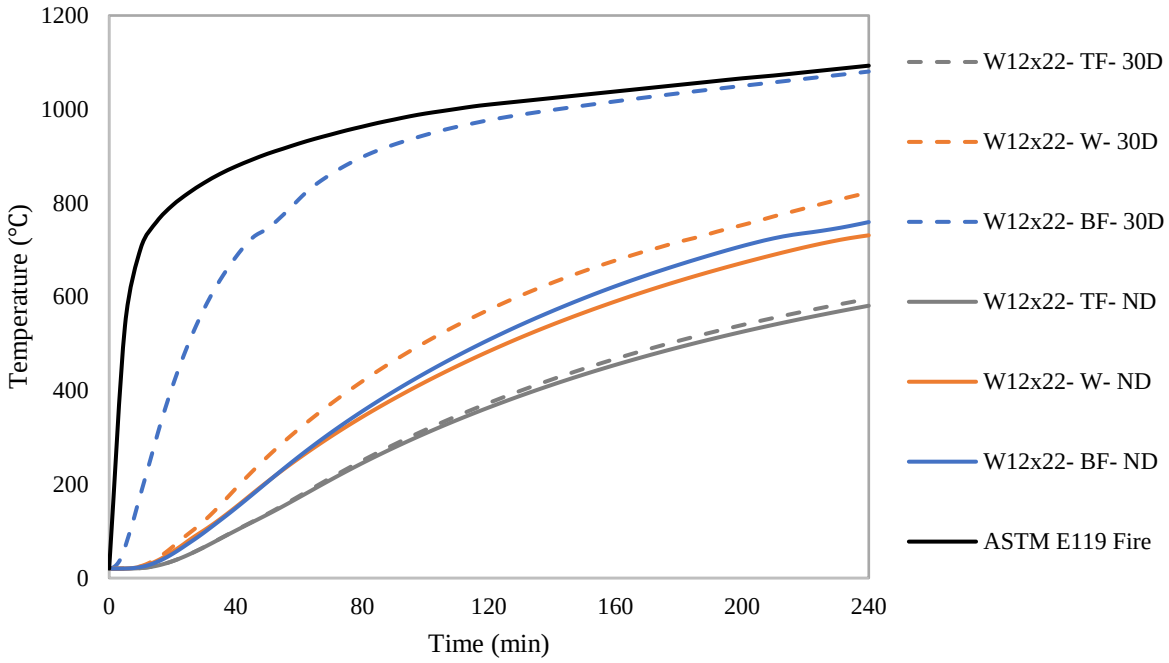

Figure 4-22. Temperature of various parts of W12×22 with 30% of span damage and fully fireproofed during the fire exposure

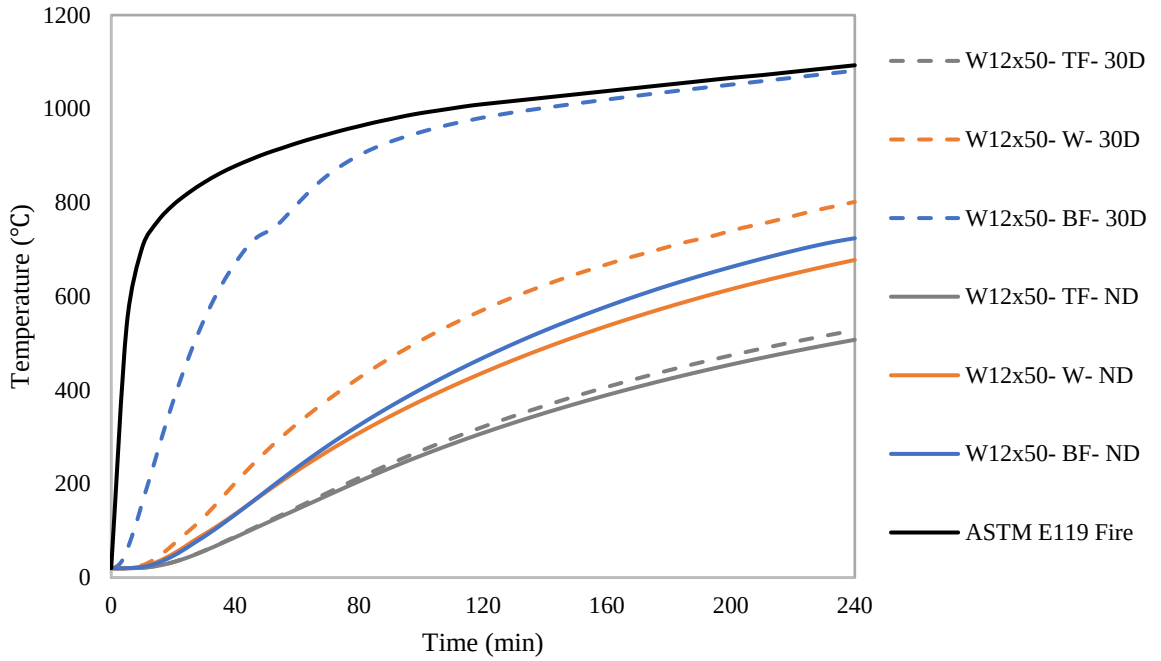

Figure 4-23. Temperature of various parts of W12×50 with 30% of span damage and fully fireproofed during the fire exposure

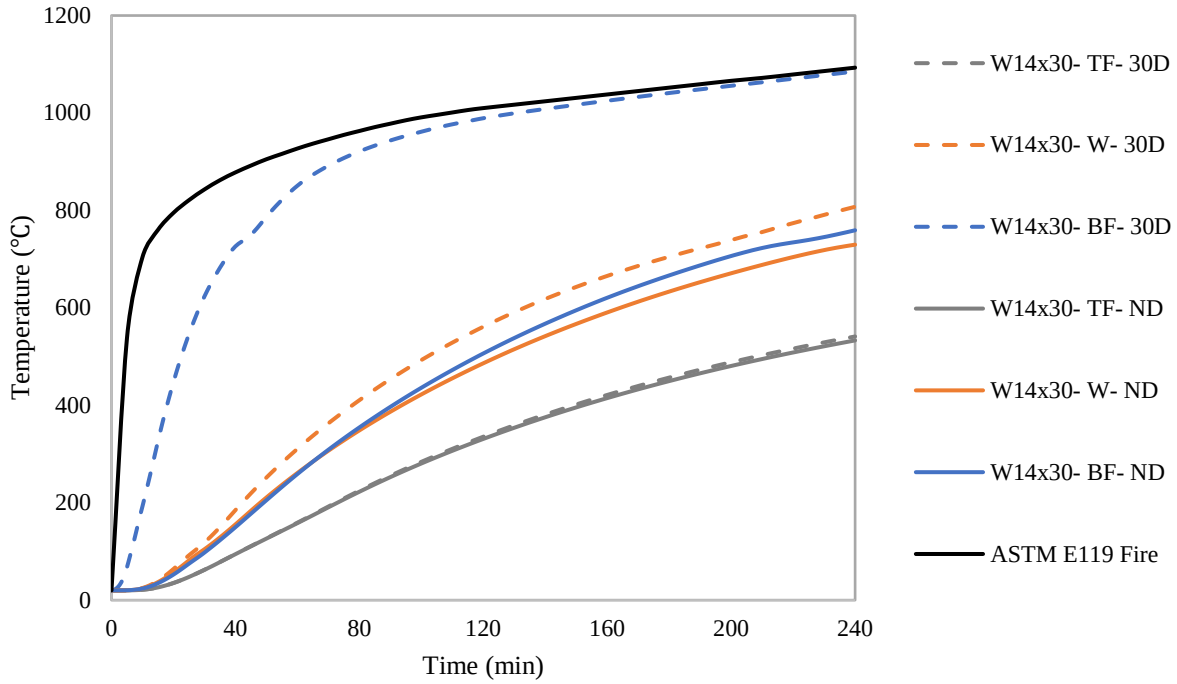

Figure 4-24. Temperature of various parts of W14×30 with 30% of span damage and fully fireproofed during the fire exposure

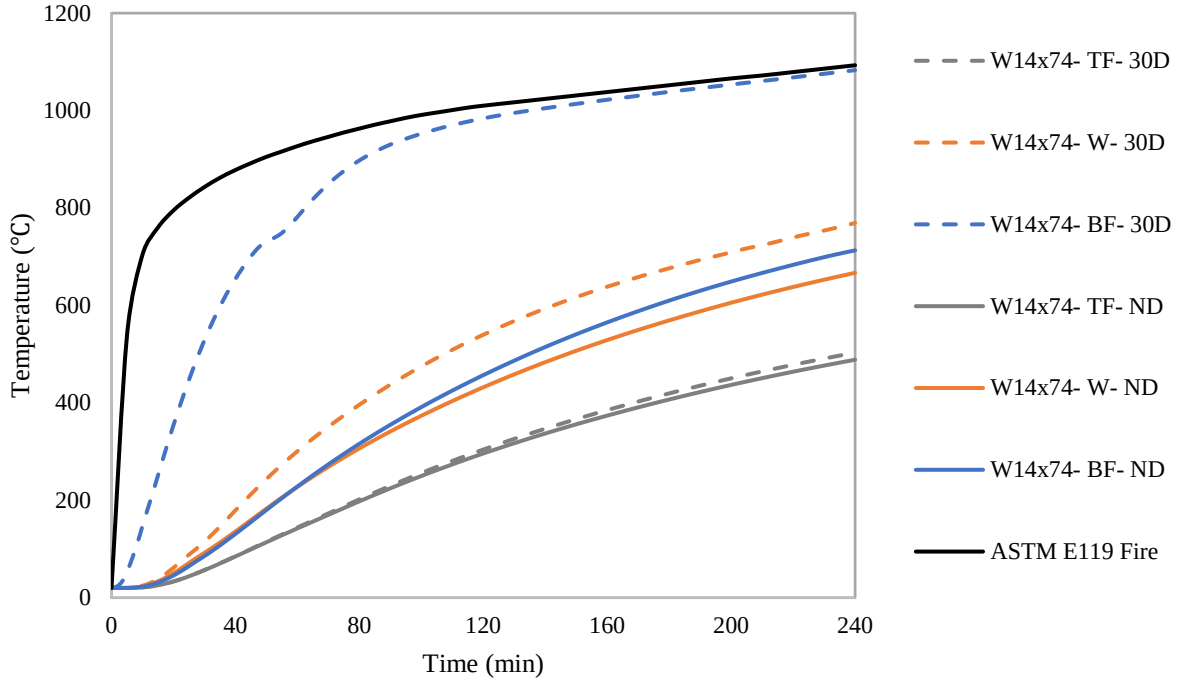

Figure 4-25. Temperature of various parts of W14×74 with 30% of span damage and fully fireproofed during the fire exposure

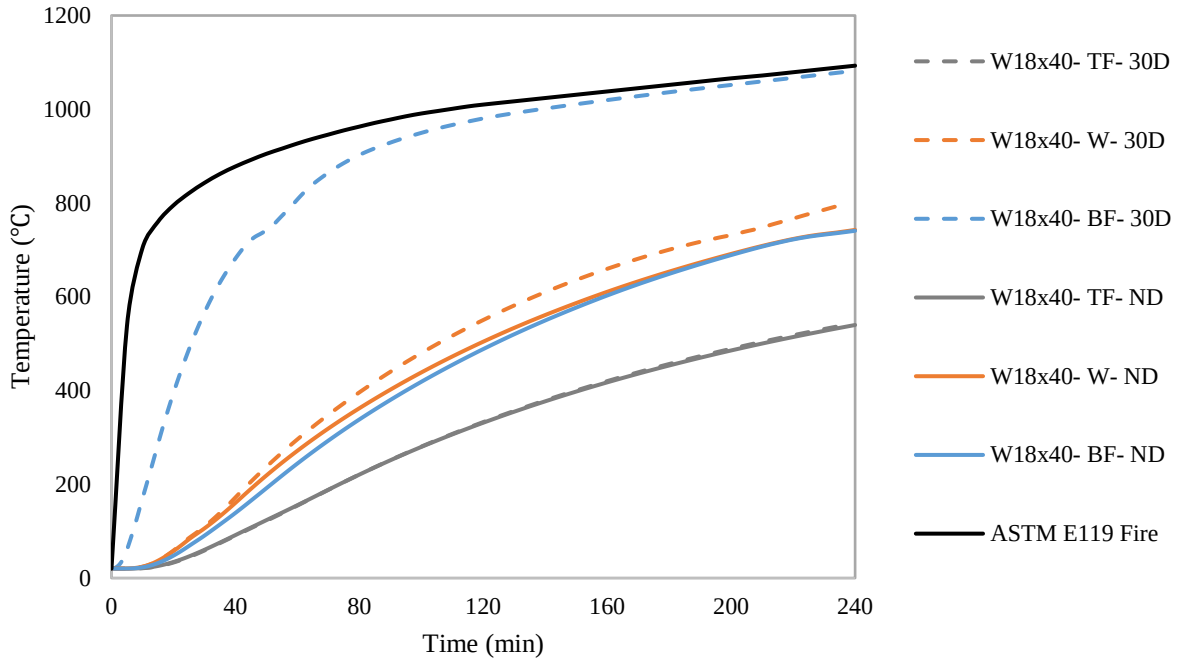

Figure 4-26. Temperature of various parts of W18×40 with 30% of span damage and fully fireproofed during the fire exposure

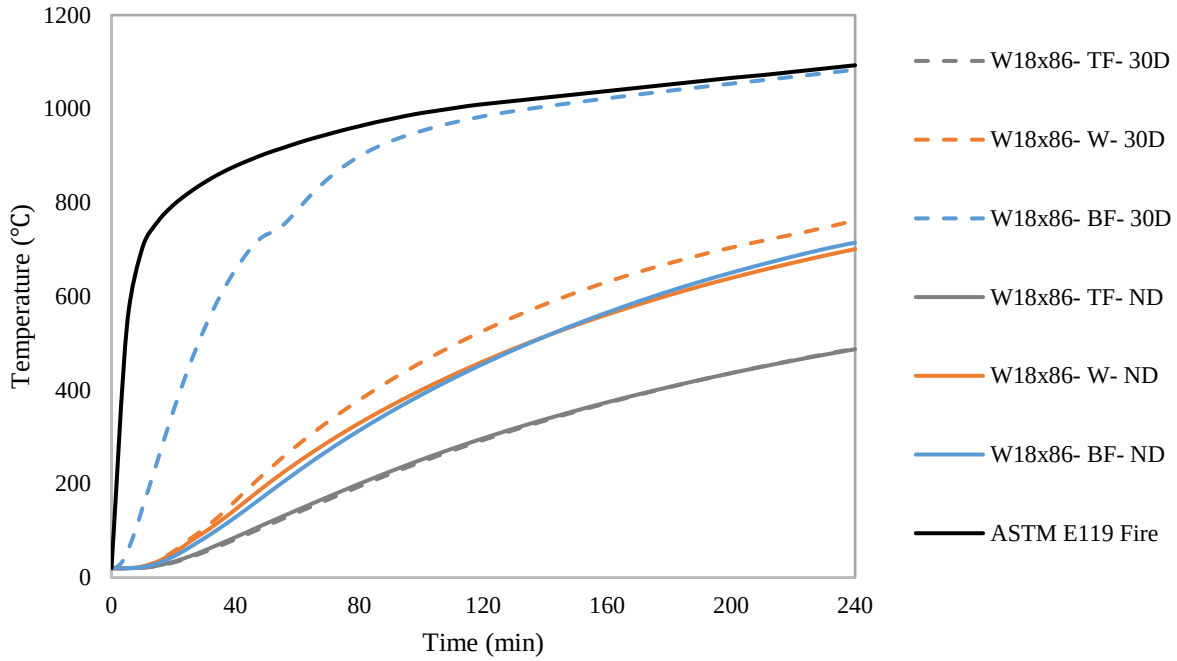

Figure 4-27. Temperature of various parts of W18×86 with 30% of span damage and fully fireproofed during the fire exposure

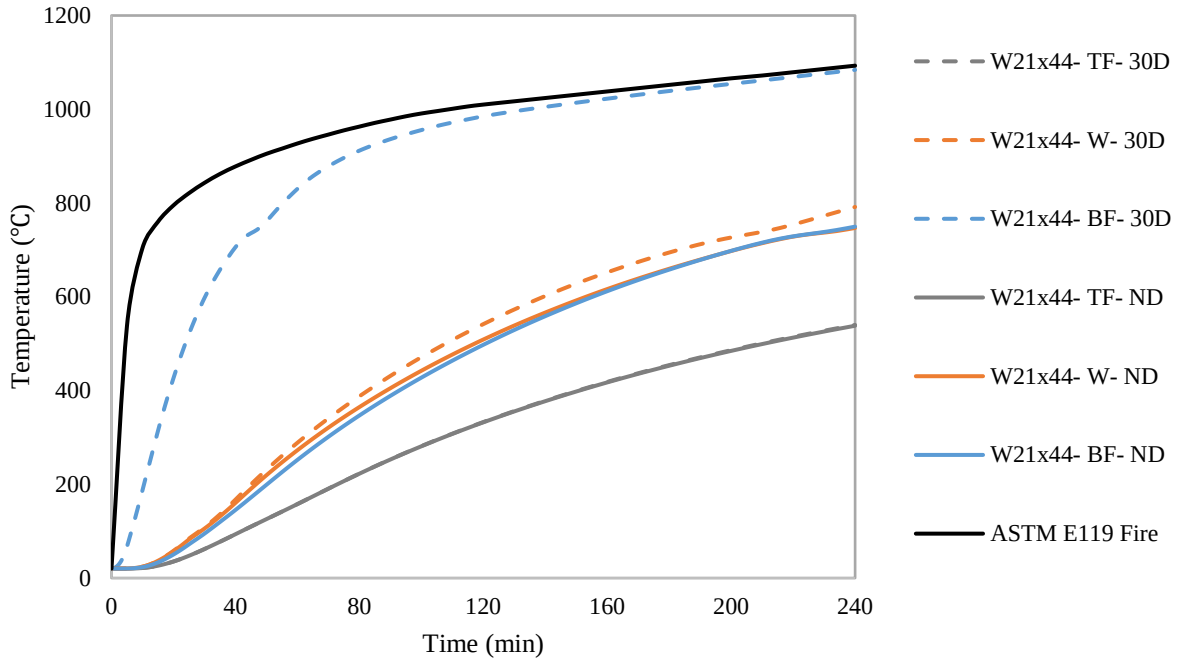

Figure 4-28. Temperature of various parts of W21x44 with 30% of span damage and fully fireproofed during the fire exposure

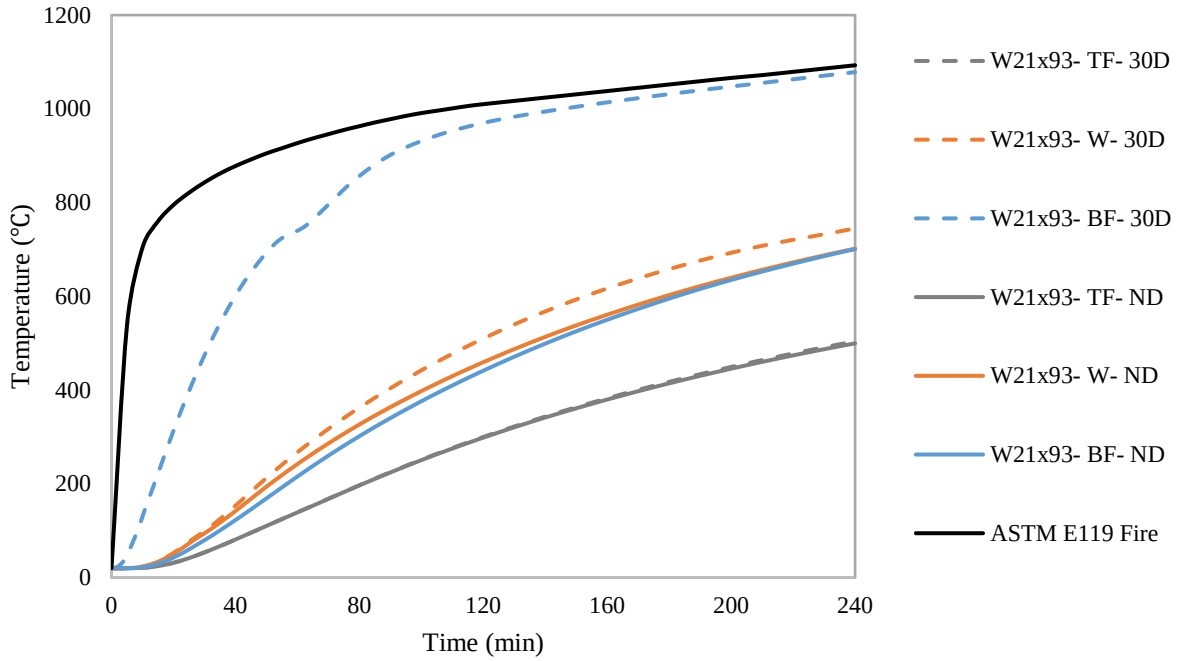

Figure 4-29. Temperature of various parts of W21×93 with 30% of span damage and fully fireproofed during the fire exposure

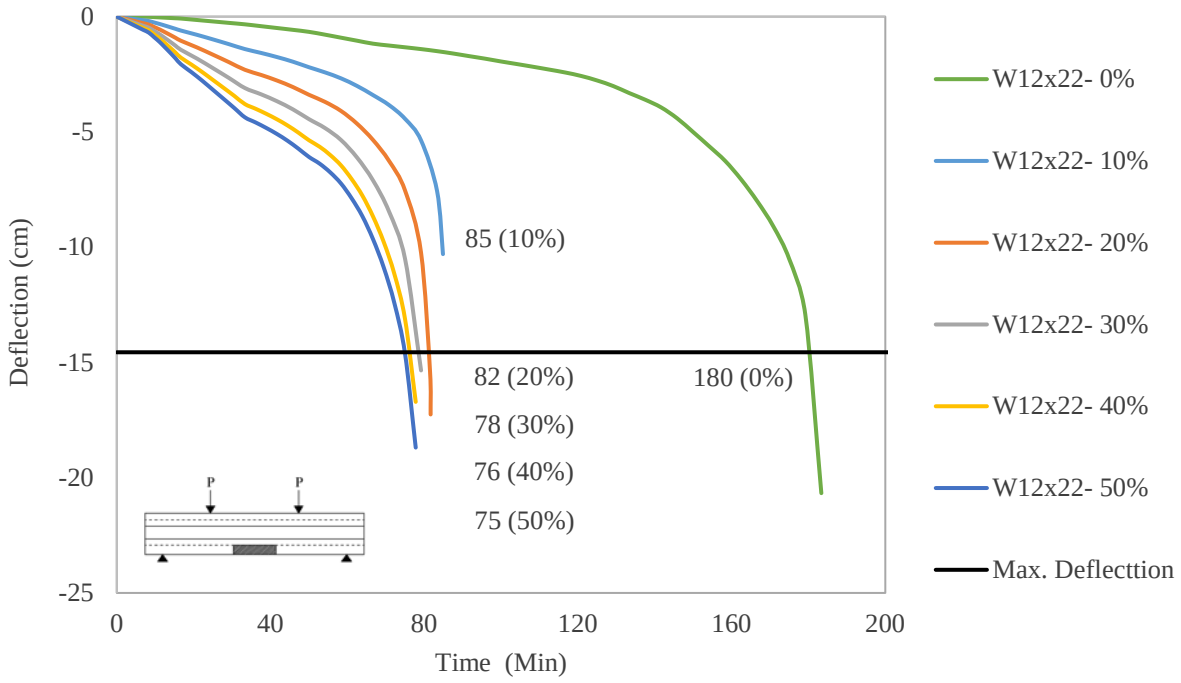

Figure 4-30. Mid-span deflection of W12×22 with 50% loading and various damage length

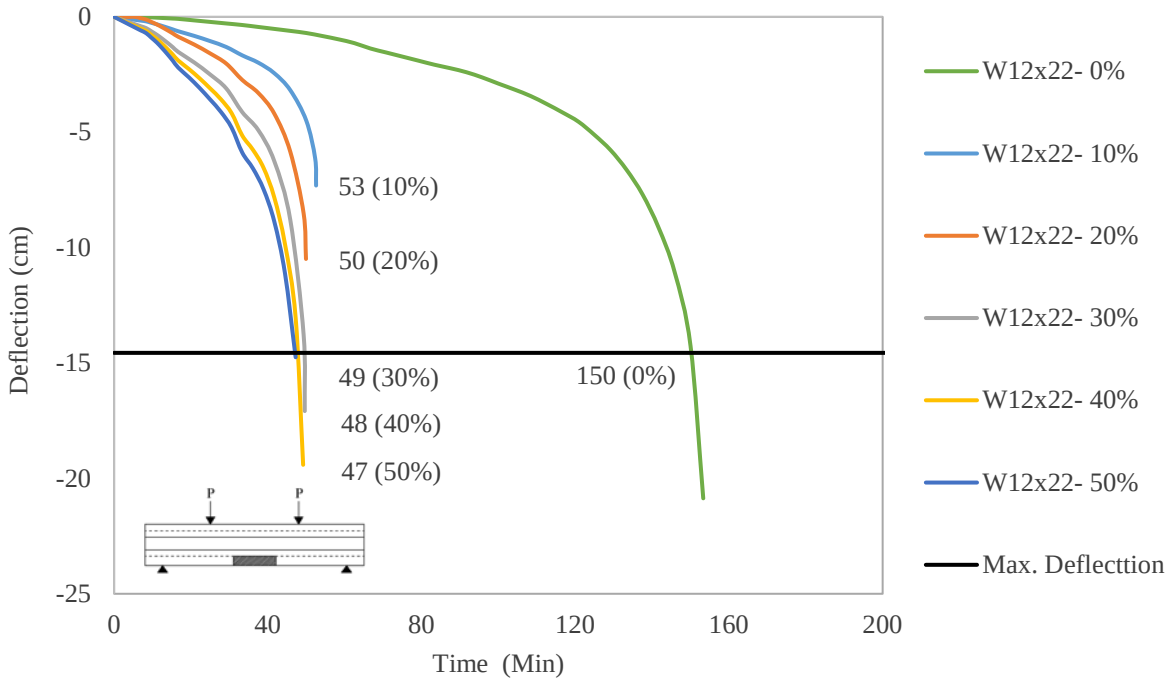

Figure 4-31. Mid-span deflection of W12×22 with 70% loading and various damage length

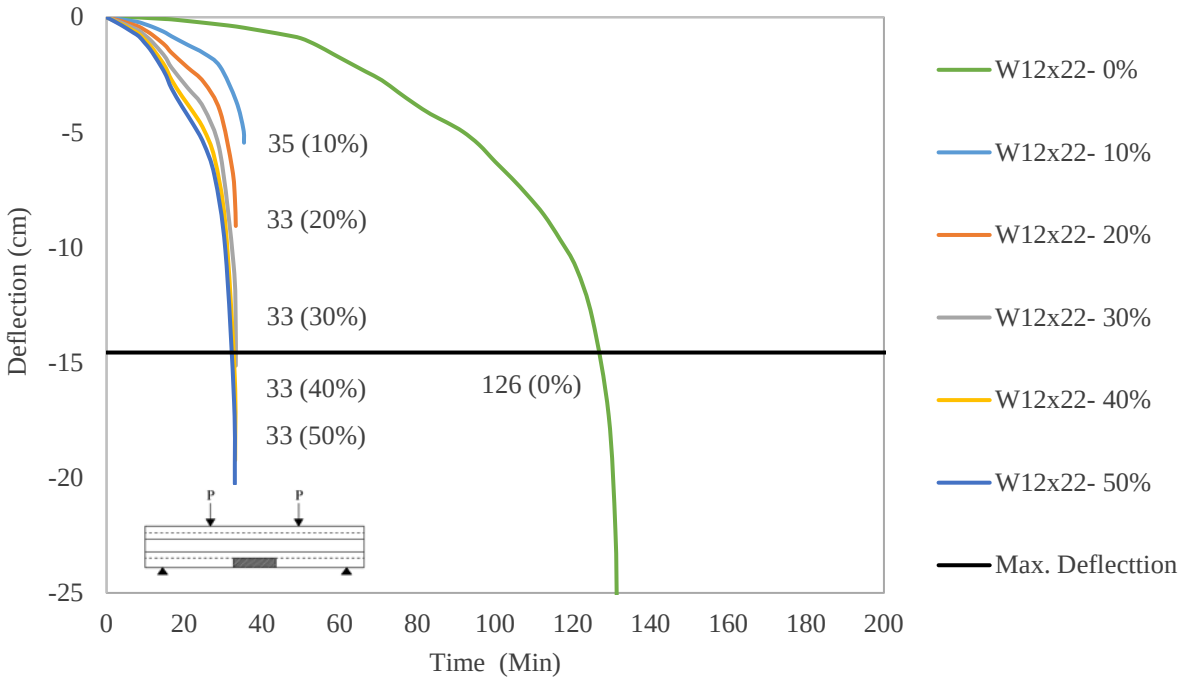

Figure 4-32. Mid-span deflection of W12×22 with 90% loading and various damage length

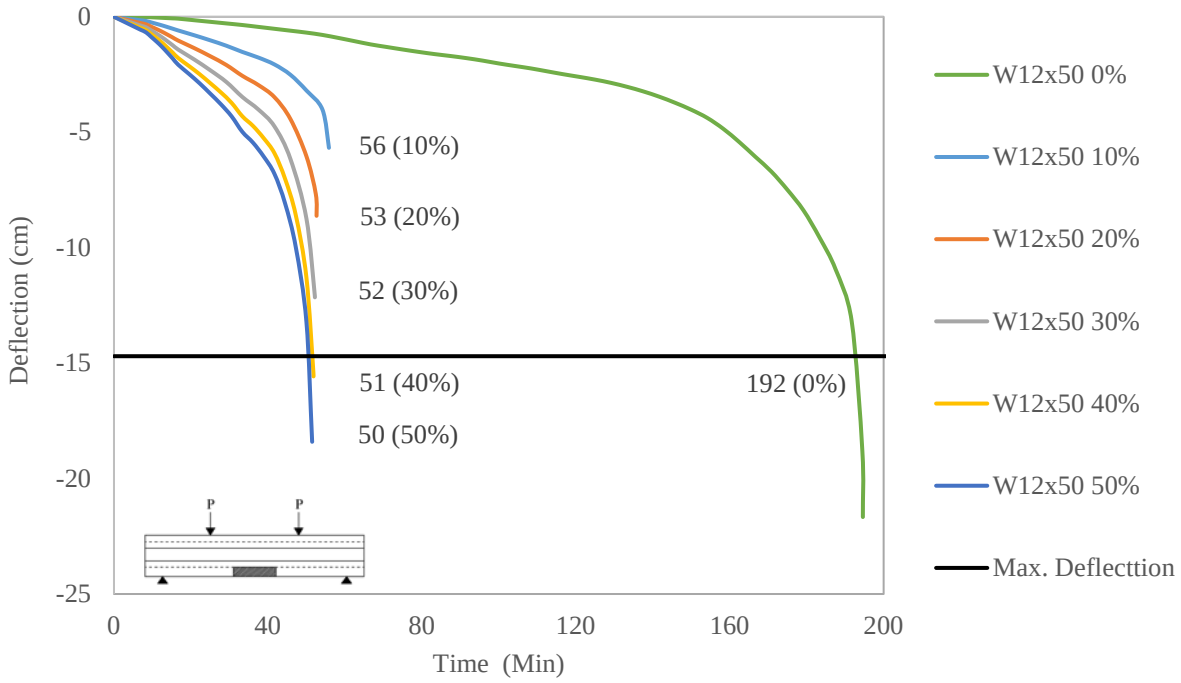

Figure 4-33. Mid-span deflection of W12×50 with 50% loading and various damage length

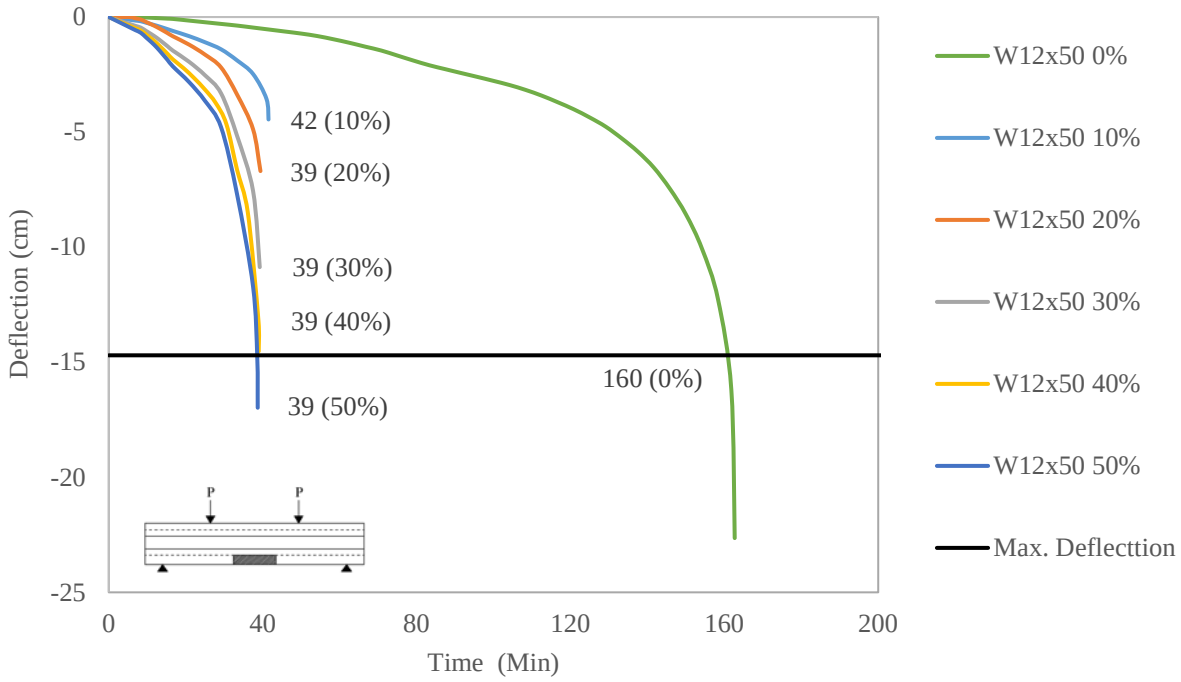

Figure 4-34. Mid-span deflection of W12×50 with 70% loading and various damage length

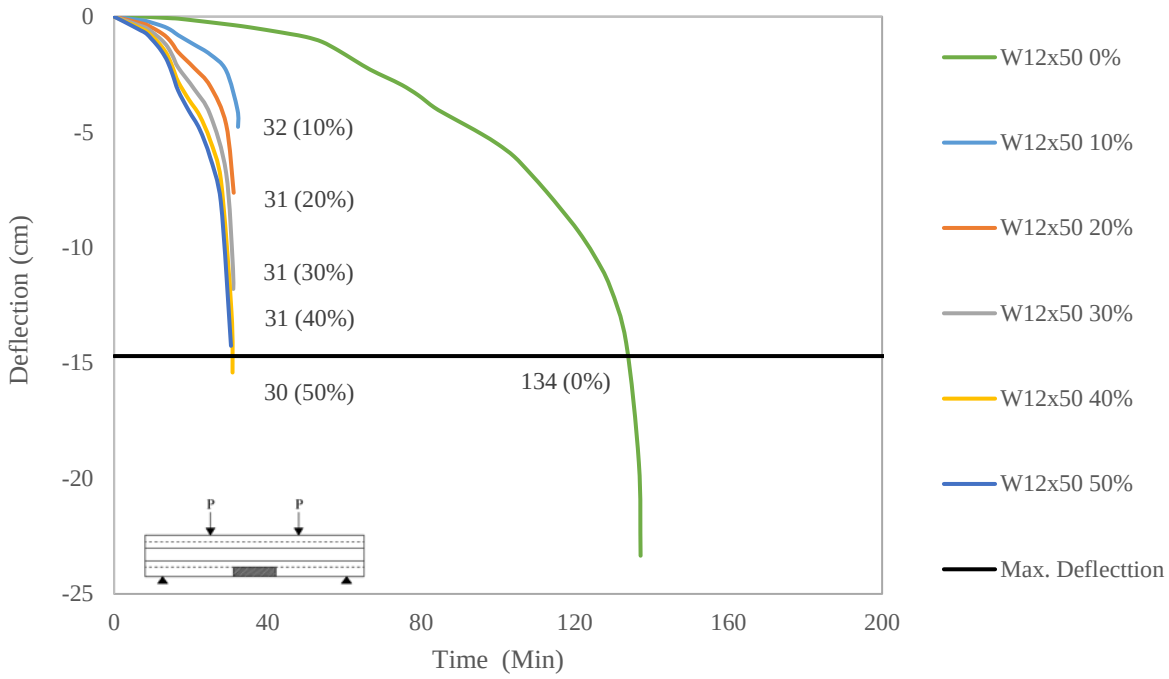

Figure 4-35. Mid-span deflection of W12×50 with 90% loading and various damage length

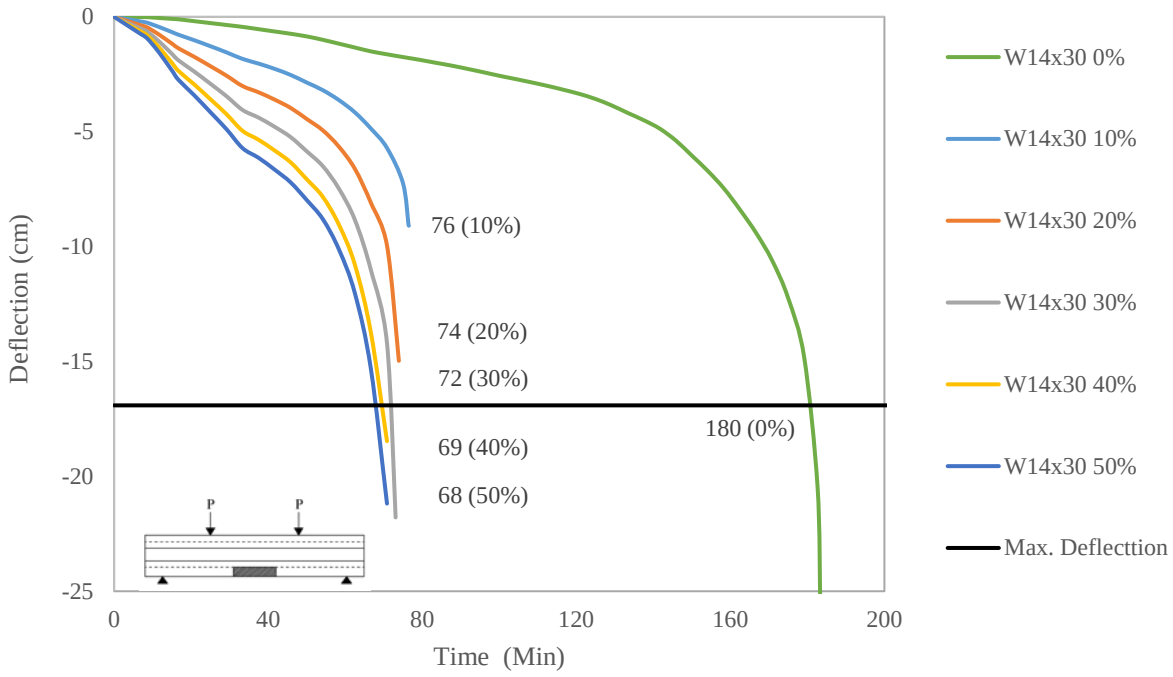

Figure 4-36. Mid-span deflection of W14×30 with 50% loading and various damage length

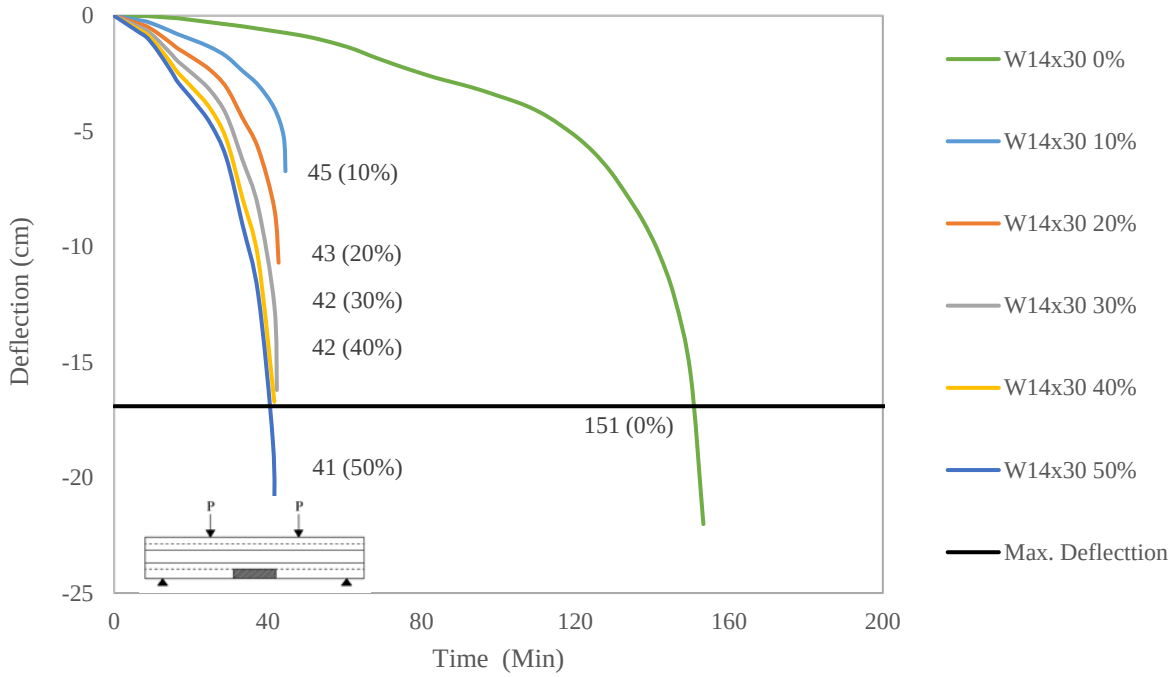

Figure 4-37. Mid-span deflection of W14×30 with 70% loading and various damage length

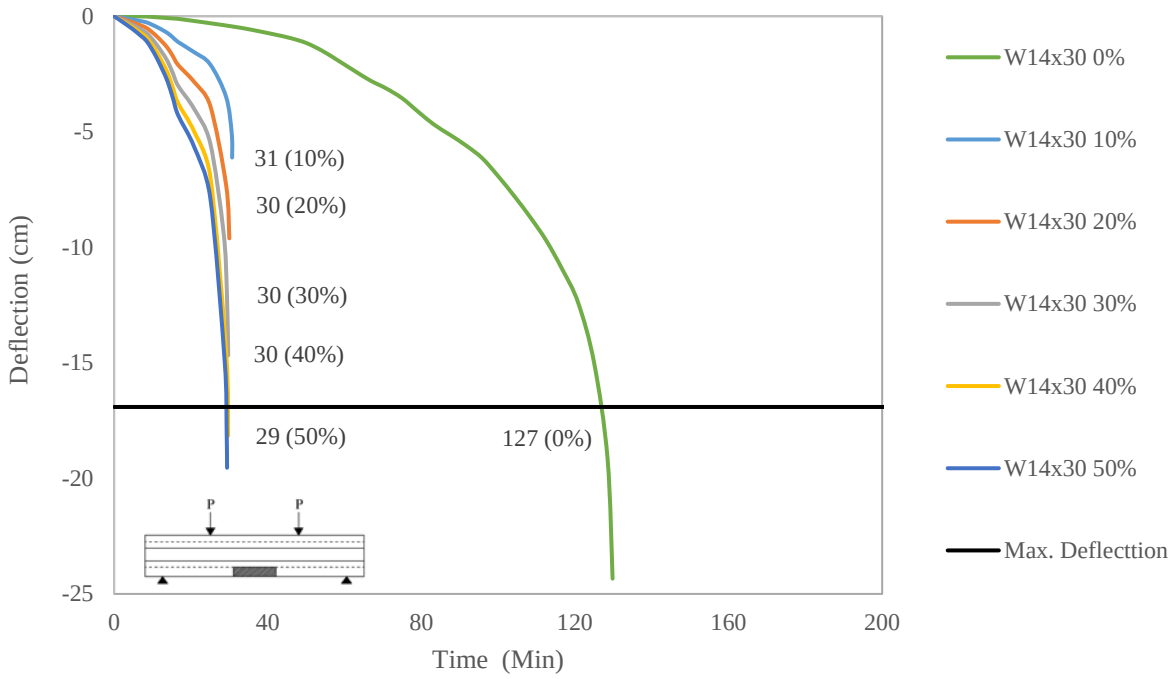

Figure 4-38. Mid-span deflection of W14×30 with 90% loading and various damage length

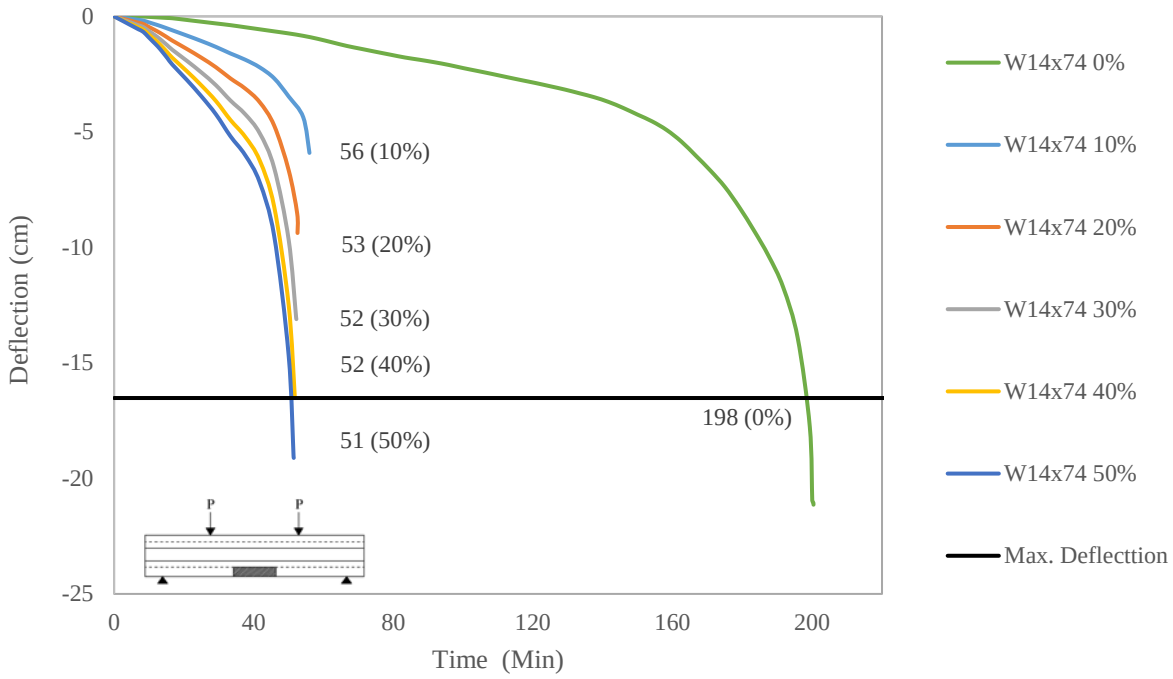

Figure 4-39. Mid-span deflection of W14×74 with 50% loading and various damage length

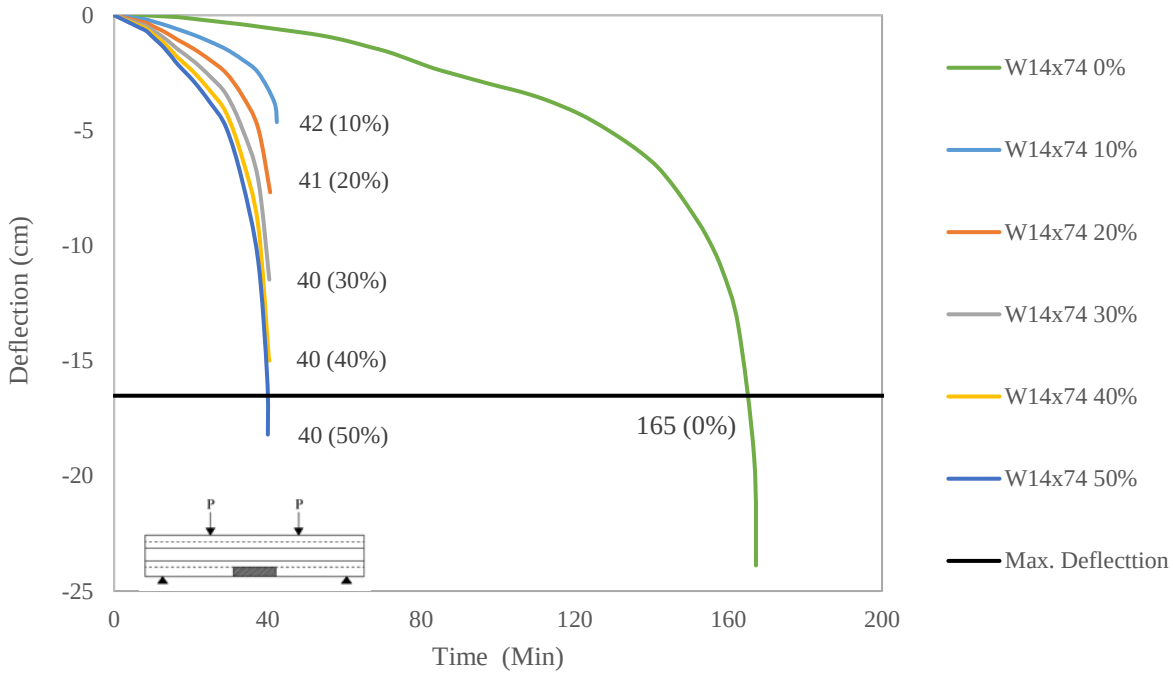

Figure 4-40. Mid-span deflection of W14×74 with 70% loading and various damage length

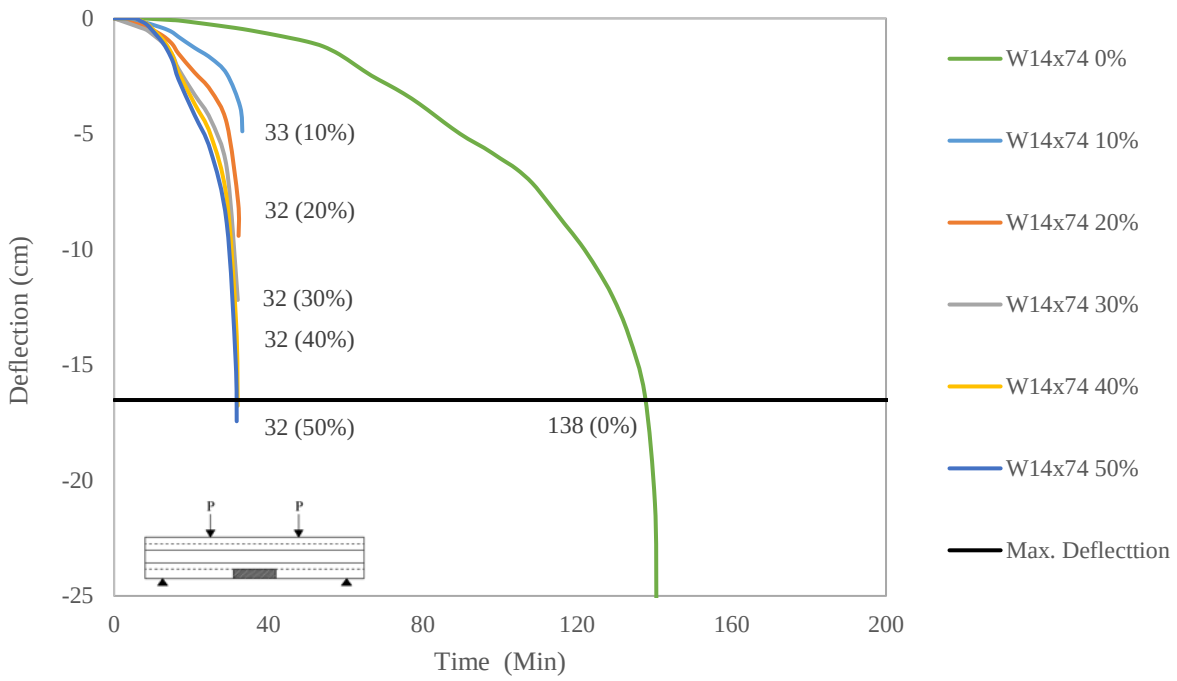

Figure 4-41. Mid-span deflection of W14×74 with 90% loading and various damage length

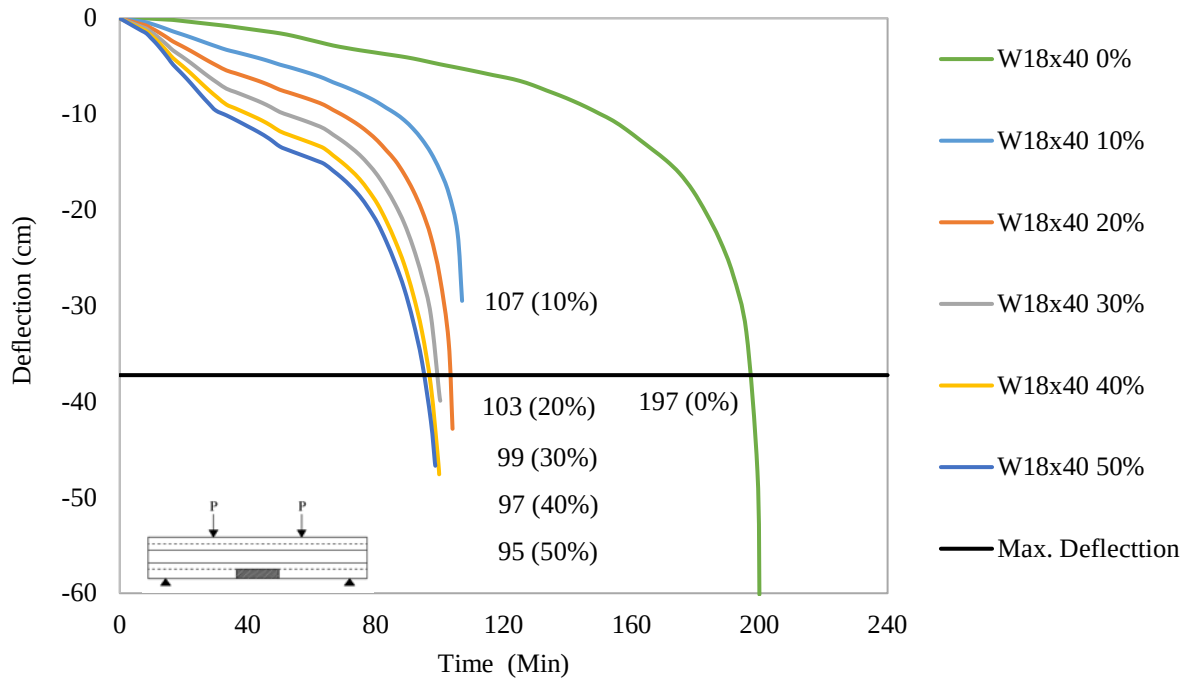

Figure 4-42. Mid-span deflection of W18×40 with 50% loading and various damage length

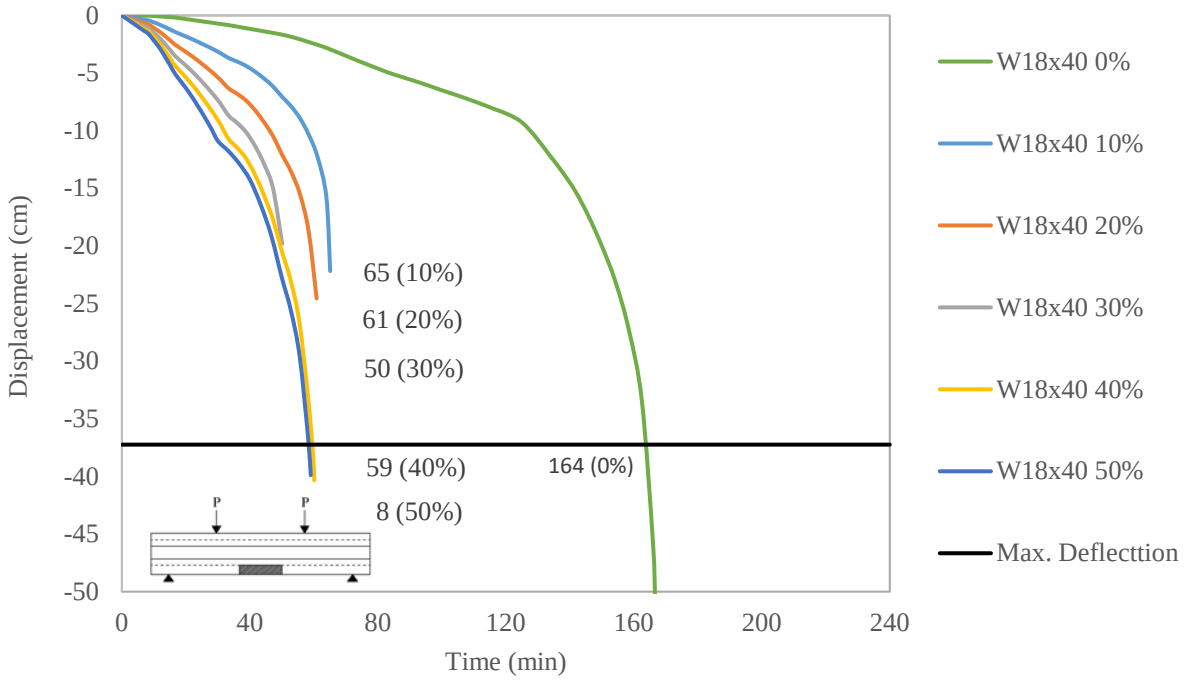

Figure 4-43. Mid-span deflection of W18×40 with 70% loading and various damage length

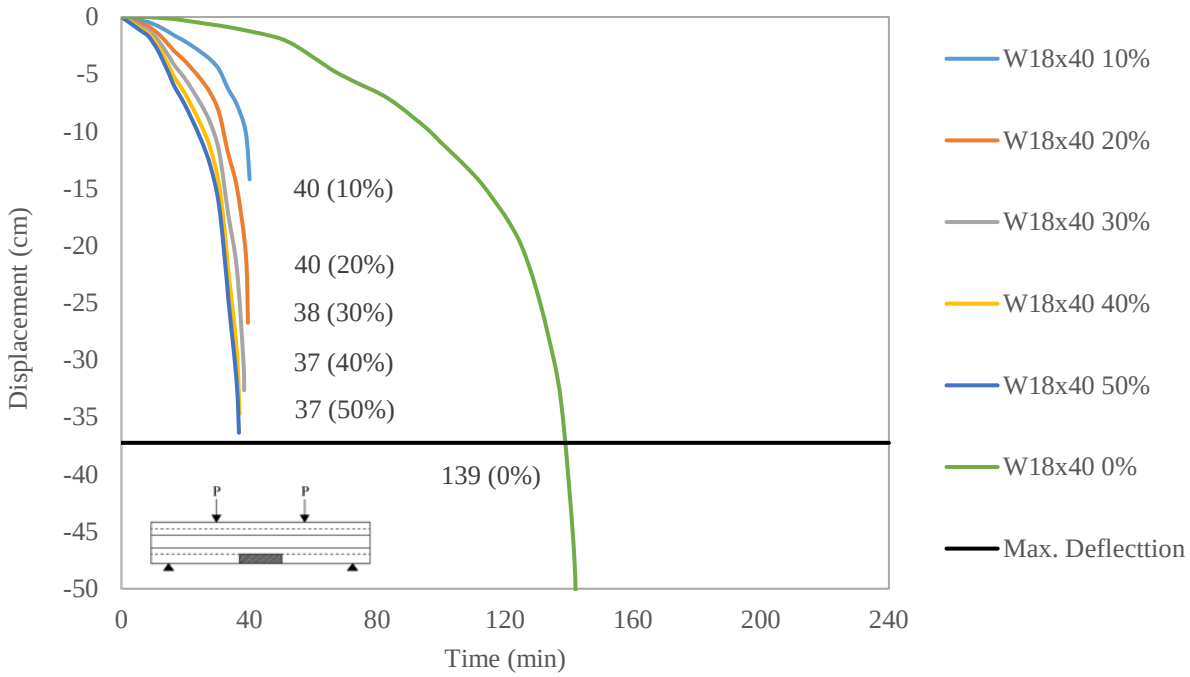

Figure 4-44. Mid-span deflection of W18×40 with 90% loading and various damage length

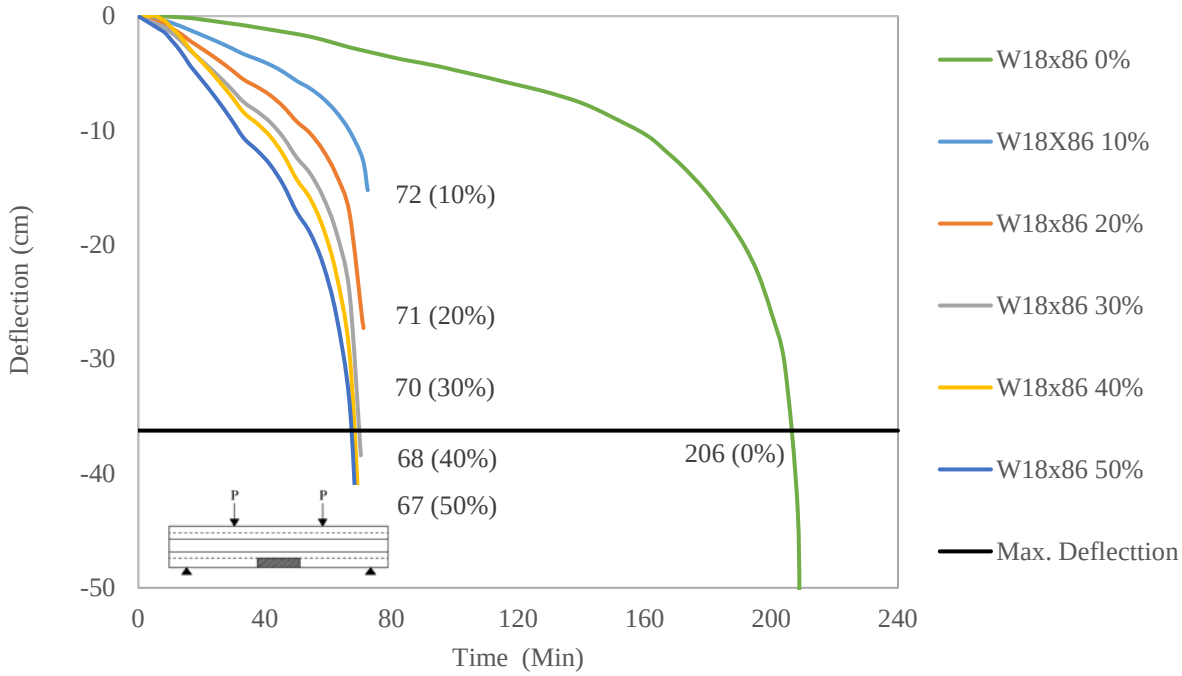

Figure 4-45. Mid-span deflection of W18×86 with 50% loading and various damage length

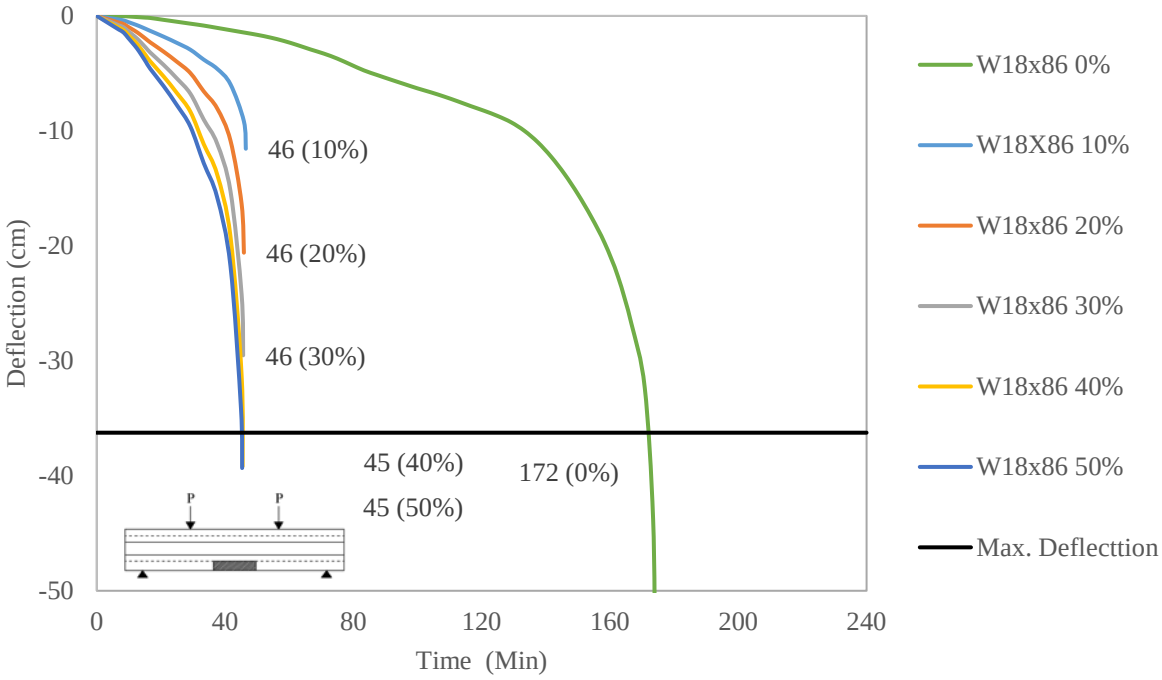

Figure 4-46. Mid-span deflection of W18×86 with 70% loading and various damage length

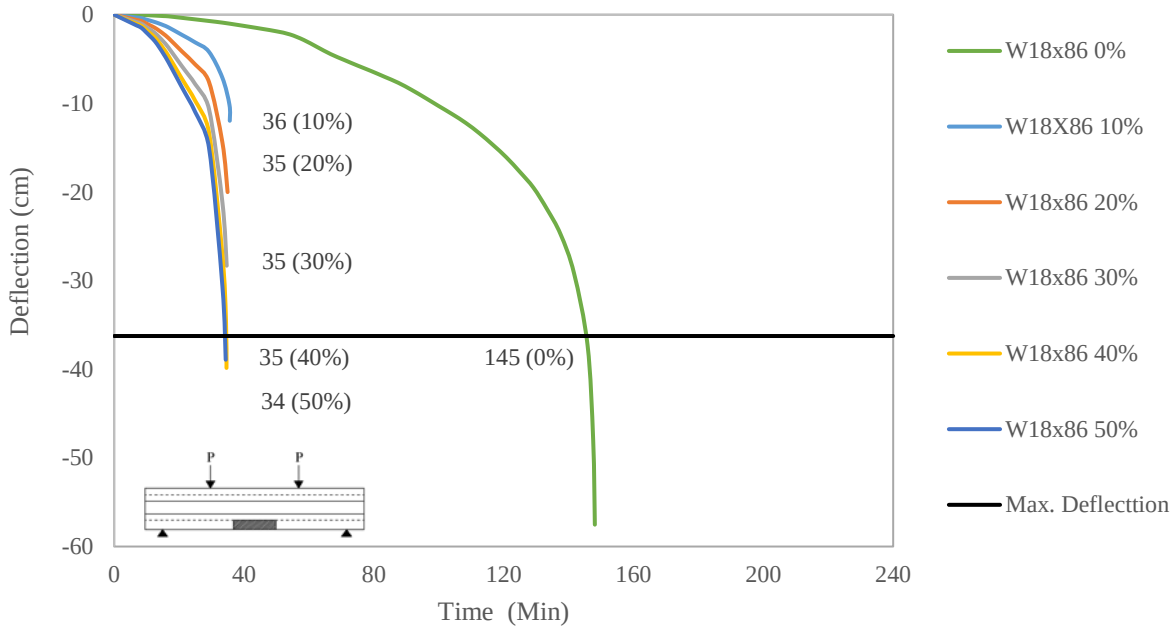

Figure 4-47. Mid-span deflection of W18×86 with 90% loading and various damage length

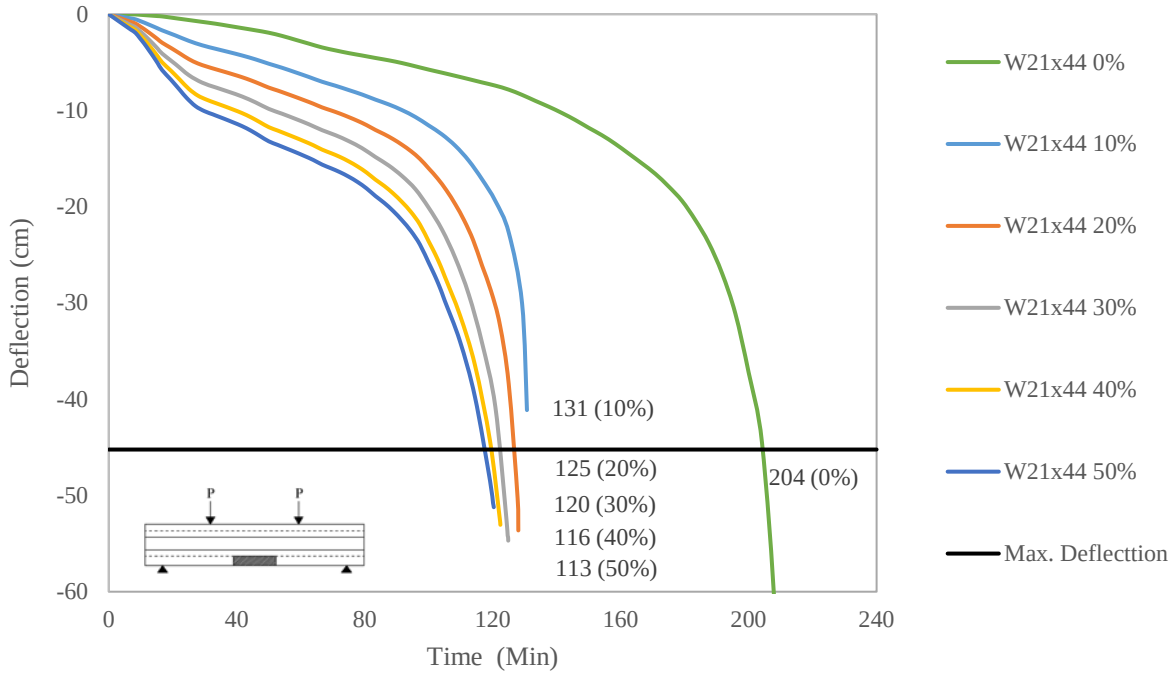

Figure 4-48. Mid-span deflection of W21×44 with 50% loading and various damage length

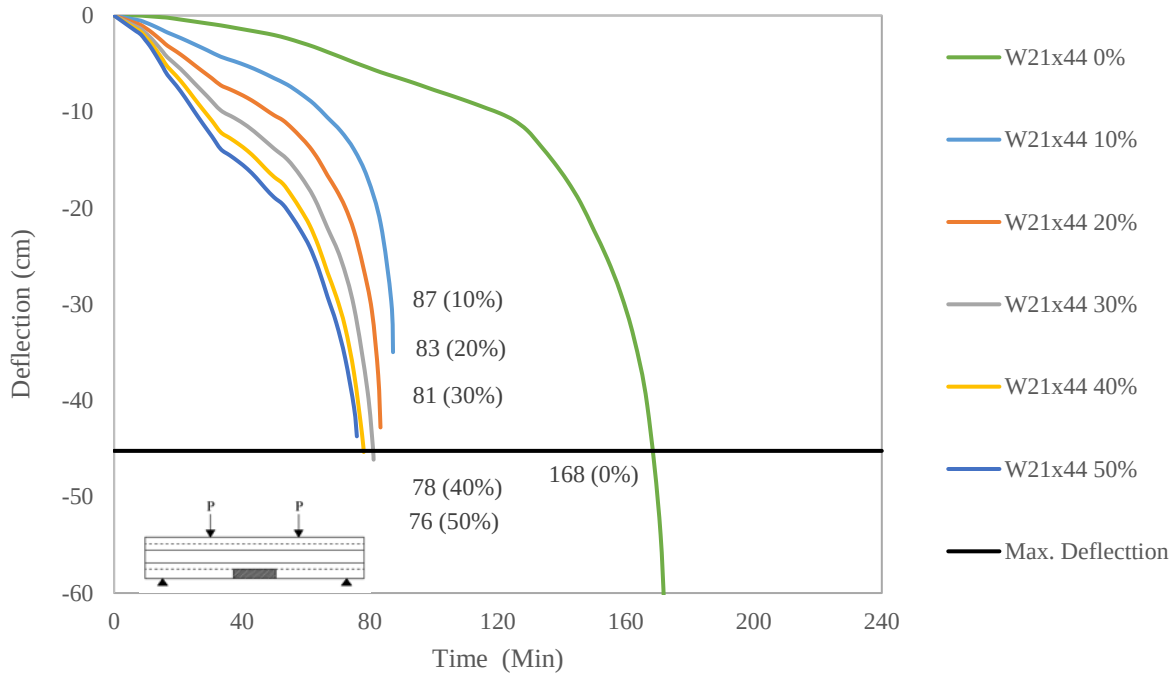

Figure 4-49. Mid-span deflection of W21×44 with 70% loading and various damage length

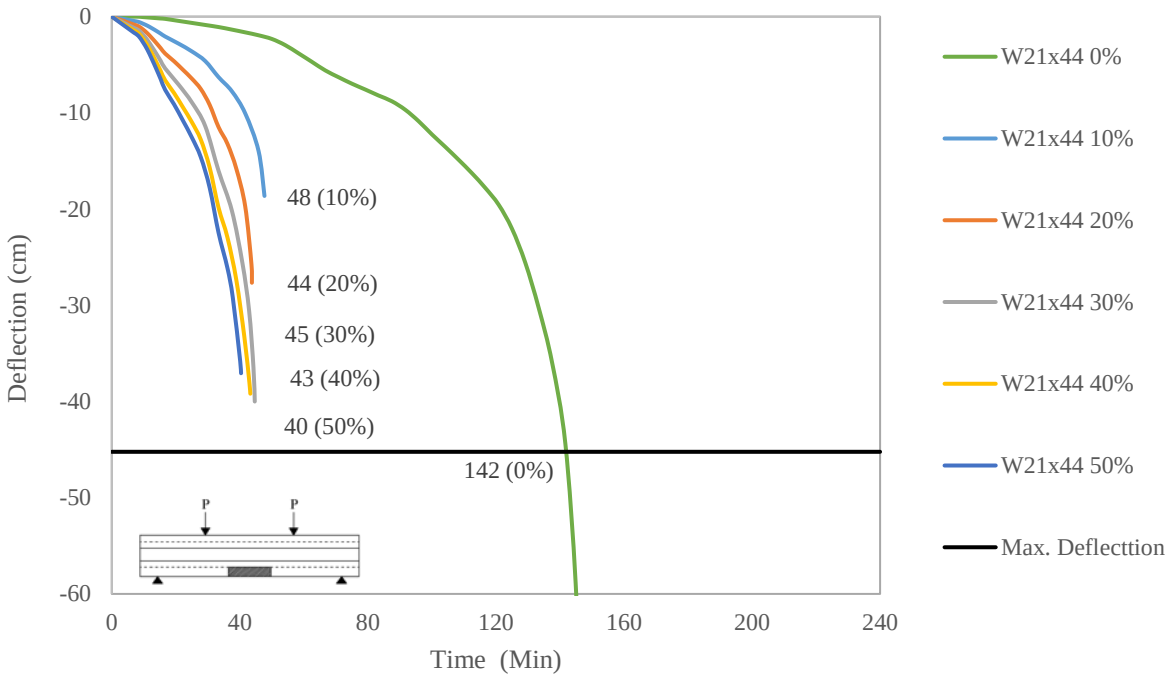

Figure 4-50. Mid-span deflection of W21×44 with 90% loading and various damage length

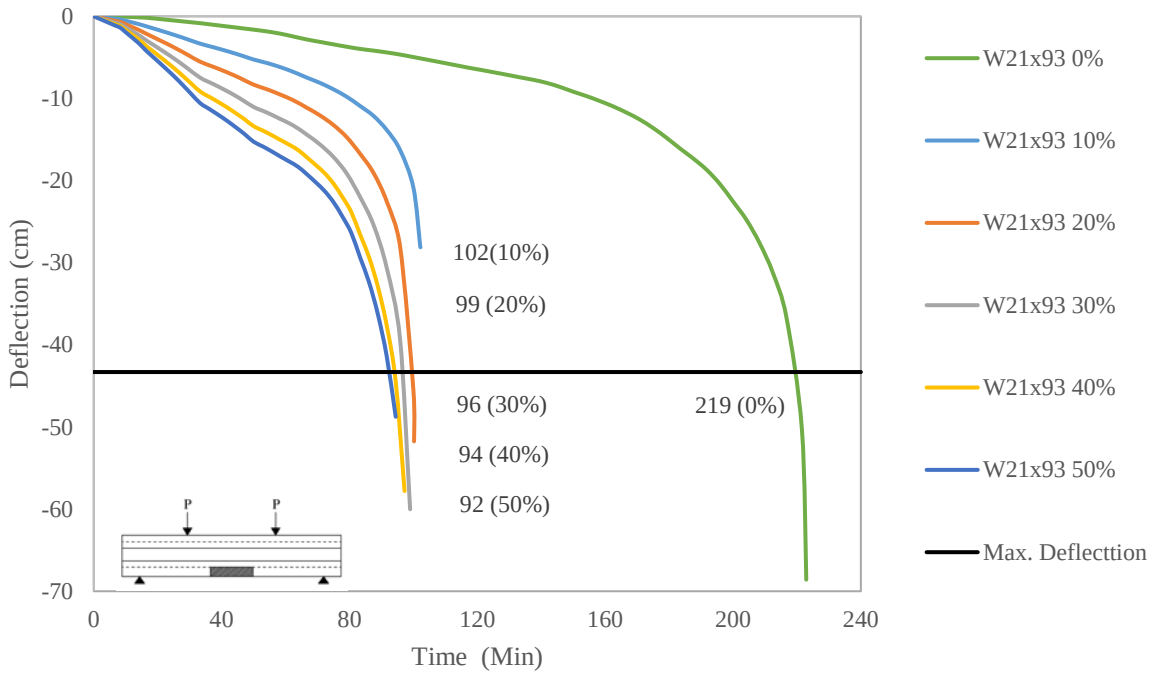

Figure 4-51. Mid-span deflection of W21×93 with 50% loading and various damage length

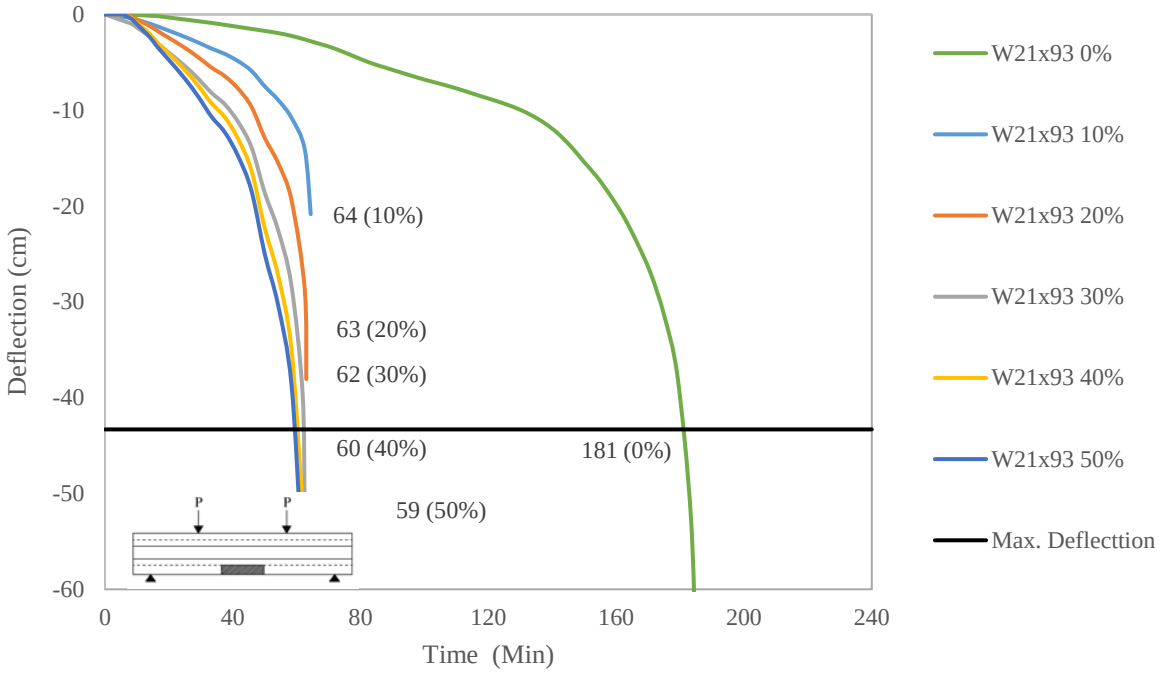

Figure 4-52. Mid-span deflection of W21×93 with 70% loading and various damage length

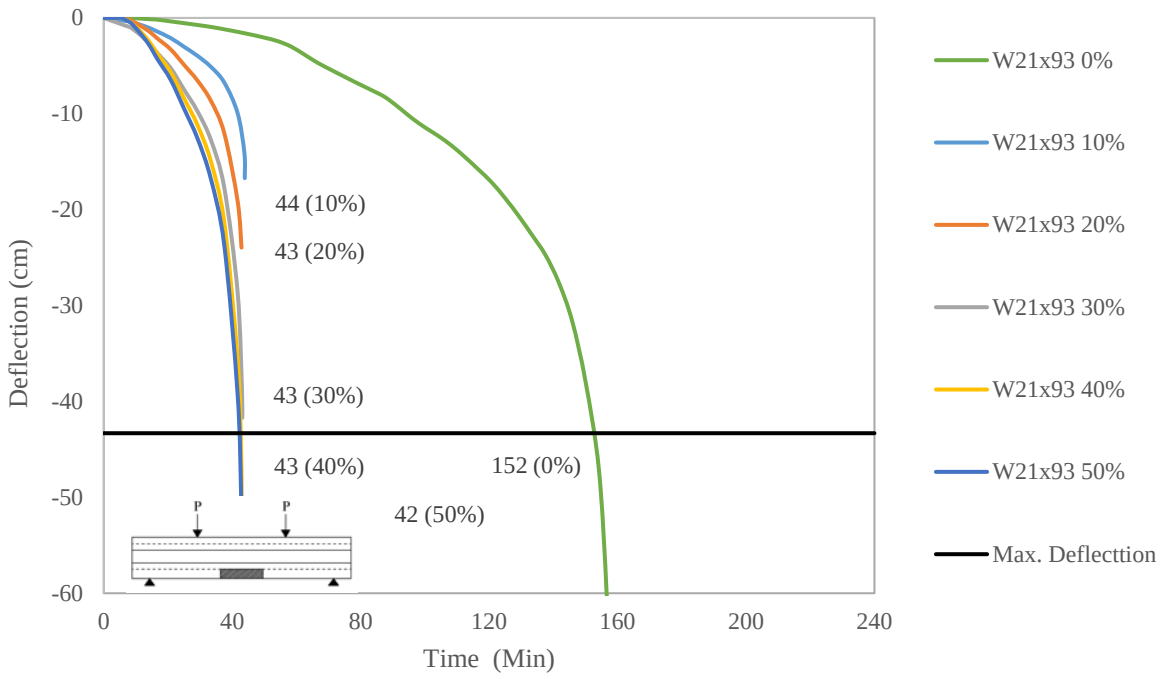

Figure 4-53. Mid-span deflection of W21×93 with 90% loading and various damage length

Table 4-4. Fire resistance of the beams (Minute)

Sections	Loading Level	Damaged region's length as a percentage of span					
		0%	10%	20%	30%	40%	50%
W12x22	50%	180	85	82	78	76	75
	70%	150	53	50	49	48	47
	90%	126	35	33	33	33	33
W12x50	50%	192	56	53	52	51	50
	70%	160	42	39	39	39	39
	90%	134	32	31	31	31	30
W14x30	50%	180	76	74	72	69	68
	70%	151	45	43	42	42	41
	90%	127	31	30	30	30	29
W14x74	50%	198	56	53	52	52	51
	70%	165	42	41	40	40	40
	90%	138	33	32	32	32	32
W18x40	50%	197	107	103	99	97	95
	70%	164	65	61	50	59	58
	90%	139	40	40	38	37	37
W18x86	50%	206	72	71	70	68	67
	70%	172	46	46	46	45	45
	90%	145	36	35	35	35	34
W21x44	50%	204	131	125	120	116	113
	70%	168	87	83	81	78	76
	90%	142	48	44	45	43	40
W21x93	50%	219	102	99	96	94	92
	70%	181	64	63	62	60	59
	90%	152	44	43	43	43	42

Due to thermal expansion of steel, the mid-span deflection of all members at early stages of fire exposure is similar and does not dependent on the load level. The increase in the damaged region's length and larger exposure area results in mid-span deflection increase at early stages of the fire exposure, and the mid-span deflection does not rely on the strength degradation of steel at early stages of a fire incident. Figure 4-54 and 4-55 show the mid-span deflection as a function of time for W12x22 and W21x44 with 30% of the span length damage and three load levels to compare the mid-span deflection at early stages of fire exposure.

The fire resistance of the members with a series of damage region's length is presented in Table 4-4. As it was concluded form the previous set of beams results, the load level has a major influence on the fire resistance of the beams. As an example, the fire resistance of fully fire protected W21x93 is reduced by about 67 minutes by increasing the load level from 50% to 90% of the moment capacity of the beam.

Table 4-5 shows the ratio of the fire resistance of beams with damaged fire protection to the fully fireproofed members' fire resistance regarding the damaged part's length and the applied load level. Other than W21x44 and W18x40 with 50% loading level, the fire resistance of the beams is reduced by more than 50% of the fully protected members. The heavier sections loose their fire resistance faster than the lighter sections with similar damage scenarios. As an example, the fire resistance of W12x22 has reduced by 52% from the fully protected member with 10% of span damage region length. Nevertheless, the fire resistance of W12x50 for same damage scenario is reduced by about 65% of that for W12x50 without any damage.

The fire resistance of lighter sections (with similar section's height) diminishes quicker than heavier sections at higher load levels. As it is shown in Table 4-4, the fire resistance of

W14x30 and W14x74 with 10% damage is reduced by about 45 and 23 minutes, respectively by increasing the load level from 50% to 90% of the member's capacity.

By comparing the failure time of the beams with damaged fire resistance in Table 4-5, it can be concluded that the fire resistance reduction rate reduces for the beams with damaged regions longer than 10% of the span. For instance, the fire resistance of W14x30 with 10% of span damaged region length and 50% load level is reduced by about 104 minutes. However, fire resistance reduction of W14x30 with 50% of span damaged region length and same loading level is about 112 minutes.

The larger exposed area and faster spread of high temperature within the length of the members results in a reduction in fire resistance of the cases with larger damage region's length. The mid-span deflection of the members with longer damaged region's length is higher at early stages of fire exposure. However, the failure time of damaged members with same load level is close. As an example, the fire resistance of W18x40 with 50% load level is reduced to 90 minutes with 10% of span damage's length. However, by 10% increment in the damaged region's length, the fire resistance is reduced by about 4 minutes.

Table 4-5. Fire resistance of damaged members as function of fire resistance of fully protected members

Sections	Loading Level	Damaged region's length as a percentage of span				
		10%	20%	30%	40%	50%
W12x22	50%	47.2	45.6	43.3	42.2	41.7
	70%	35.3	33.3	32.7	32.0	31.3
	90%	27.8	26.2	26.2	26.2	26.2
W12x50	50%	29.2	27.6	27.1	26.6	26.0
	70%	26.3	24.4	24.4	24.4	24.4
	90%	23.9	23.1	23.1	23.1	22.4
W14x30	50%	42.2	41.1	40.0	38.3	37.8
	70%	29.8	28.5	27.8	27.8	27.2
	90%	24.4	23.6	23.6	23.6	22.8
W14x74	50%	28.3	26.8	26.3	26.3	25.8
	70%	25.5	24.8	24.2	24.2	24.2
	90%	23.9	23.2	23.2	23.2	23.2
W18x40	50%	54.3	52.3	50.3	49.2	48.2
	70%	39.6	37.2	30.5	36.0	35.4
	90%	28.8	28.8	27.3	26.6	26.6
W18x86	50%	35.0	34.5	34.0	33.0	32.5
	70%	26.7	26.7	26.7	26.2	26.2
	90%	24.8	24.1	24.1	24.1	23.4
W21x44	50%	64.2	61.3	58.8	56.9	55.4
	70%	51.8	49.4	48.2	46.4	45.2
	90%	33.8	31.0	31.7	30.3	28.2
W21x93	50%	46.6	45.2	43.8	42.9	42.0
	70%	35.4	34.8	34.3	33.1	32.6
	90%	28.9	28.3	28.3	28.3	27.6

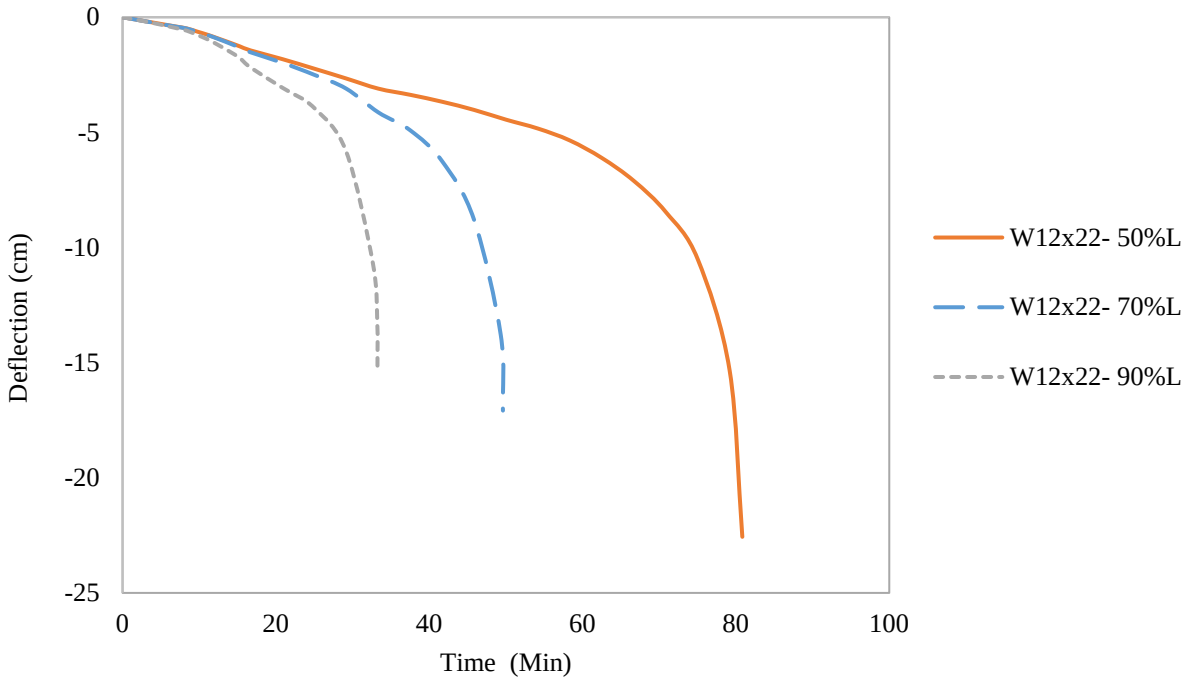

Figure 4-54. The mid-span deflecting of W12x22 with 30% of span damage length during fire exposure

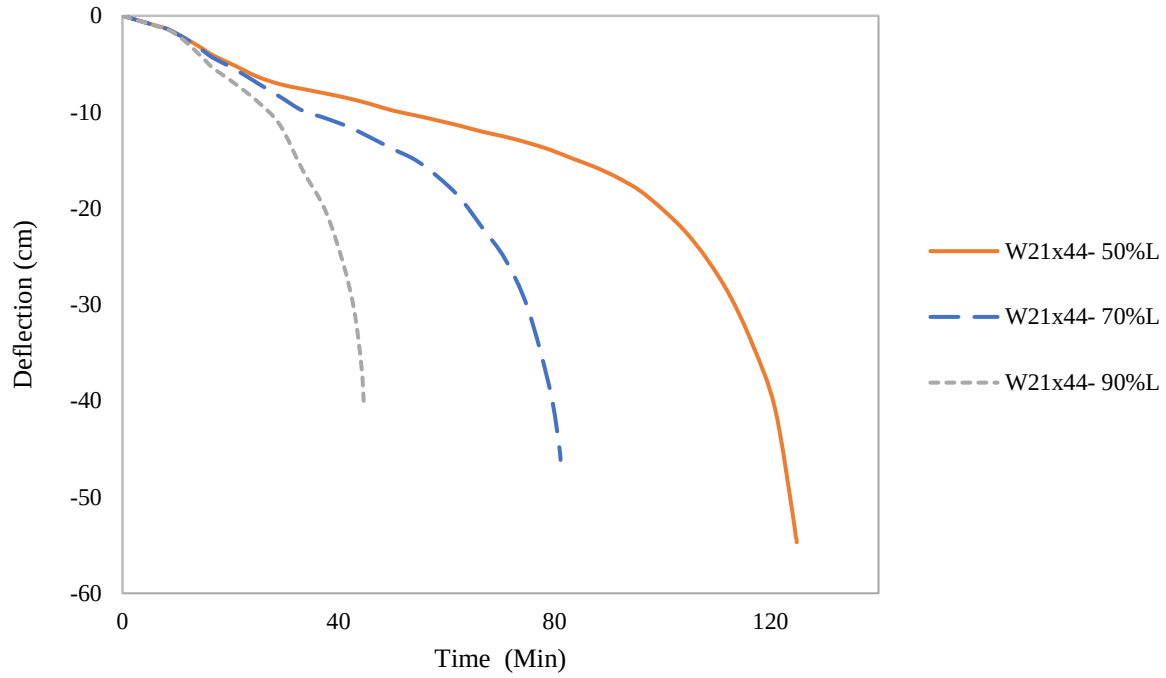

Figure 4-55. The mid-span deflecting of W21x44 with 30% of span damage length during fire exposure

CHAPTER 5. CONCLUSIONS AND FUTURE WORK

5.1 Summary

Passive fire protections methods prevent rapid temperature rise in structural steel members. However, the deterioration of the fire protections of the members influences the behavior of the members. Numerical analysis was carried out to better understand the response of structural steel beams with such damages to the fire protections. The partial loss of fire protection on the structural steel beams leads to a rapid increase in temperatures of the steel members at the damaged region. The degradation of strength stiffness of the steel material at elevated temperatures leads to the reduction of the fire resistance and so the load carrying capacity of the beams. In this study, the influence of the load level, damaged region's length and the penetration of damage on various concrete encased steel beams as primary variables of the parametric study were investigated. Thermal and structural analyses were performed for each beam with different damage scenarios using the ASTM E119 standard fire exposure. ANSYS was utilized to perform the thermal and structural analysis of the beams with partial loss of fire protection. The thermal and structural material properties of steel and concrete at elevated temperatures were applied according

to the equations provided by the Eurocode. The validation of the thermal and structural models was performed by comparison of the experimental fire test's results from the literature with the responses obtained from numerical analysis. The mid-span deflection of each studied case was traced as a function of time. All possible failure limit states were investigated to determine the failure time (fire resistance) of the studied cases. Finally, results were employed to evaluate the influence of the parametric studies' variables.

5.2 Conclusions

- The fire protection loss at the bottom flanges causes a significant reduction in the fire resistance of the steel beams. However, there are no any particular consideration in codes and standards for possible fire resistance reduction due to any partial loss of fire protection during the service life of the members.

- A small length of fire protection loss at the bottom flanges of the beams has a major effect on the load carrying capacity and fire resistance of the beams. However, increasing the length of the damaged part's by more than a specific limit does not increase the reduction rate of the fire resistance of the beams with damaged fire protection.

- The developed finite element results compare well with the measured temperatures and deflections obtained by experiments. These models and modeling procedure were utilized to determine the thermal and structural response of the steel beams with partial loss of fire protection and determine the fire resistance of the beams with different damage scenarios.

- The load level has a significant influence on the structural response of the beams. Steel beams experience more degradation in their fire resistance at higher load levels. Also, heavier steel beam sections' fire resistance drops at a higher rate than the lighter sections with same section's depth.

- The fire protection damages with shallower penetration cause a minor reduction in the fire rating of the beams. The remaining fire protection at the damaged region prohibits the steel beam to be exposed to the radiation portion of the fire heat transfer.

- The degradation of the steel material properties at the flanges has the significant contribution to the deflection and flexural capacity of the beams. Beams with such damages, at the middle of the span, fail through flexural yielding at the location of the damaged part.

5.3 Future Work

This study demonstrate the impact of the partial loss of fire protection on the fire rating (failure time) of the beams, further studies are proposed to gain more understating of fire protection damages' effect:

- There is a lack of experimental studies on the members with damaged fire protection. Experiments would lead to more realistic comprehension of the consequences of fire protection loss on the structural member's behavior. experiments also help in recognizing the fire protection damage parameters that affect the failure of the beams during a fire incidents.

- There is no specific fire exposure coefficients for damaged regions in codes and standards. The accuracy of the analysis with application of accurate fire exposure coefficients results in precise structural analysis for the material with temperature-dependent properties.

- Parametric studies of the beams with damaged fire protections at various fire conditions by application of other fire scenarios, different load configurations and different support conditions provides better insight into the behavior of such beams.

- The slenderness of the web and flanges of the beams has a significant impact on the mode and failure time of the beams. Studies on the beams with different slenderness ratios can help understanding the behavior of plate girders with deteriorated fire protections.

REFERENCES

1. NIST, GCR. "GCR 04-872,"." Fire Protection of Structural Steel in High-Rise Buildings," National Institute of Standards and Technology, Gaithersburg, MD, 2004.

2. Milke, James A., N. Ryder, and S. Wolin. "Analyses of the impact of loss of spray-applied fire protection on the fire resistance of steel columns." Fire Safety Science 7 (2003): 1025-1036.

3. Kang, Y., G. V. Hadjisophocleous, and H. A. Khoo. "Effect of Partial loss of Spray-on Protection on the Load Capacity of Steel Beams during a Standard Fire." Journal of Fire Protection Engineering 18, no. 1 (2008): 5-27.

4. Tomecek, David V., and James A. Milke. "A study of the effect of partial loss of protection on the fire resistance of steel columns." Fire Technology 29, no. 1 (1993): 3-21.

5. Underwriters' Laboratories. Fire Resistance Directory. Vol. 1 Underwriters' Laboratories. 1992

6. Dwaikat, M. M. S., and V. K. R. Kodur. "A simplified approach for predicting temperature profile in steel members with locally damaged fire protection." Fire technology 48, no. 2 (2012): 493-512.

7. Wang, Wei-Yong, and Guo-Qiang Li. "Behavior of steel columns in a fire with partial damage to fire protection." Journal of constructional steel research 65, no. 6 (2009): 1392-1400.

8. Faber, Michael H Michael Havrbro, Oliver Kbler, Mario Fontana, and Markus Knobloch. "Failure Consequences and Reliability Acceptance Criteria for Exceptional Building Structures.",2004.

9. ANSYS® Academic Research. Release 17.1, 2016.

10. CEN Eurocode. "Eurocode 2: Design of Concrete Structures Part 1.2: General Rules - Structural Fire Design ENV 1992-1-2: 2004." .

11. CEN, Eurocode. 2005. "Eurocode 3: Design of Steel Structures Part 1.2: General Rules Structural Fire Design ENV 1993-1-2: 2005." .

12. Aziz, Esam Mohammed. "Response of Fire Exposed Steel Bridge Girders."ProQuest Dissertations Publishing, 2015.

13. Aziz, Esam M., Venkatesh K. Kodur, Jonathan D. Glassman, and Maria E. Moreyra Garlock. "Behavior of steel bridge girders under fire conditions." Journal of Constructional Steel Research 106 (2015): 11-22.

14. ANSYS® Academic Research, Release 17.1, Help System. Coupled-Field Analysis Guide, ANSYS, Inc., 2016.

15. ASTM International. ASTM E119-16a Standard Test Methods for Fire Tests of Building Construction and Materials. West Conshohocken, PA: ASTM International, 2016. doi: https://doi.org/10.1520/E0119-16A.

16. CEN, Eurocode. Eurocode 1: Actions on Structures Part 1.2: General Actions - Actions on Structures Exposed to Fire ENV 1991-1-2: 2002.

17. Phan, Long T., Therese P. McAllister, John L. Gross, and Morgan J. Hurley. 2010. Best Practice Guidelines for Structural Fire Resistance Design of Concrete and Steel Buildings NIST Technical note 1681,National Institute of Standards and Technology, Technology Administration, U.S. Department of Commerce, Gaithersburg, MD.

18. Gewain, Richard G., and Emile WJ Troup. "Restrained fire resistance ratings in structural steel buildings." ENGINEERING JOURNAL-AMERICAN INSTITUTE OF STEEL CONSTRUCTION 38, no. 2 (2001): 78-89.

19. ANSYS® Academic Research, Release 17.1, Help System. Thermal Analysis Guide, ANSYS,Inc., 2016.

20. AISC Committee. "Specification for Structural Steel Buildings (ANSI/AISC 360-10)." American Institute of Steel Construction, Chicago-Illinois (2010).

21. ANSYS® Academic Research, Release 17.1, Help System. Element Reference, ANSYS, Inc., 2016.

22. Krishnamoorthy, Renga Rao. "The analysis of partial and damaged fire protection on structural steel at elevated temperature." (2011).

23. Chang, Yun-Fei, Yih-Houng Chen, Maw-Shyong Sheu, and George C. Yao. "Residual stress–strain relationship for concrete after exposure to high temperatures." Cement and Concrete Research 36, no. 10 (2006): 1999-2005.

24. ANSYS® Academic Research, Release 17.1, Help System. Material Reference, ANSYS, Inc., 2016.

VITA

Mr. Ataollah Taghipour Anvari graduated from Azarbaijan Shahid Madani University with a Bachelors degree in Civil Engineering. Mr. Taghipour is currently a graduate student at University of Illinois at Chicago in the Department of Civil and Material Engineering. He worked on the effect of the partial loss of concrete fireproofing on the fire resistance of the steel beams for his master thesis project. He will earn Master of Science degree from University of Illinois at Chicago. He will pursue a Doctorate Degree in the field of Structural Civil Engineering.